SYNTHESIS AND CHARACTERIZATION OF BORON-NITROGEN DATIVELY BONDED SUPRAMOLECULAR ASSEMBLIES AND ROTORS

A thesis presented to the faculty of the Graduate School of
Western Carolina University in partial fulfillment of the
requirements for the degree of Masters of Science in Chemistry

By

Jeffrey Edward Lux

Director: Dr. William R. Kwochka
Associate Professor of Chemistry
Department of Chemistry and Physics

Committee Members: Dr. Channa R. De Silva, Chemistry
Dr. Brian D. Dinkelmeyer, Chemistry

June 2012

ACKNOWLEDGEMENTS

I would like to thank my thesis research advisory committee, especially Dr. Kwochka for his years of patience, understanding, and gentle pushing. I thank everyone in the Chemistry and Physics Department for helping me by talking about my ideas in an endless quest to understand the how and the why. Acknowledgement is also due to Robert Pike of the College of William and Mary for his analysis of crystal structures for us. I would also like to thank the people at Oak Ridge National Laboratory and the South Carolina Universities Research and Education Foundation for giving me the motivation to push through this last year. Finally, I am thankful to my editor, Danielle Pattee, whose mind can work in ways that mine does not. I owe all of this to others: my family for instilling and nurturing my curiosity to understand the world and the way it works, the professors who provided the knowledge to understand it, and my friends for making it all worthwhile.

TABLE OF CONTENTS

LIST OF TABLES

Page

LIST OF FIGURES

Page

LIST OF SCHEMES

Page

ABSTRACT

SYNTHESIS AND CHARACTERIZATION OF BORON-NITROGEN DATIVELY BONDED SUPRAMOLECULAR ASSEMBLIES AND ROTORS

Jeffrey Edward Lux, M.S.

Western Carolina University (June 2012)

Director: Dr. William R. Kwochka

The synthesis of three adducts of ferrocene boroxine $(C_{10}H_9Fe)_3B_3O_3$ with dative bonds to amines (pyridine, 4-picoline, 4-aminomethyl pyridine, and p-bromoaniline), as well as to two diamines (4,4-bipyridine and 1,4-diazabicyclo[2.2.2]octane) to form bis-complexes which have the potential to be simple molecular rotors was completed. In a related project, complexes of either diphenylborinic acid or 9-borabicyclononane with Lewis base/ hydroxyl group pairs (picolinic acid, nicotinic acid, isonicotinic acid, picolinic acid *N*-oxide, nicotinic acid *N*-oxide, isonicotinic acid *N*-oxide, benzoic acid, 3,5-dibromobenzoic acid, 2-pyridinmethanol, L-Leucine, and L-Phenylalanine) were formed. These primarily intramolecular reactions formed rings of either 5 or 6 atom members. There was also evidence that some of the more geometrically challenged systems could form dimers. The characterization of all of these complexes was performed by ^{1}H NMR and, when possible, LCMS and single crystal x-ray diffraction.

CHAPTER ONE: INTRODUCTION

1.1 Boron and Dative Bonding

Boron typically forms three bonds to form a stable, neutral atom, which leaves it with an empty p-orbital. This empty orbital allows it to form an additional type of bond. Similar to how transition metals function with ligands, if an atom with a lone pair of electrons is present then it may “donate” its pair of electrons to form what is known as a dative (or coordinate covalent) bond (figure 1).

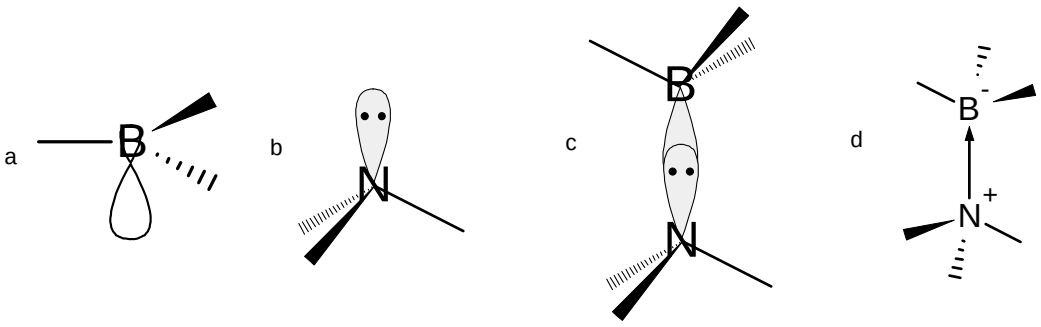

Figure 1. The properties of boron-nitrogen dative bonding. a) Boron with its empty orbital. b) Nitrogen with its lone pair of electrons. c) Nitrogen donating both electrons to boron. d) This dative bond, is represented by an arrow which shows the directionality of the electron density in the bond

This dative bond is sometimes necessary for stability of the boron atom. The lower the oxidation state of boron atoms, the lower the stability of the compound (figure 2). The lowest oxidation level, boranes, is unstable and does not exist in nature as it reacts violently with water. Borinic acids, the next level, are not stable in nature by themselves and will decompose, but will become stable if an additional dative bond forms to the boron atom. Following that are the boronic acids, these are fairly stable but will slowly decompose if exposed to moisture, and again a dative bond will provide even more stability. The final level is boric acid and is found in nature.

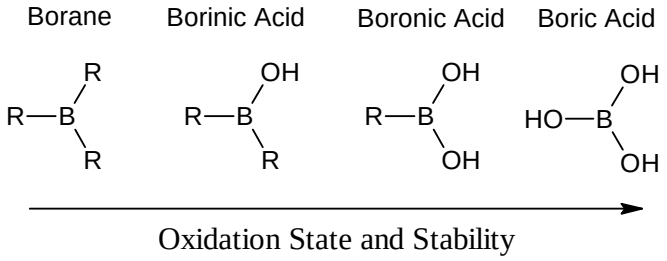

Figure 2. As the oxidation state of the boron atom increases the stability also increases

Boronates are a type of boron compound that has two oxygen atoms bonded to it, with the third bond being an 'R' group (figure 3). Boroxines are similar to boronates except that the 'R' groups attached to the oxygen atoms are other boronates. This leads to compounds characterized by a six membered ring made up of alternating boron and oxygen atoms (figure 3). The three 'R' groups allow for a great deal of variety in both boronates and boroxines.

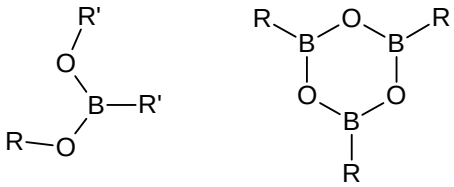

Figure 3. The basic structures of a boronate (left) and a boroxine (right)

These compounds are stable, but will slowly decompose when exposed to water in the air. The decomposition will either return the compound to its original boronic acid or cleave the bond between the boron and 'R' group. When a boronate or boroxine is complexed with an amine through a dative bond they become very stable (figure 4). This process of forming a dative bond will happen at room temperature within a few minutes when the reactants are dissolved in a solvent. An interesting property of boroxines is that despite having three boron atoms, only one dative bond is needed to stabilize the compound. This enhanced stability has been demonstrated by Hursthouse and Beckett and shows some of the typical characteristics of these dative bond systems (figure 5) [1].

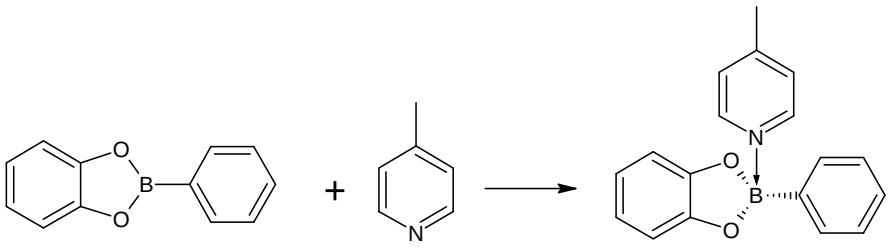

Figure 4. Pyridine complexed with 2-phenyl-1,3,2-benzodioxaborole

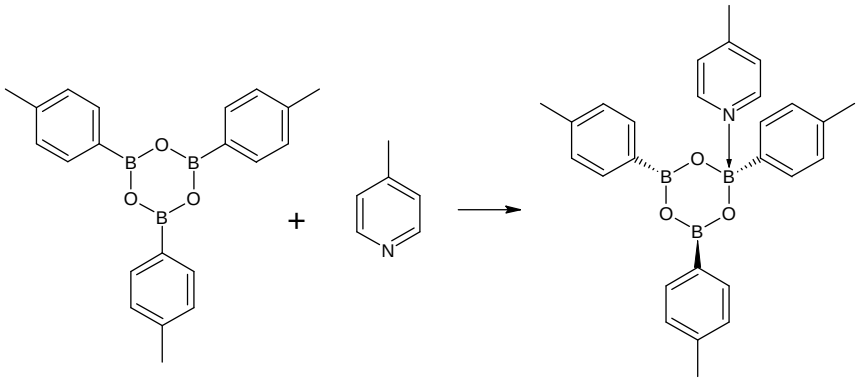

Figure 5. Pyridine complexed with methylphenylboroxine

1.2 Molecular Rotors

One area of research that has garnered a lot of attention lately has been in synthesizing molecules which behave analogously to macroscopic devices such as rotors or gyroscopes. Rotors that have two heads and an internal piece that can freely rotate have been synthesized (figure 6) and have the ability to rotate internal portions of the molecule in the solid state [2]. If the middle group is non-symmetrical and can be affected by things like electromagnetic fields then they have been called molecular compasses.

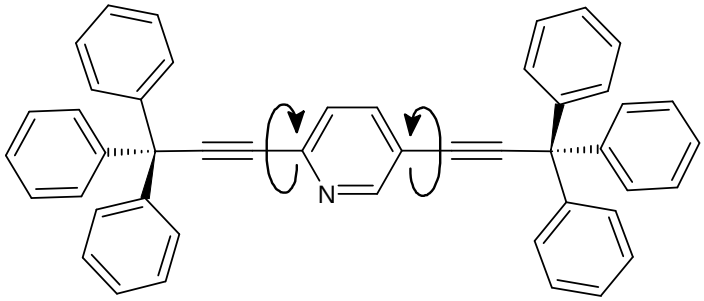

Figure 6. Molecular rotor with two bulky stator groups, triphenylmethyl, and a rotator, a pyridine diene, in the middle that can spin freely

In theory, a molecular rotor could be formed with boroxines and a diamine (figure 7). This rotor has two large stator groups, the phenyl boroxines, much like the triphenylmethyl groups in (figure 6). It also contains a rotator, 4,4-bipyridine, analogous to the polar pyridine in (figure 6). The main difference is in the (figure 6) rotator which is physically bound to the stator by carbon-carbon bonds, while in (figure 7) the rotator is connected only through coordinating dative bonds.

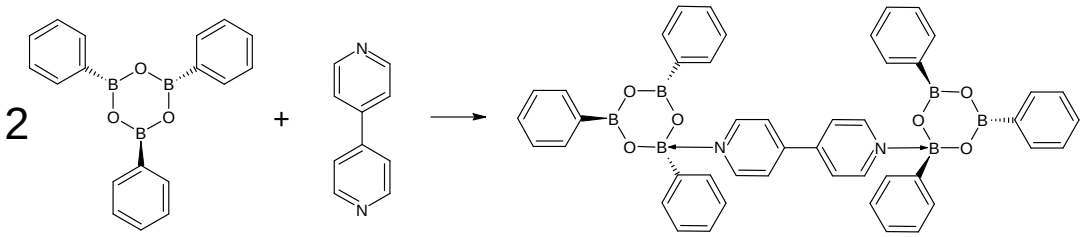

Figure 7. Phenyl boroxine complexed with 4,4-bipyridine to form a molecular rotor

1.3 Self-Assembling Macrocycles

Dative bonds of several types have been used as a means of preparing supramolecular assemblies; these bonds are easily interchangeable if a more favorable electron donator is introduced. This approach is quite flexible and is an ideal method for self-assembling supramolecular systems. Stang, for example, has used nitrogen - Pd or - Pt dative bond interactions in the directed self-assembly of supramolecular systems

(figure 8) [3]. These molecules, all mixed together and allowed to come to equilibrium over a period of 120 hours, will form the self-recognized products in over 90% yield.

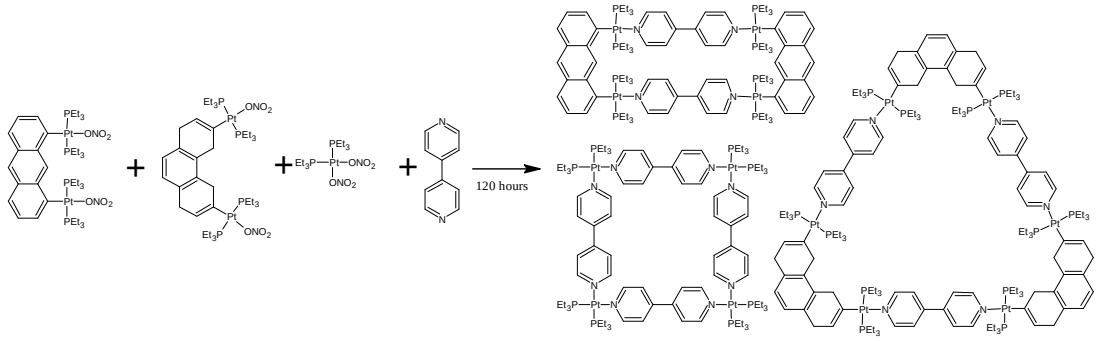

Figure 8. Self-assembling and self-recognizing organometallics by the Stang group

There has been increasing interest in creating supramolecular assemblies and one specific area of interest has been in the utilization of boron compounds for this purpose [4]. The dative bond formed between boron and nitrogen allows for self-assembling supramolecules, as demonstrated by Severin (figure 9). For example, when phenyl boronic acid is combined with 2,3-dihydroxypyridine, the two molecules undergo a condensation reaction to yield a boronic ester complexed with an amine. This compound self-assembles into a cyclic tetramer with 16-atom members in the ring. Other macrocylic systems were also reported which contained additional functional groups on the acid and amine.

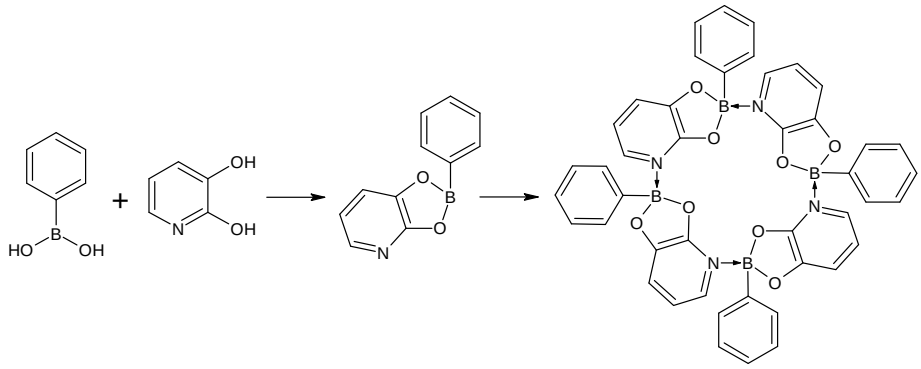

Figure 9. Phenyl boronic acid reacted with 2,3-dihydroxypyridine to form a macrocycle with four boronate subunits

The previously mentioned borinic acids contain only one oxygen group and two other 'R' groups. This low oxidation state of boron is quite unstable but the dative bond greatly enhances that stability. It also allows for additional variety in possible structures and potentially more options for self-assembling macrocycles (figure 10).

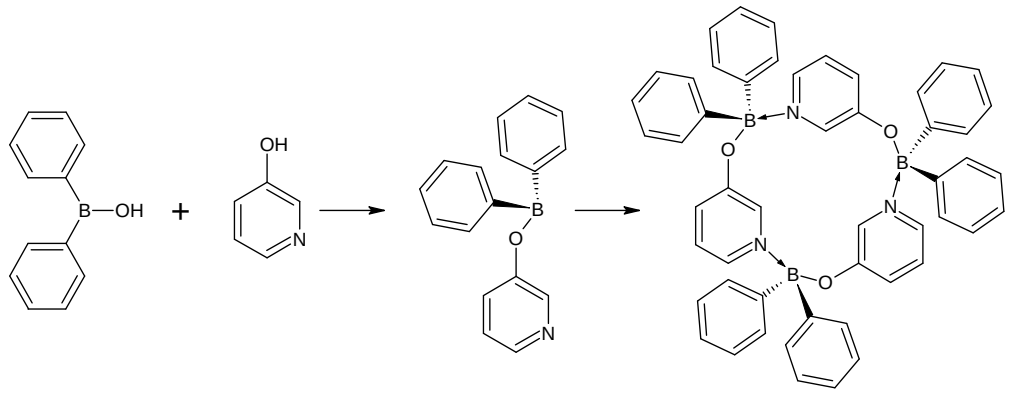

Figure 10. Hypothetical example of self-assembling macrocycle with borinic acid through dative bonding

CHAPTER TWO: RESULTS AND DISCUSSION

When the dative bond forms, the basic nitrogen atom donates electron density to the acidic boron atom. As a consequence of this electron donation, the hydrogen atoms nearest the nitrogen become electron deficient. This loss of electron density deshields those hydrogen nuclei and causes their respective signals to shift downfield in ^{1}H NMR. Conversely, the hydrogen atoms nearest the boron atom have an increased electron density causing them to shift upfield. The downfield shifting will be the primary evidence in ascertaining whether or not a dative bond formed and thus a successful complexation.

2.1 Ferrocene Boroxine Complexes

This project focused around the study of boron-nitrogen dative bonds and attempting to use them to make solid-state molecular rotors via a self-assembly process. A system with ferrocene boroxine as a stator and a diamine as a rotator was chosen for two reasons. First, the ferrocene moiety's sheer bulk was postulated to prevent intercalation of neighboring rotor molecules which might inhibit rotation of the internal rotor. Second, by incorporating ferrocene moieties into the rotor structure, it was hoped that these systems would be more amenable to single crystal x-ray analysis.

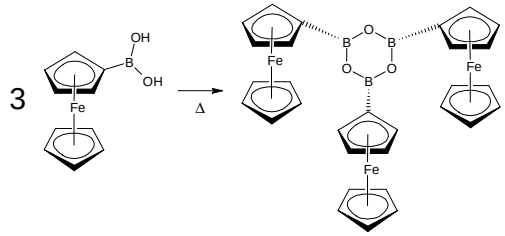

1 **2**

The first step in any of these reactions is the production of the ferrocene boroxine **2** from ferrocene boronic acid **1**. To do this a significant amount of the boronic acid **1**

was placed in a beaker in an oven at 80℃ for a 24 hour period to make material for several reactions. Both the starting material **1** and the boroxine product **2** are orange powders; however there would always be several small red crystals formed on the sides of the beaker during the baking process. The orange powder was confirmed by ^{1}H NMR to be ferrocene boroxine **2** with an impurity (figure 11).

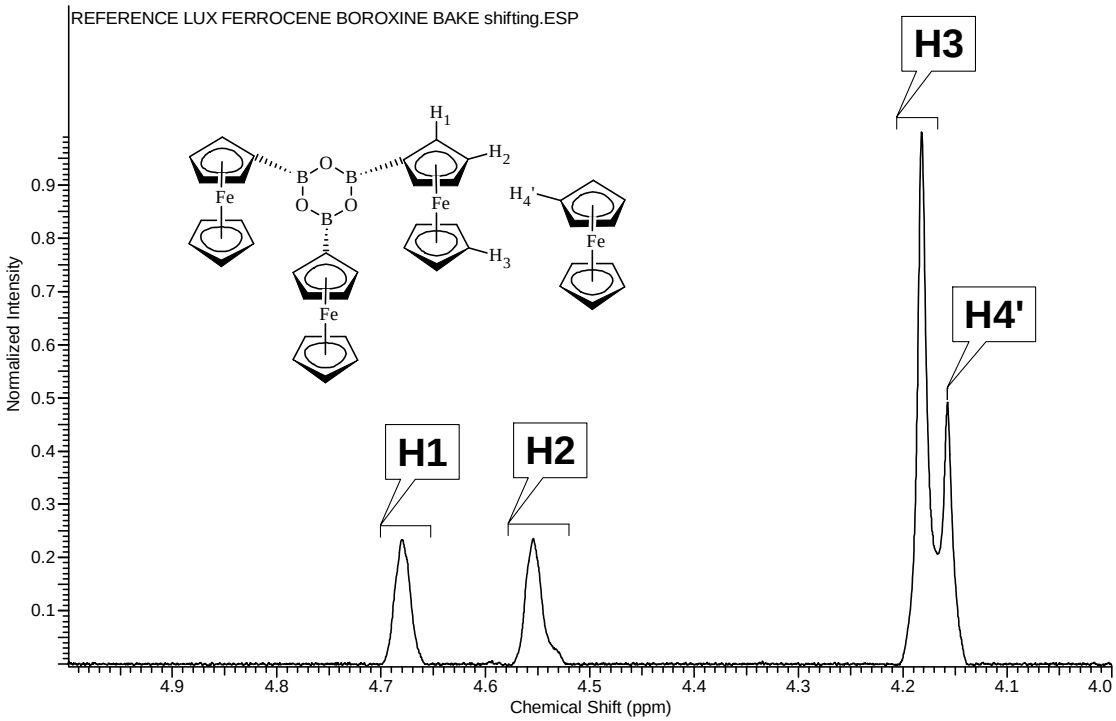

Figure 11. ^{1}H NMR spectrum of ferrocene boroxine **2** powder after baking

The red crystals were determined by ^{1}H NMR to be plain ferrocene with trace amounts of the boroxine **2** (figure 12). The exact mechanism by which these ferrocene crystals were produced is uncertain, but the impurity in the ferrocene boroxine **2** used as a starting material for the rest of the reaction was ferrocene. Consequently, the ferrocene peak appears in the spectra of most of the compounds produced and causes some problems with integration due to overlap.

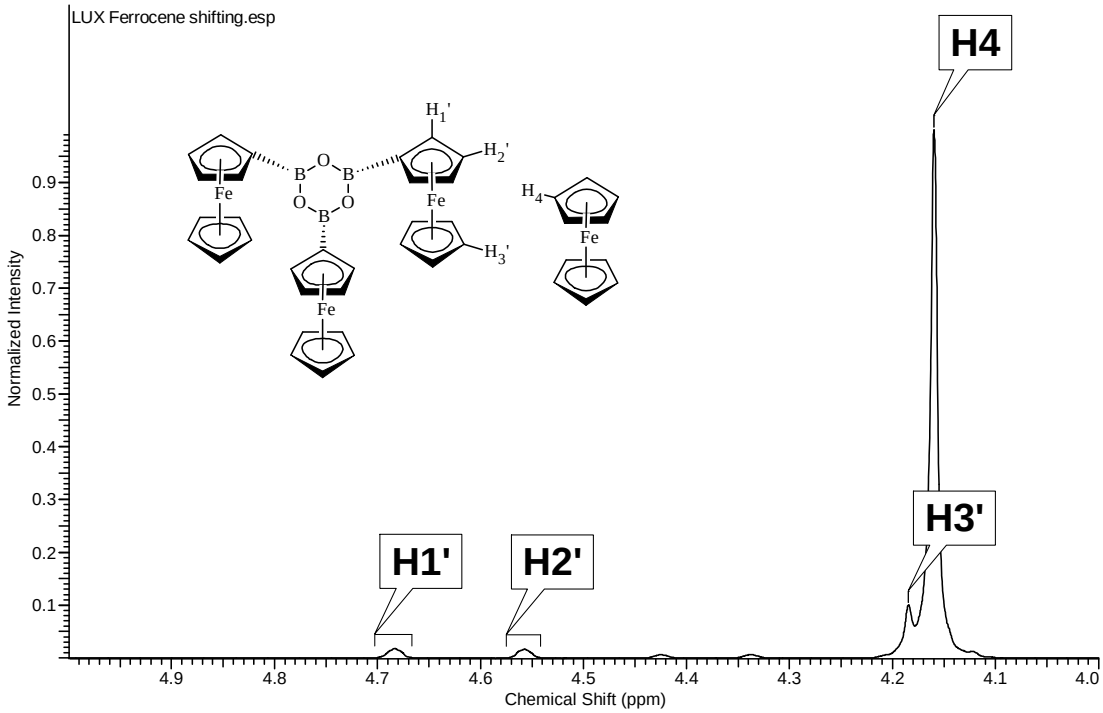

Figure 12. ^{1}H NMR spectrum of ferrocene crystals with trace amount of ferrocene boroxine **2**.

Key to the formation of a rotor is that there are two stator groups (ferrocene boroxine) for each internal rotator (diamine). In order to determine this ratio the integrations of the ^{1}H NMR peaks from the ferrocene boroxine portion of the complex will be compared to the integrations from the diamine portion of the complex. Ferrocene boroxine has three peaks associated with it, one of which is impossible to get an accurate integration for due to the contamination of ferrocene. The other two can be compared to the diamine to demonstrate the ratio except in cases where there is extreme peak broadening. In these instances the entire ferrocene boroxine region must be integrated together and compared to the diamine; however, due to the ferrocene contamination the ratio will appear larger than it actually is. If the ratio is 2:1 then a rotor is possible, but if the ratio is only 1:1 then it formed a non-rotor complex.

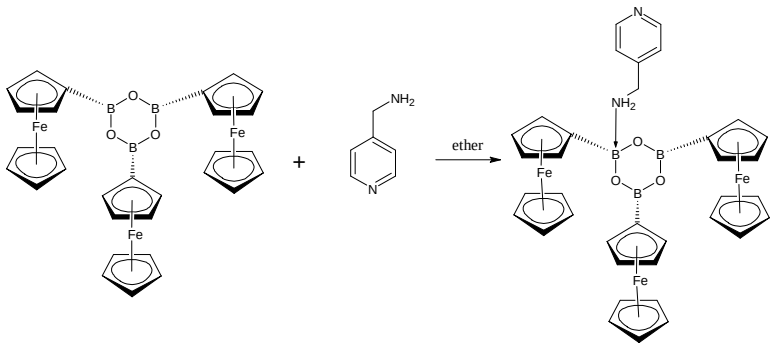

2 **3** **4**

The first reaction selected for the ferrocene boroxine series was with 4-aminomethyl pyridine **3**. This complex had the potential to form a rotor as it contained two nitrogen atoms, though the stator portions of the rotor would not be parallel. The previously synthesized boroxine **2** was dissolved in diethyl ether and changed from an orange powder to a cloudy green liquid. The 4-aminomethyl pyridine **3** was added and the solution was stirred for 48 hours. The resulting cloudy green solution was gravity filtered to yield a green filtered solid and a yellow-orange filtrate. The filtrate had its solvent removed *in vacuo* and analyzed by ^{1}H NMR. The results of this were unclear but recrystallization attempts were made, one of which yielded promise.

One of these crystals was dissolved in $CDCl_3$ and a ^{1}H NMR revealed that it was the desired product **4**. All peaks for both the ferrocene boroxine **2** and 4-aminometyl pyridine **3** components were present and the 4-aminomethyl pyridine peaks were properly shifted from the starting material (figure 13). The peak associated with the proton *ortho* to the nitrogen atom, H_1, shifts from 8.48ppm to 8.68ppm, the *meta* H_2 shifts from 7.19ppm to 7.36ppm, and the aliphatic H_3 shifts from 3.84ppm to 3.96ppm.

Another of the crystals from the same batch was sent off for single crystal x-ray diffraction. The results confirmed that the crystal was the desired product **4** (figure 14) and it also demonstrated that, at least in the solid state, the amine nitrogen formed the dative bond rather than the pyridine nitrogen.

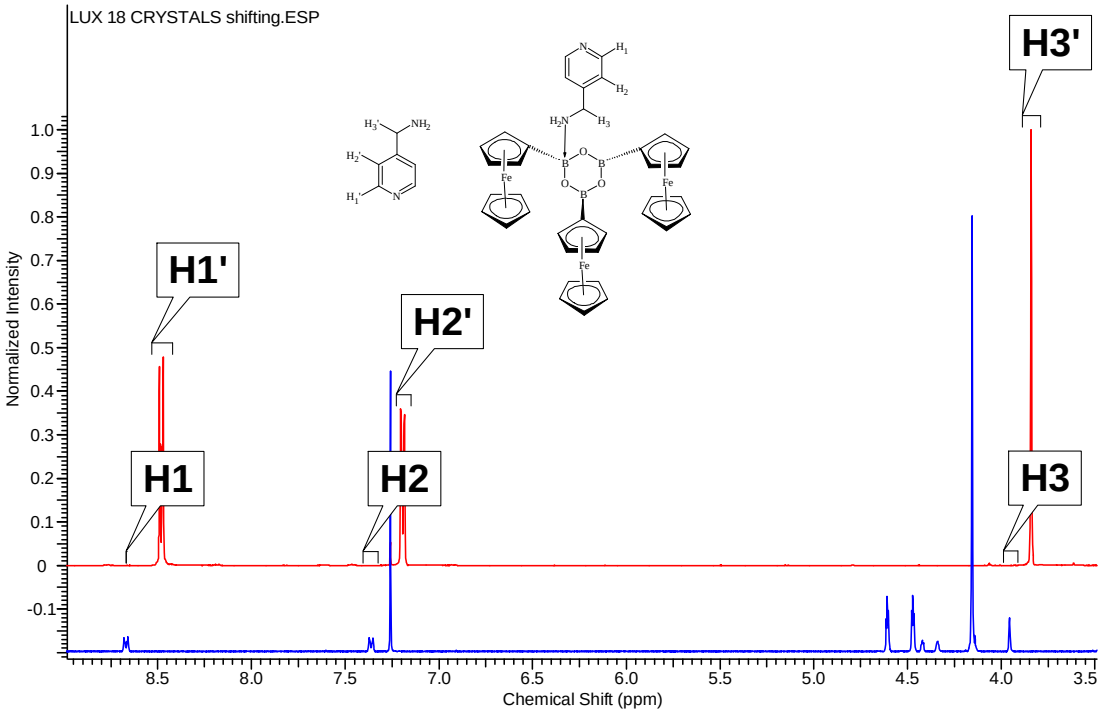

Figure 13. ^{1}H NMR spectra of 4-aminomethyl pyridine **3** (red) and its complex with ferrocene boroxine **4** (blue)

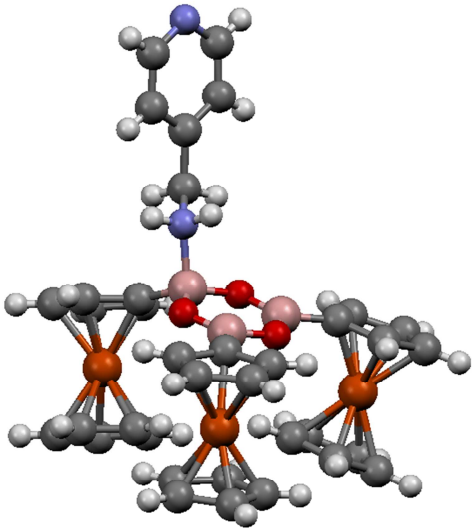

4

Figure 14. Crystal structure of the complex **4** formed between ferrocene boroxine **2** and 4-aminomethyl pyridine **3** as determined by x-ray crystal diffraction

Attempts were made using both diethyl ether and dioxane as a solvent and in 1:1 and 2:1 ratios of boroxine:amine. Unfortunately, a rotor was never formed and the only complex formed was with ether as a solvent in a 1:1 ratio that later yielded the above-mentioned crystals. Despite this drawback, this was the most successful of the ferrocene boroxine series of reactions due to clear evidence of formation from both ^{1}H NMR and x-ray crystal structure.

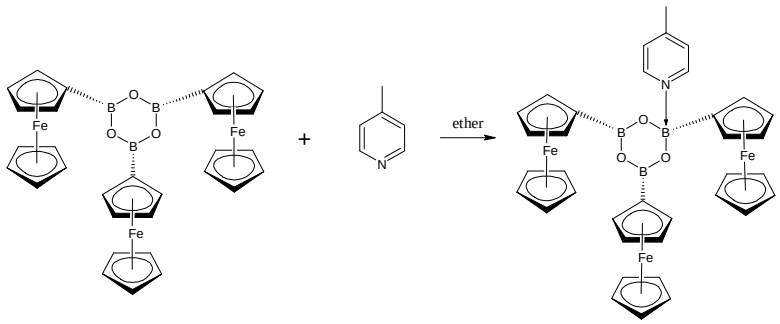

2 **5** **6**

Following the success of the complex formed, but with several failed attempts on the mind as well, a more simple reaction was undertaken. This time, a rotor was not to be attempted but rather a simple complexation with the single nitrogen containing picoline **5**. This reaction proceeded as with the previous; beginning with the formation of a cloudy green solution and 48 hours of stirring, followed by filtration and removal of solvents from the filtrate. Recrystallizations were attempted but the crystals formed were only ferrocene boroxine **2**. The filtrate before recrystallization was analyzed by ^{1}H NMR and, due to shifting of the peaks, was determined to be the predicted complex **6** (figure 15). The peak associated with the proton *ortho* to the nitrogen atom, H_1, shifts from 8.46ppm to 8.54ppm, the *meta* H_2 shifts from 7.10ppm to 7.18ppm, and the methyl H_3 shifts from 2.35ppm to 2.39ppm. The ferrocene peaks integrated to slightly less than a 1:1 ratio in all of the attempts for this reaction.

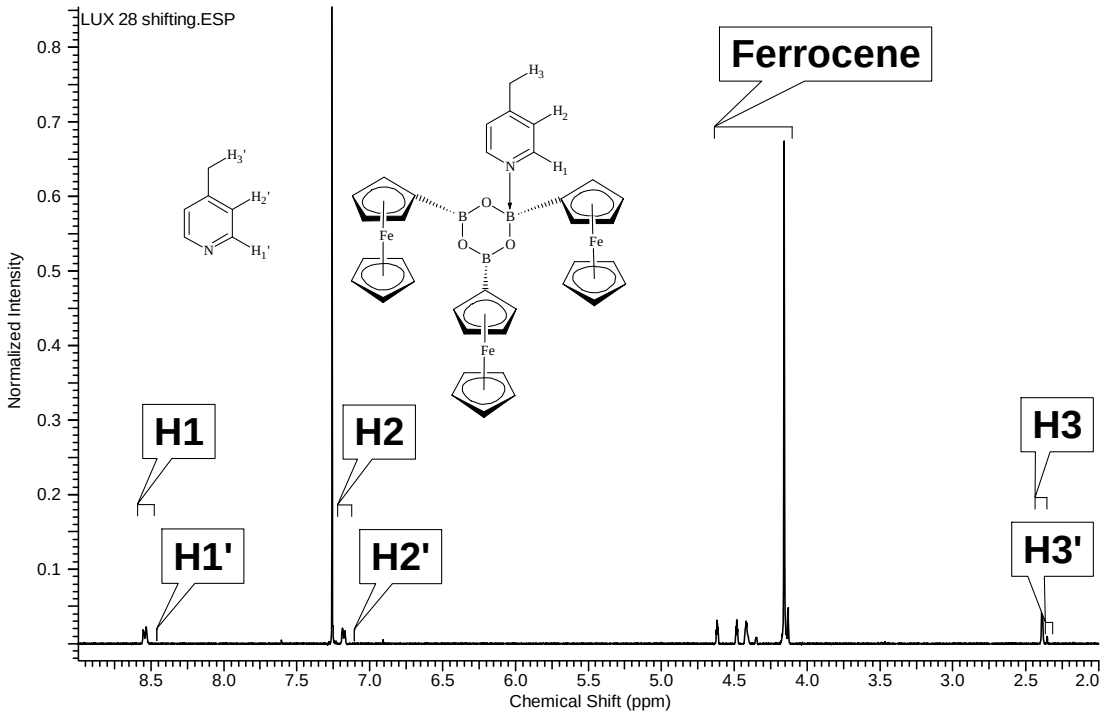

Figure 15. ^{1}H NMR spectrum of complex with ferrocene boroxine and picoline **6**

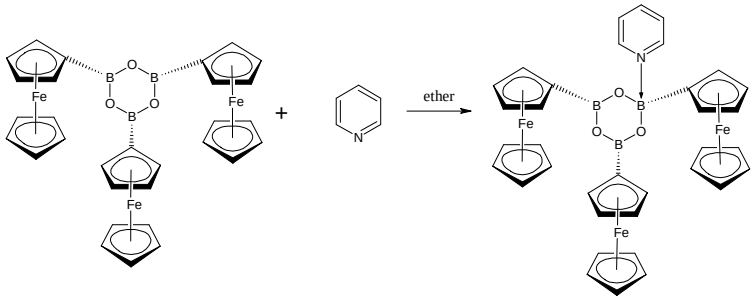

2 **7** **8**

Continuing the non-rotor exploration, pyridine **7** was selected for the next reaction. The process followed the same pattern as the previous ones with the same color changes evident. No crystals were formed during recrystallization attempts, but a few of the reaction attempts did produce compounds with appropriate shifting of peaks when analyzed by ^{1}H NMR to suggest the desired product **8** (figure 16). The peak associated with the proton *ortho* to the nitrogen atom, H_1, shifts from 8.59ppm to 8.80ppm, the *meta* H_2 shifts from 7.23ppm to 7.43ppm, and H_3, *para*, shifts from 7.60ppm to 7.81ppm. Again, the ferrocene peaks never integrated properly and some

even demonstrated patterns that were not able to be explained, such as the pyridine peaks not integrating to each other equally.

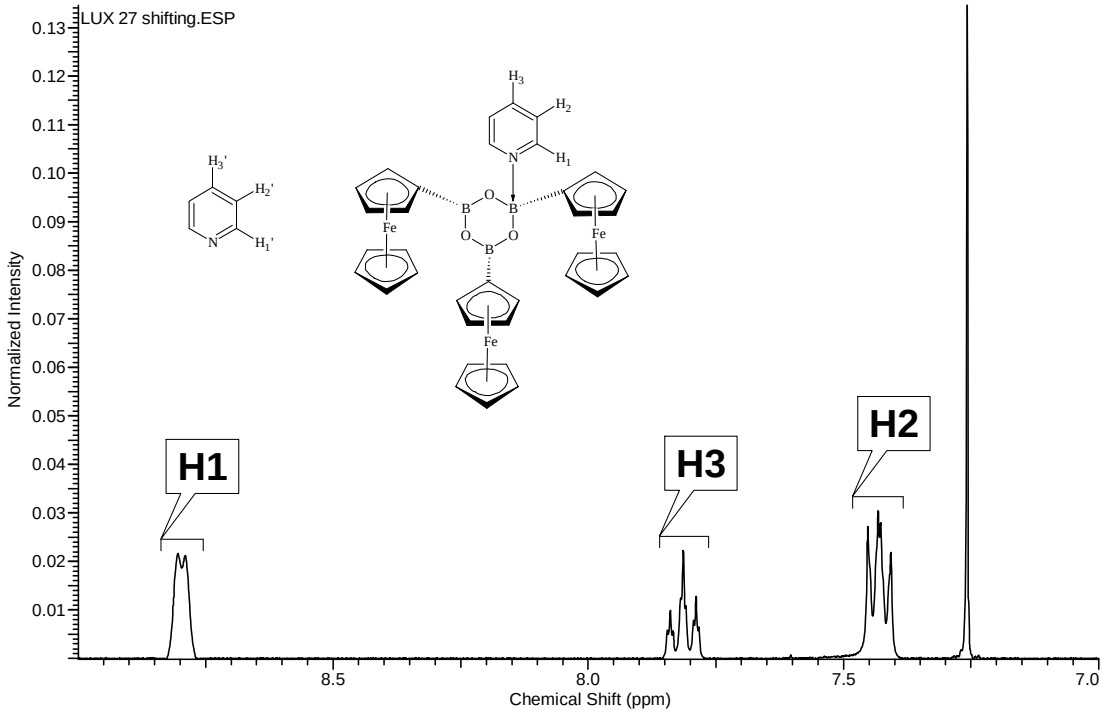

Figure 16. ^{1}H NMR spectrum of complex with ferrocene boroxine and pyridine **8**

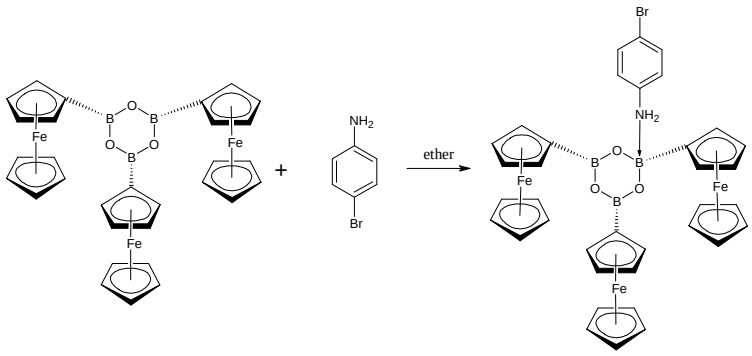

2 **9** **10**

With the difficulties of the previous reactions, p-bromoaniline **9** was selected for the next reaction as it also contained only a single nitrogen atom. However, this nitrogen was an amine nitrogen, not a pyridine nitrogen and similar to the crystal **4** formed earlier. This reaction again used the same procedure as the previous ones with the same visual changes. Crystals were formed during recrystallization but turned out to

be purely ferrocene boroxine **2**. When analyzed by ^{1}H NMR, the filtrate showed the presence of both ferrocene boroxine **2** and p-bromoaniline **9** but no shifting of peaks nor proper integration to suggest the desired product (figure 17). While there were peaks that could have represented the shifted product they did not even integrate properly with themselves, reinforcing the fact that this product **10** did not form.

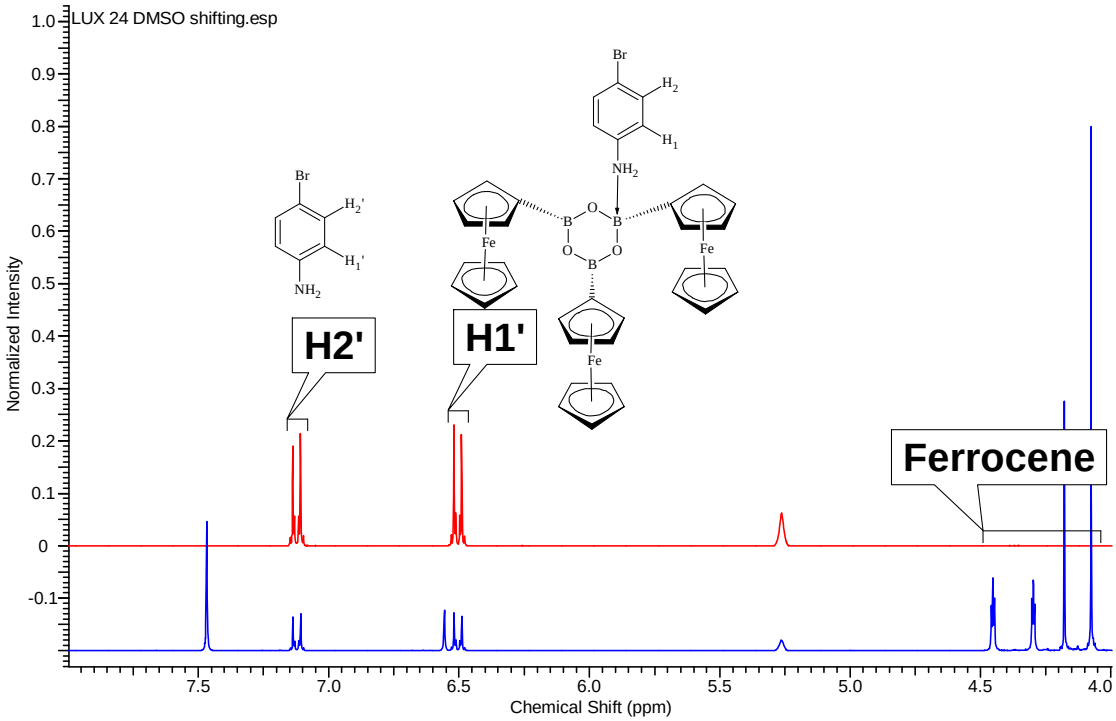

Figure 17. ^{1}H NMR spectra of p-bromoaniline **9** (red) and the product of its reaction with ferrocene boroxine **2** (blue)

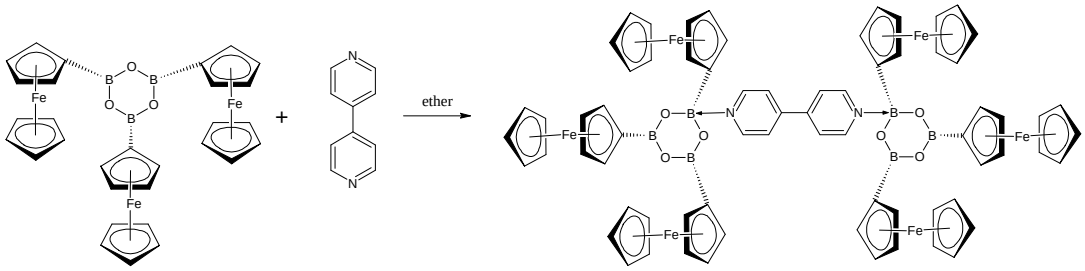

2 **11** **12**

After exploring several non-rotor forming reactions it was decided to return to the potentially rotor forming reactions. The first new rotor attempt was with 4,4'-bipyridine **11**. This reaction proceeded the same as the others except that it was done in a 2:1

ratio with twice as much boroxine **2** in order to form the rotor. No crystals were formed but, based pm shifting, the filtrate did appear to form the desired complex **12** when analyzed by ^{1}H NMR. (The ^{1}H NMR data file for this sample was corrupted but a scan of the hard copy is in Appendix A.) The peak associated with the proton *ortho* to a nitrogen atom, H_1, shifts from 8.74ppm to 8.88ppm and the *meta* H_2 shifts from 7.53ppm to 7.63ppm. The problem came from the integrations of the ferrocene boroxine peaks, since all of the ferrocene boroxine peaks overlapped each other and the inclusion of ferrocene meant that an accurate integration was not possible but it was clearly less than a 2:1 ratio.

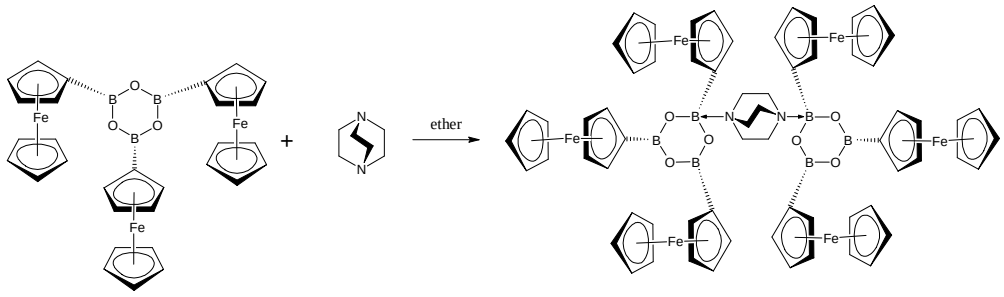

2 **13** **14**

The final attempt at forming a rotor was done with 1,4-diazabicylo(2.2.2)octane (DABCO) **13**. This reaction was done the same as the one before it with the 2:1 ratio and again no crystals were formed. According to the shifting on the ^{1}H NMR, the filtrate held what appeared to be the desired product **14** (figure 18). The only peak on the diamine shifts from 2.78ppm to 3.03ppm. The ferrocene boroxine peaks demonstrated extreme overlap once more and combined with the ferrocene peak. It was not possible to accurately determine the actual ratio. The ratio appears higher than it truly is but as it is greater than a 2:1 ratio, it is possible that a rotor formed.

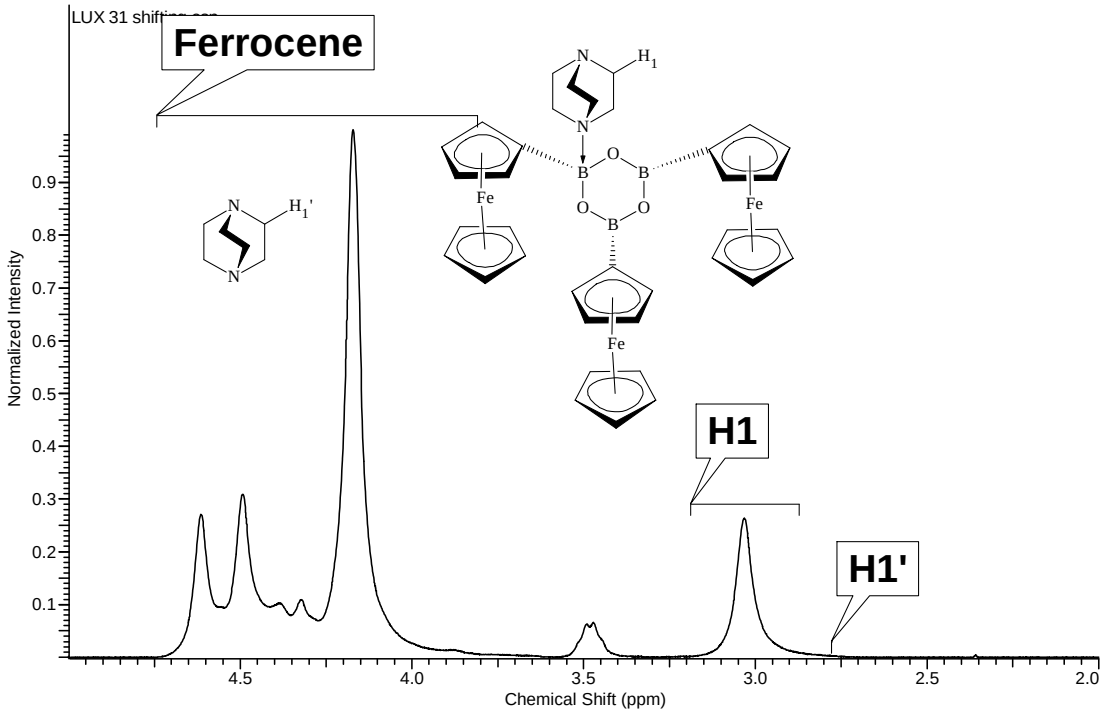

Figure 18. ^{1}H NMR spectrum of complex with ferrocene boroxine and DABCO **14**

It was discovered later that the ferrocene boronic acid **1** could be placed in one reaction vessel with the nitrogen containing compound in solution and heated through reflux or microwave. The components would all self-assemble in a “one pot” method. This method was attempted for many of these compounds and several additional ones and had similar results but also similar difficulties.

Due to the difficulties in interpreting the peaks associated with the ferrocene protons that were pervasive throughout this project, few definitive conclusions could be made. Exact ratios of ferrocene boroxine to amine could not be determined, uncertainty as to what some of the peaks in the ferrocene region were, and molecular ferrocene existing in the samples were some of the major problems that were not able to be overcome. These problems brought this project to an end as it became evident that we had no method to avoid them; thus another task was begun. Continuing the concept of boron-nitrogen dative bonding, self-assembling molecular structures were to be attempted.

2.2 Macrocycles Via Self-Assembly of Borinic Acid Derivatives

The monomer subunits would be made from a diphenyl borinic acid **16** and one of a variety of carboxylic acids containing a nitrogen atom (figure 19). The structures of these carboxylic acids are similar, the first few of the series being isomers of picolinic acid; the nitrogen atom in the aromatic ring is located in the *ortho*, *meta*, or *para* positions relative to the carboxylic acid group. Other varieties being used were the N-oxide versions of the picolinic acid series, some amino acids, as well as a few other variations. The reasoning for these variations was to determine whether or not we could control the intramolecular vs. intermolecular interactions to form either macrocycles or polymeric systems.

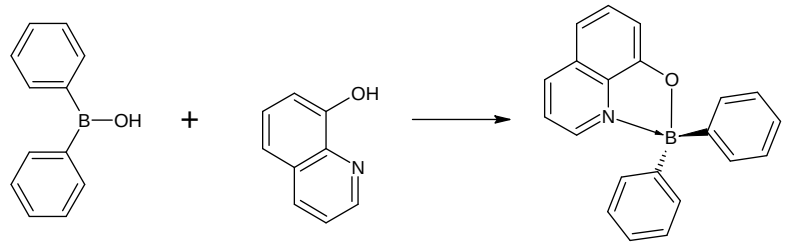

Figure 19. Basic theory for the self-assembling macrocycles of diphenyl borinic acid ester complexes as demonstrated by Benkovic and Baker [5]

The diphenyl borinic acid **16** used in these reactions has one major problem, it is unstable by itself. For this reason it has a protecting group on it while it is being stored that must be removed prior to its reaction with the carboxylic acid. Due to the instability of this compound, the reaction must be completed within a few hours and formed into a stable compound before it begins to decompose.

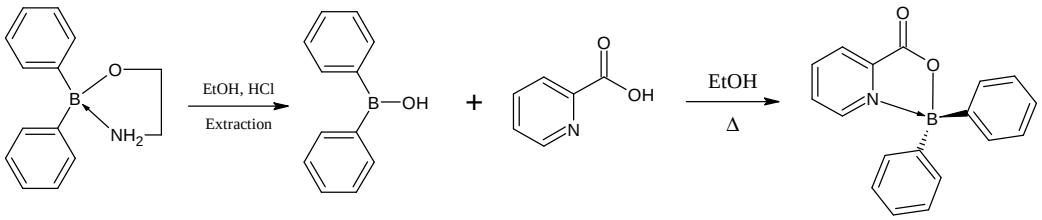

15 **16** **17** **18**

The first reaction in this series is the diphenyl borinic acid **16** with picolinic acid **17**, having the nitrogen in the *ortho* position. First, the ethanolamine protecting group is removed by dissolving the starting material **15** in ethanol and a small amount of water with a few drops of concentrated hydrochloric acid. This solution is stirred for approximately 20 minutes, extracted with ether, dried with magnesium sulfate, and the solvent removed *in vacuo*. The deprotected borinic acid **16** is combined with picolinic acid **17** and ethanol and refluxed for 15 minutes. Following reflux, approximately 75% of the ethanol was distilled off and the product **18** allowed to recrystallize. The end result was a white crystalline solid with a 69% yield.

The crystals dissolved well in DMSO-d_6 and the ^{1}H NMR showed a clear shifting of the peaks as well as the separation of two of the peaks (figure 20). The peak associated with the proton *ortho* to the nitrogen atom, H_1, shifts from 8.71ppm to 9.18ppm, H_2, *meta*, and H_3, *para*, separate and shift from ~8ppm to 8.47ppm and 8.64ppm respectively, and H_4, *ortho* to the carboxylic acid, shifts from 7.62ppm to 8.18ppm. Having all of these peaks shift in this way is indicative of the expected reaction taking place where electrons from the nitrogen are donated to the boron and thus the protons on the nitrogen-containing ring lose electron density.

The crystals were also sent off for x-ray crystal diffraction. The results show that the reaction worked as expected and that the nitrogen datively bonds to the boron of the same molecule forming a monomer with a five membered ring (figure 21).

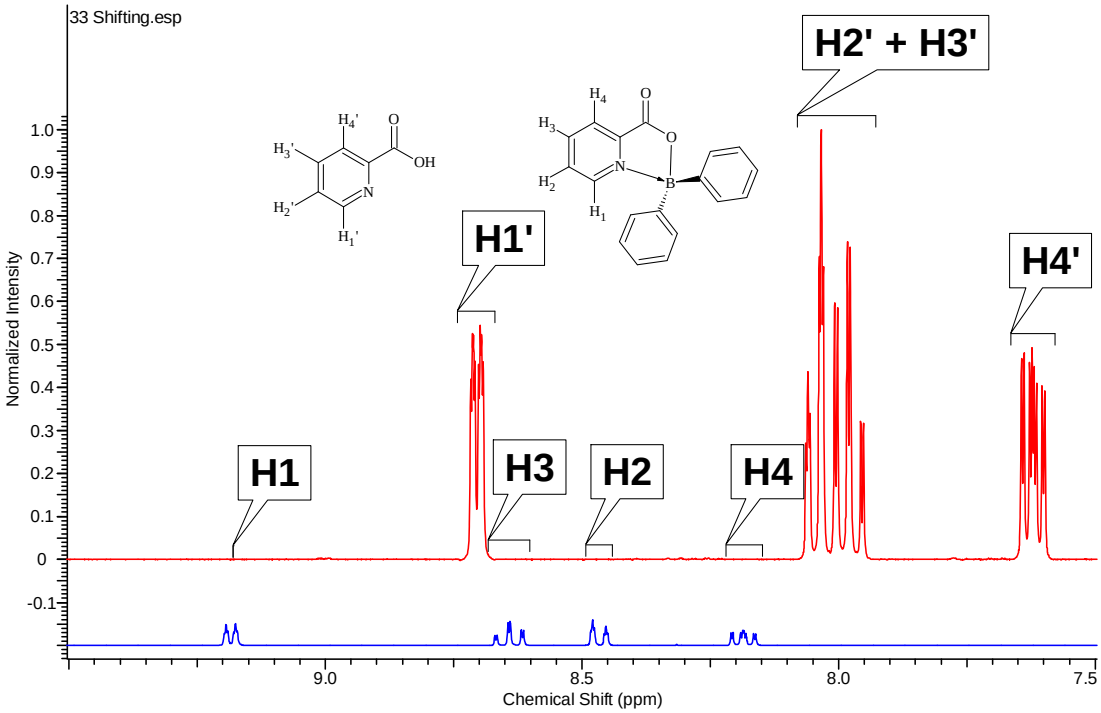

Figure 20. ^{1}H NMR spectra of picolinic acid **17** (red) and its complex with diphenyl borinic acid **18** (blue)

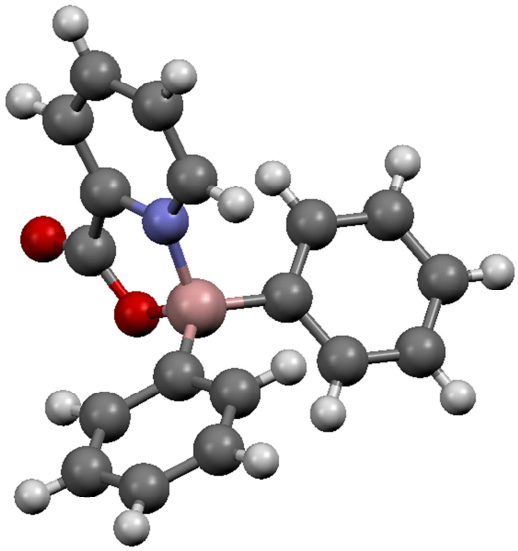

18

Figure 21. Crystal structure of the complex formed between picolinic acid and diphenyl borinic acid **18** as determined by x-ray crystal diffraction

These crystals were dissolved in methanol for an LC/MS analysis and revealed some interesting properties. The monomer was indeed the base peak at 310.09 $^{m}/_{z}$ for

[M]+Na and 288.09 $^{m}/_{z}$ for [M]+1 about half the intensity. Molecular fragments such as picolinic acid+1 at 123.91 $^{m}/_{z}$ and the monomer minus pyridine+1 at 210.00 $^{m}/_{z}$ were also detected (figure 22). The intriguing result is that the second largest peak, at 597.00 $^{m}/_{z}$, indicated the dimer plus sodium as 2[M]+Na demonstrating that while in its crystal structure it is indeed a monomer; it can become a dimer in solution at very dilute concentrations. Additionally, all of the peaks that represent a compound that contains boron have a peak one $^{m}/_{z}$ unit lower at approximately 20% of the relative abundance of its parent peak, indicative of the B^{10} isotope.

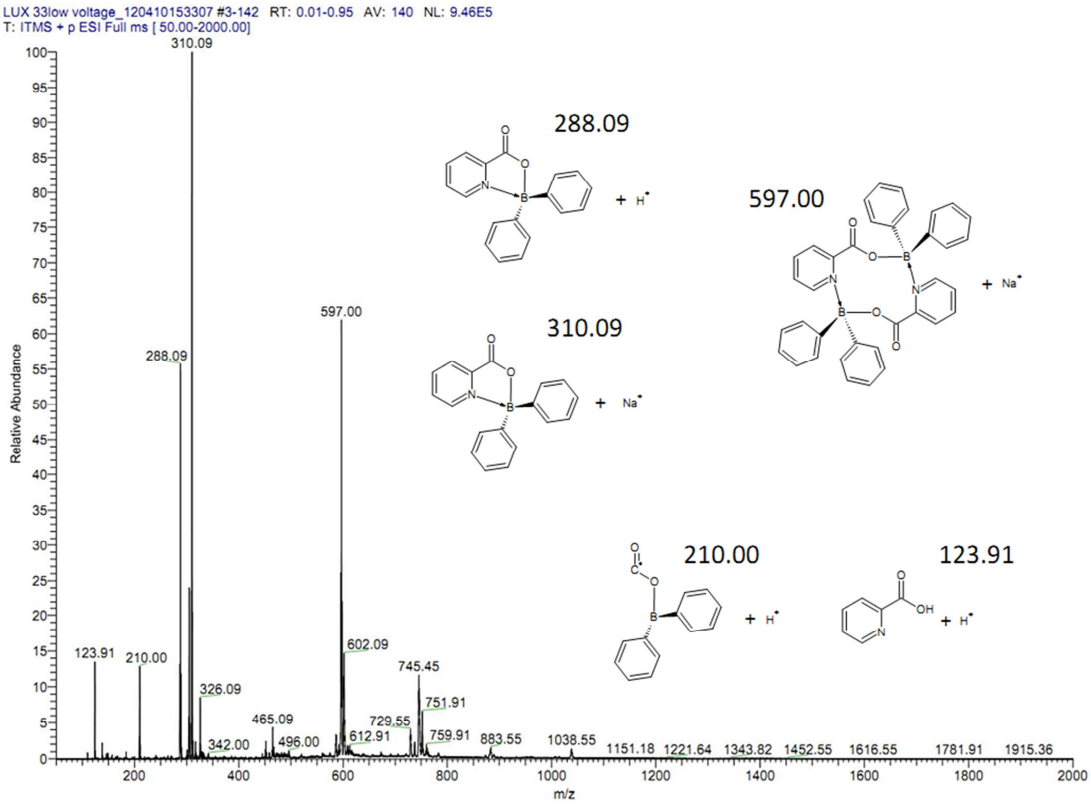

Figure 22. Mass spectrum of the complex formed between picolinic acid and diphenyl borinic acid **18** dissolved in methanol

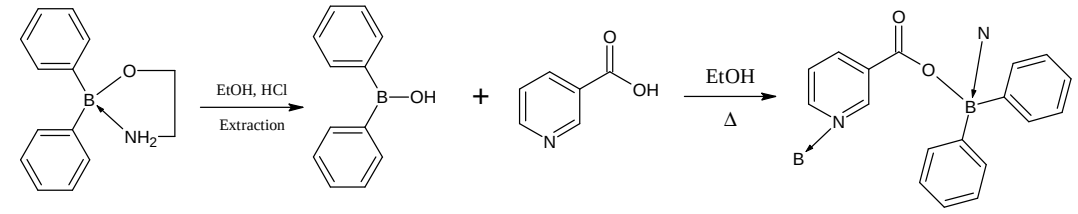

15 **16** **19** **20**

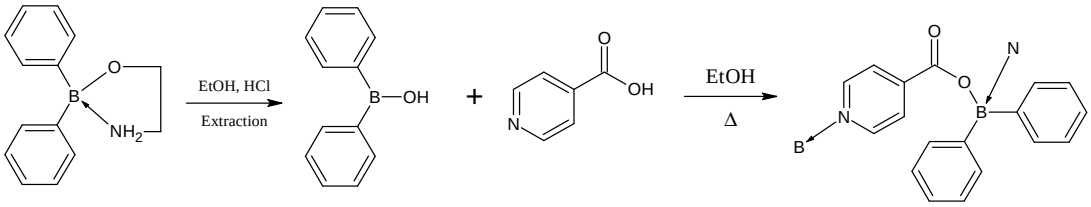

15 **16** **21** **22**

Following the success of the picolinic acid reaction, the next two isomers of it were nicotinic acid **19** and isonicotinic acid **21**, with the nitrogen *meta* and *para* to the carboxylic acid. Unfortunately, these isomers did not have the same quality results that the previous reaction had and the instability of the diphenyl borinic acid **16** became apparent. The reaction conditions for these isomers were the same; the color descriptions and spectral analyses were also similar. The protecting group was removed and the solution of diphenyl borinic acid **15** in ethanol **6** was then mixed with the corresponding nicotinic acid **19** or isonicotinic acid **21**. The reaction mixture then refluxed and approximately 75% of the ethanol was removed by distillation.

Up to this point the reaction appeared much like the previous successful reaction but differed after distillation. The distilled product formed a white precipitate and colorless liquid which turned to an orange precipitate and orange liquid the next day. Within a few days, the product became a brown precipitate and brown liquid. The reaction was attempted several times and each time the results were the same. ^{1}H NMR was taken of both the filtrate and filtered solid of these attempts and the filtered solid appears to be the carboxylic acid starting material with no evidence of the borinic acid

(figure 23). The filtrate, however, appears to be a collection of products including the decayed borinic acid (figure 24).

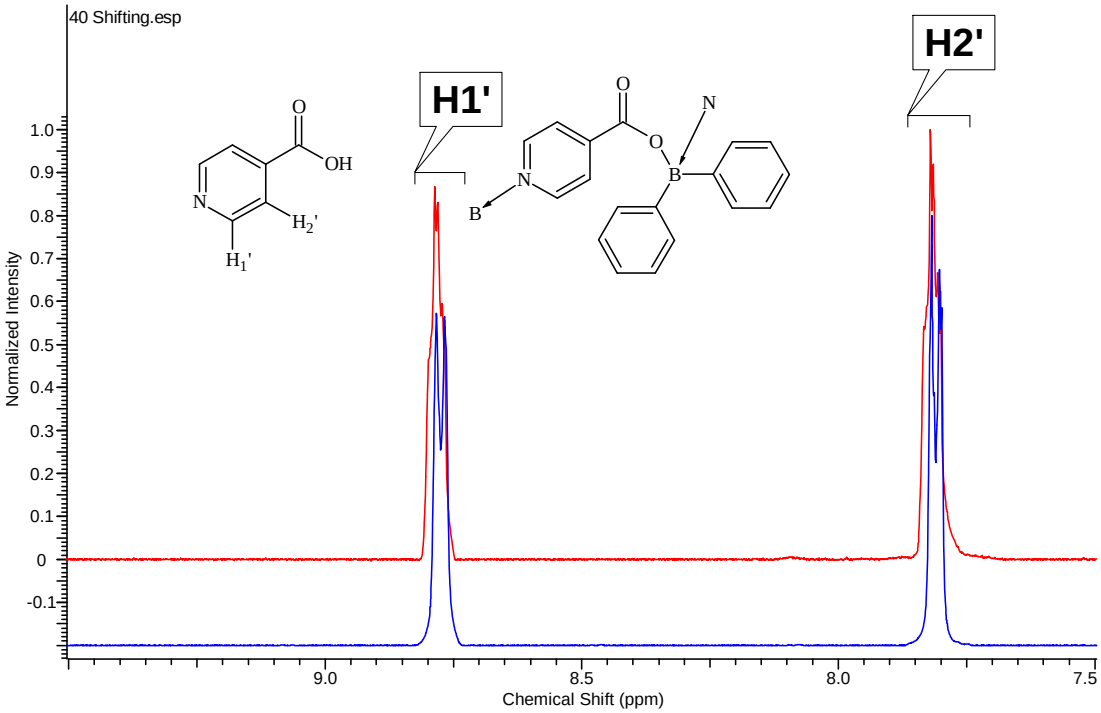

Figure 23. ^{1}H NMR spectra of isonicotinic acid **21** (red) and the filtered solid product of its reaction with diphenyl borinic acid (blue)

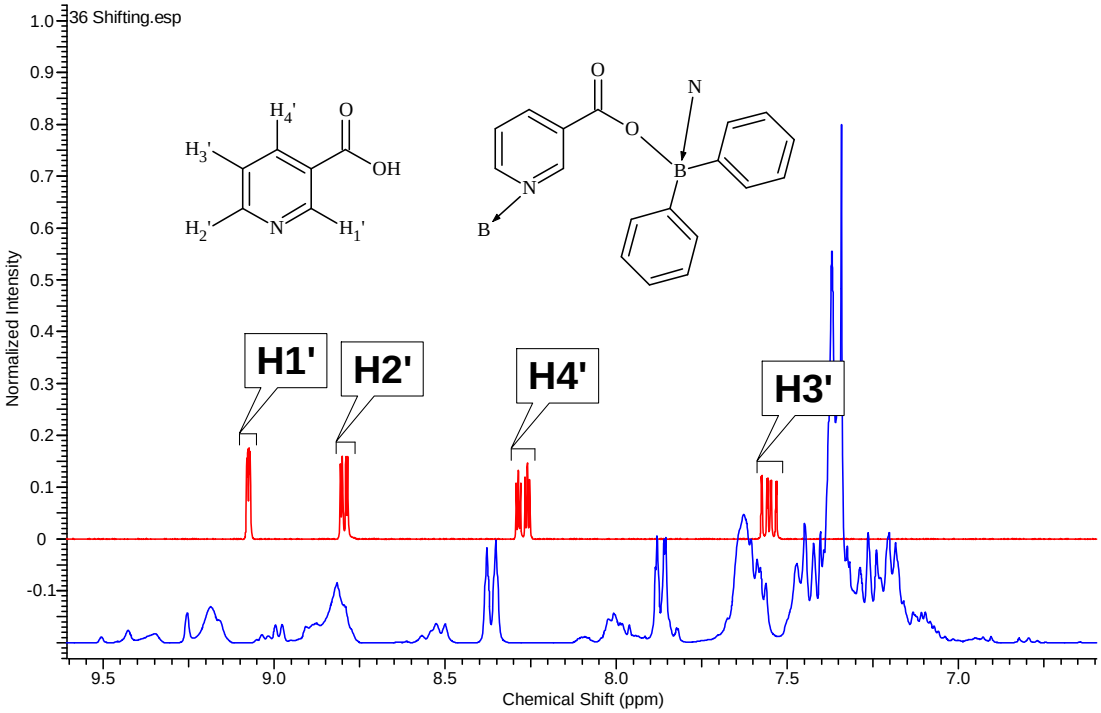

Figure 24. ^{1}H NMR spectra of nicotinic acid **19** (red) and the filtrate product of its reaction with diphenyl borinic acid (blue)

As stated previously, the diphenyl borinic acid **16** is unstable and will decay without its protecting group. The complexes formed in the first reaction, have an ester linkage and a dative bond to the boron that gives it the stability to sit on a shelf without decomposing. Since the products from the reaction mixtures of the *meta* and *para* isomers is clearly decomposing, it must not be able to form either the ester linkage or the dative bond. After several attempts at this reaction and all indicators, visible and spectral, suggesting that the product was decaying or was never properly formed, it was decided to move on to the N-oxide versions of the picolinic, nicotinic, and isonicotinic acid isomers. If the reaction proceeded via an intramolecular pathway, the picolinic n-oxide would form a six-membered ring instead of a five-membered ring. If the reaction proceeded via an intermolecular route, these n-oxide isomers could potentially form macrocyclic system due to less steric hindrance around the reaction centers.

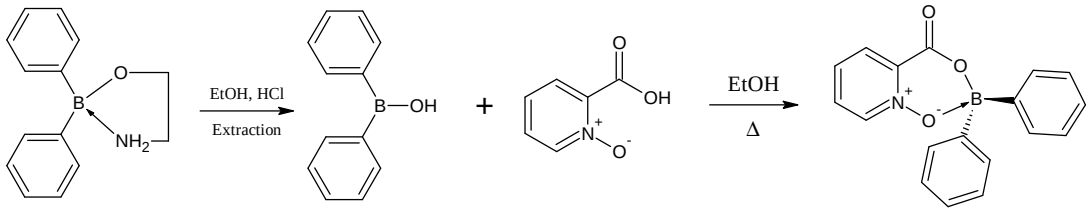

15 **16** **23** **24**

Since picolinic acid **17** worked previously it was chosen to go first in the N-oxide versions. The N-oxide reactions behave just like the previous non-oxide versions. The deprotecting procedure is the same as is the reaction procedure. The visual indicators for the picolinic acid N-oxide complex **24** all appeared the same as with the picolinic acid complex **18** with no color change after distillation which indicated a successful reaction. The product **24** was a white solid and the ^{1}H NMR showed separation of peaks as well as shifting of peaks (figure 25). The peak associated with the proton *ortho* to the nitrogen atom, H_1, shifts from 8.75ppm to 8.52ppm, H_2, *meta*, and H_3, *para*, separate and shift from ~7.9ppm to 7.75ppm and 7.99ppm respectively, and H_4, *ortho* to the carboxylic acid, shifts from 8.32ppm to 8.44ppm.

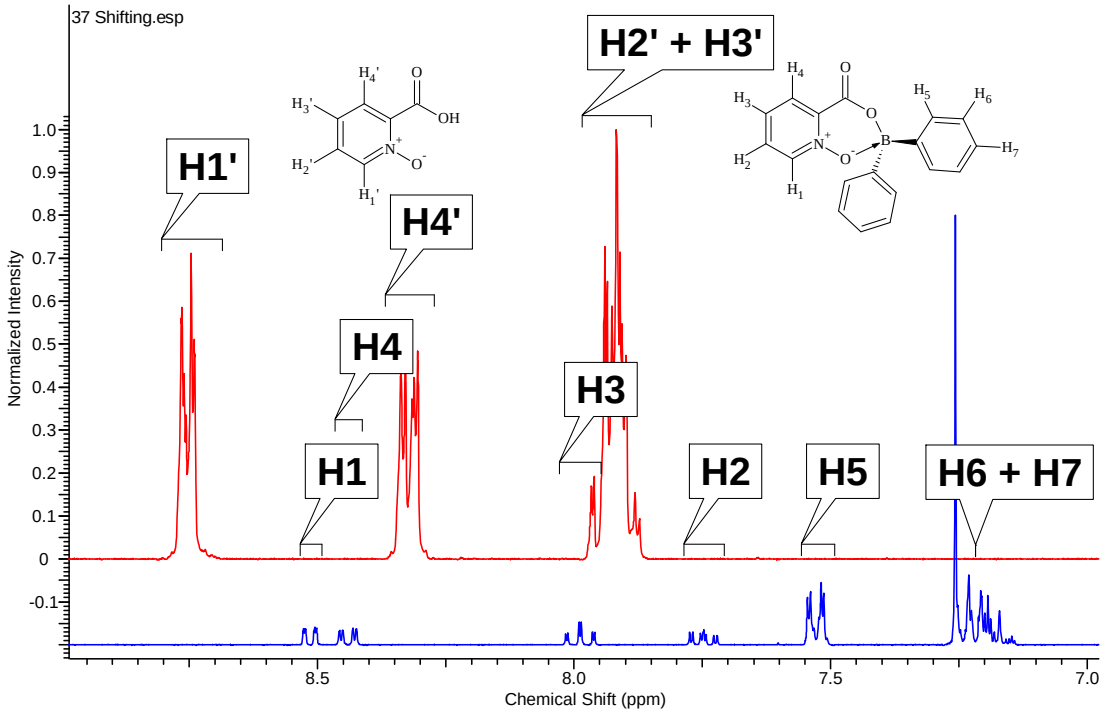

Figure 25. ^{1}H NMR spectra of picolinic acid N-Oxide **23** (red) and its complex with diphenyl borinic acid **24** (blue)

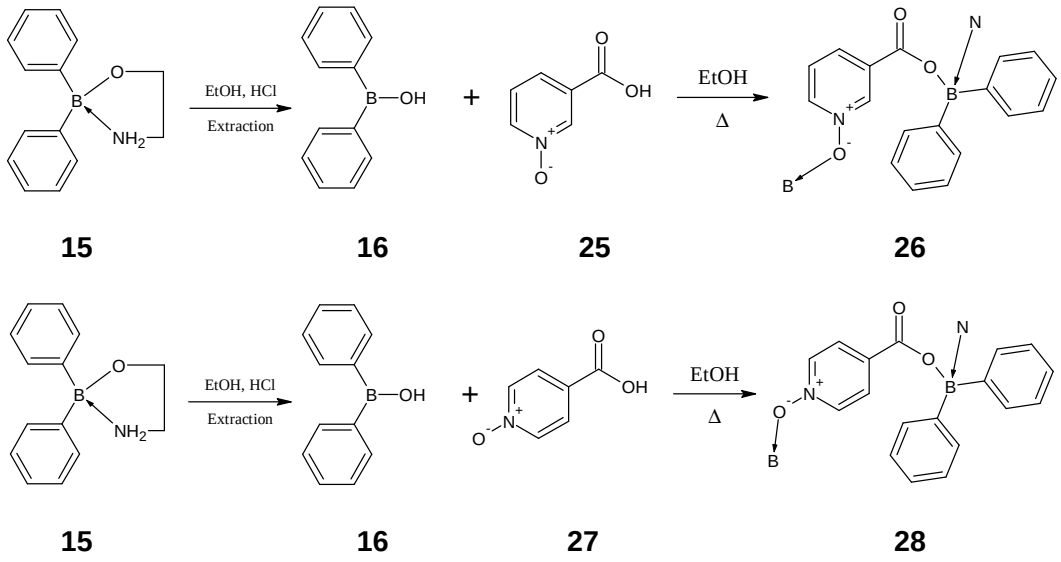

With the success of the picolinic acid N-oxide complex **24**, work moved onto the nicotinic and isonicotinic acid N-oxides **25** and **27**. The test here was to see if the oxygen atom of the n-oxide would form the dative bond to the boron and permit the formation of the ester linkage between the carboxylic acid and the borinic acid. Unfortunately, as time would tell, these reactions had the same fate as their non-oxide

forms. The reactions proceeded as those before with the deprotection, extraction, drying, and reaction. As before, everything appeared normal until the distillation, the same white to orange to brown color changes occurred as with the nicotinic **19** and isonicotinic acids **21**. The ^{1}H NMR spectra also showed the same problems with the filtered solid containing only the carboxylic acid starting material and the filtrate being a undecipherable collection of peaks.

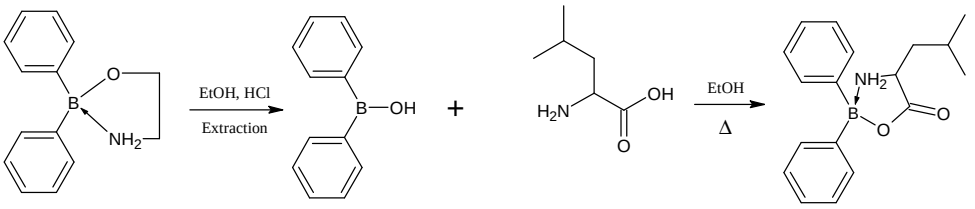

15 **16** **29** **30**

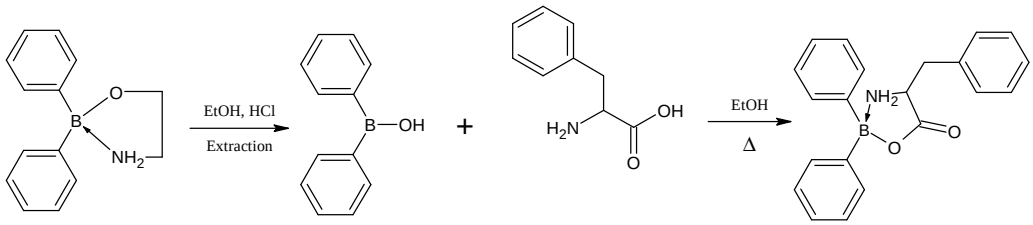

15 **16** **31** **32**

The next area explored with the diphenyl borinic acid **16** was combining it with amino acids as they are similar to the previously successful reactions **18** and **24**. Leucine **29** and phenylalanine **31** were selected for this experimentation. The preparation of the borinic acid worked the same as in previous syntheses. Subsequent reaction of borinic acid **16** with leucine **29** seemed to proceed smoothly. However, not all of the leucine dissolved in the ethanol solvent; the product precipitated as a white amorphous solid. In the reaction involving borinic acid 16 and phenylalanine **31**, the amino acid dissolved completely in the ethanol and the product **32** became a more crystalline white solid. In neither case did the color of the products change to orange or brown, indicating potentially successful reactions.

The ^{1}H spectrum for the leucine compound **30** was taken and seemed to confirm that the desired product was formed (figure 26) but the original amino acid **29** and the product were not soluble in the same two deuterated NMR solvents so shifting could not be demonstrated. The phenylalanine compound **32** was soluble in the same solvent as its starting material **31**; the NMR seemed to confirm it (figure 27) and although shifting was present, it was not as strong as in previous experiments. The peak associated with the proton sharing the carbon bonded to the nitrogen atom, H_1, shifted from 3.36ppm to 3.70ppm and the chiral H_2 and H_3 shifted from 3.17ppm to 3.19ppm and 2.83ppm to 2.94ppm respectively.

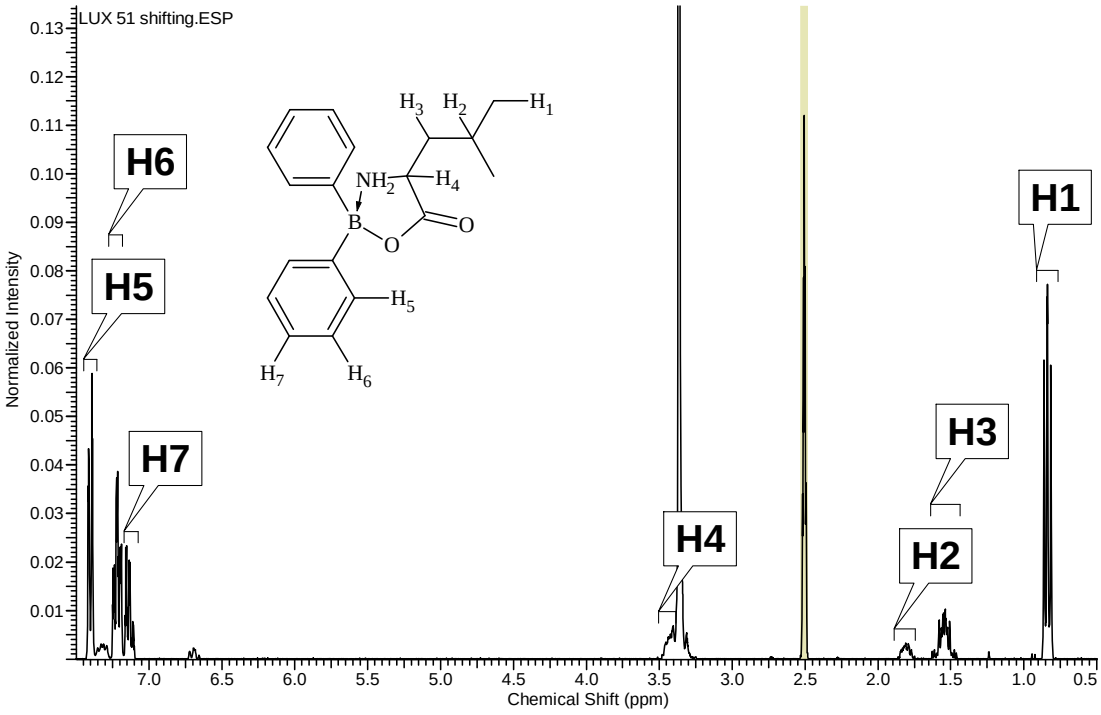

Figure 26. ^{1}H NMR spectrum of the product of leucine and diphenyl borinic acid **30**.

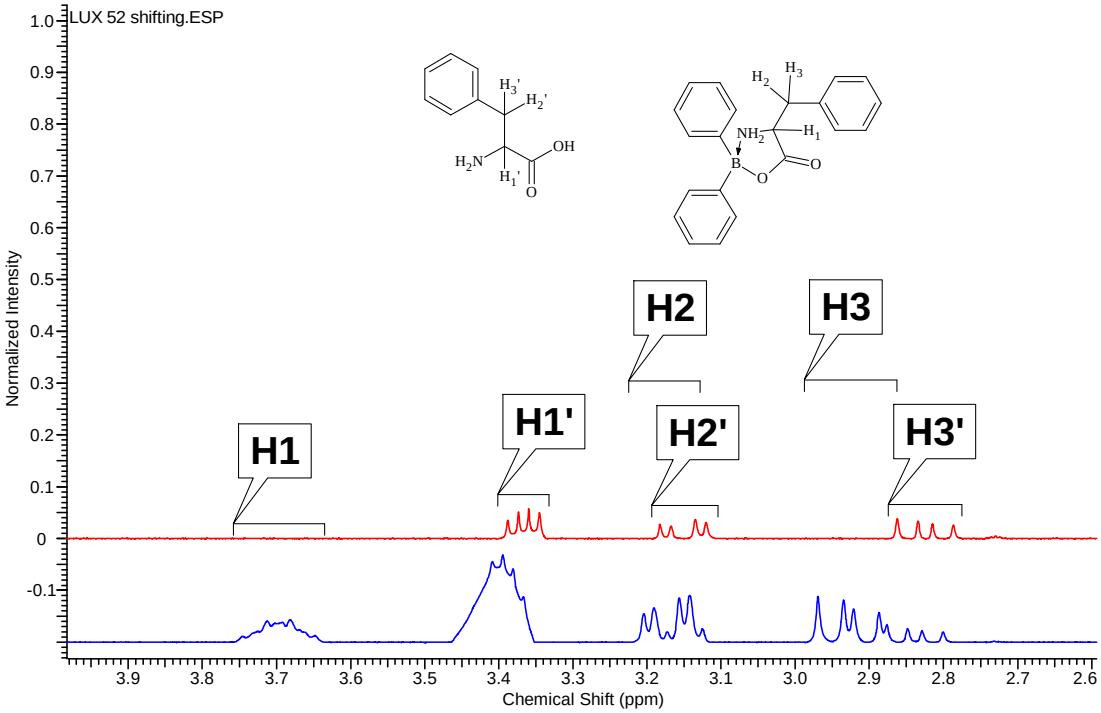

Figure 27. ^{1}H NMR spectra of phenylalanine **31** (red) and its complex with diphenyl borinic acid **32** (blue)

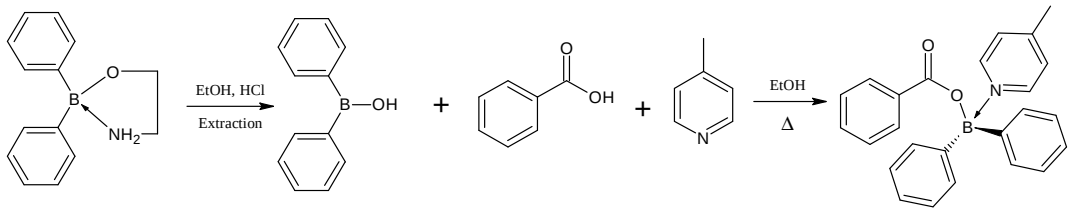

15 **16** **33** **5** **34**

In order to further explore the scope of these borinic acid complexations, several other carboxylic acids and amine components were selected to explore different possibilities. The first of these was to use benzoic acid **33** as it is similar to the original carboxylic acids in this series but without the nitrogen and thus cannot form an intramolecular bond. Picoline **5** was chosen as the Lewis base component since the methyl group would be an obvious indicator for ^{1}H NMR. The reaction followed the same procedure as the others in this series except that both benzoic acid **33** and picoline **5** were added in the step where normally only a carboxylic acid is added.

The product **34** was a white solid and did not decay to orange or brown, the first indicator of a successful reaction. When the product was characterized by ^{1}H NMR there were some difficulties. Many of the peaks were overlapped and could not be separated out and there was a substantial amount of benzoic acid **33** which made integration for many of the peaks in the aromatic region difficult (figure 28). There were three peaks that were able to be separated out and integrated properly that corresponded to the methyl peak on picoline, H_6, shifted from 2.35ppm to 2.51ppm, the protons *ortho* to the nitrogen atom, H_4, shifted from 8.46ppm to 8.64ppm, and the protons *ortho* to the carboxylic acid on the benzoic acid, H_3, shifted from 8.16ppm to 8.23ppm. Due to no evidence of decay and the evidence collected from ^{1}H NMR it appears that this reaction was successful.

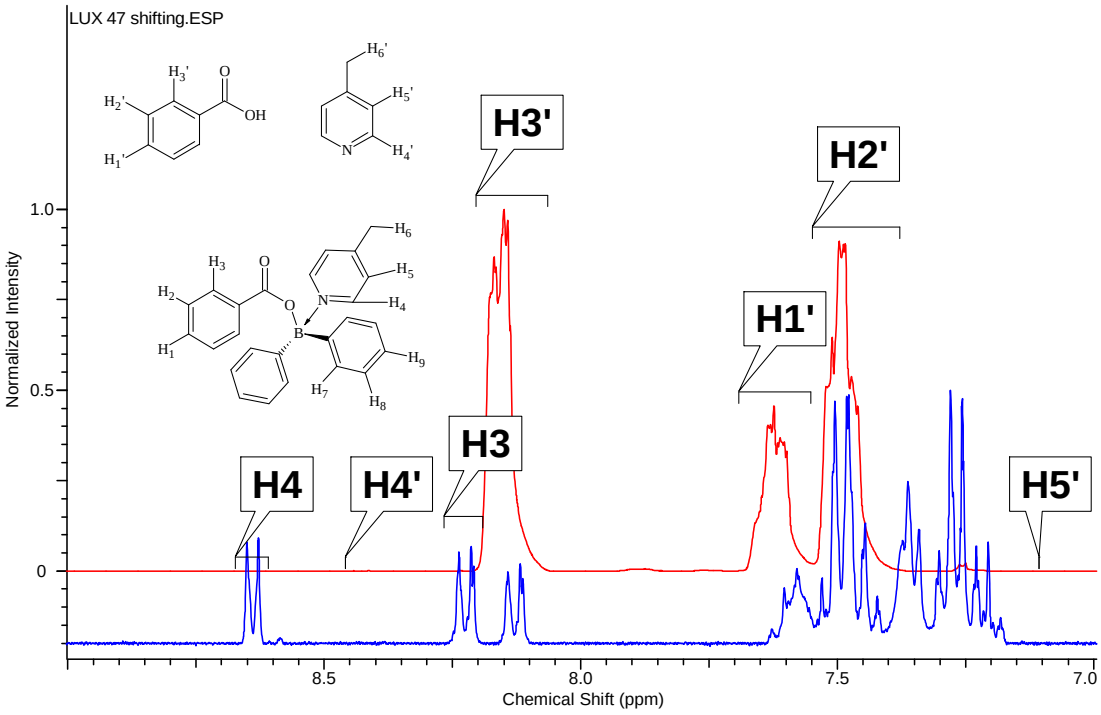

Figure 28. ^{1}H NMR spectra of benzoic acid **35** (red), picoline **5**, and its complex with diphenyl borinic acid **34** (blue)

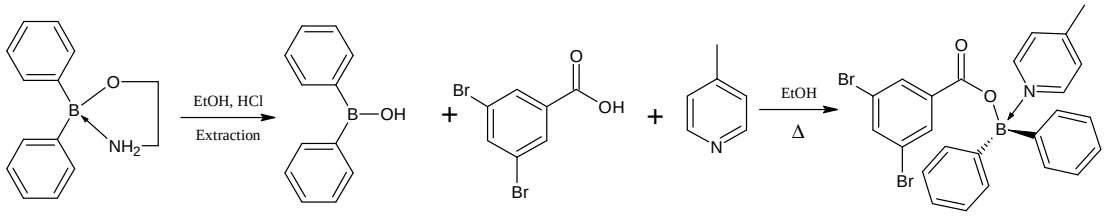

15 **16** **35** **5** **36**

The next reaction chosen was similar to the previous one except that it contained two bulky bromine atoms *meta* to the carboxylic acid. Again the starting material **35** contains no nitrogen and thus picoline **5** was added. The reaction proceeded as previously with the addition of the 3,5-dibromobenzoic acid **35** and picoline **5** at the same time after isolation of the diphenyl borinic acid **16**. The final product **36** was brown instead of white but this was acceptable as the 3,5-dibromobenzoic acid **35** was brown due to the bromine atoms. The ^{1}H NMR worked better than the previous as most peaks were non-overlapping, integrated properly and showed clear shifting of the peaks from the starting material (figure 29). The peak associated with the proton between the two bromine atoms, H_1 shifts from 8.17ppm to 8.14ppm and the proton between the carboxylic acid and a bromine, H_2, shifts from 7.91ppm to 8.03ppm. The peak associated with the proton *ortho* to the nitrogen atom, H_3, shifts from 8.56ppm to 8.44ppm, and H_4, *meta*, shifts from 7.21ppm to 7.29ppm.

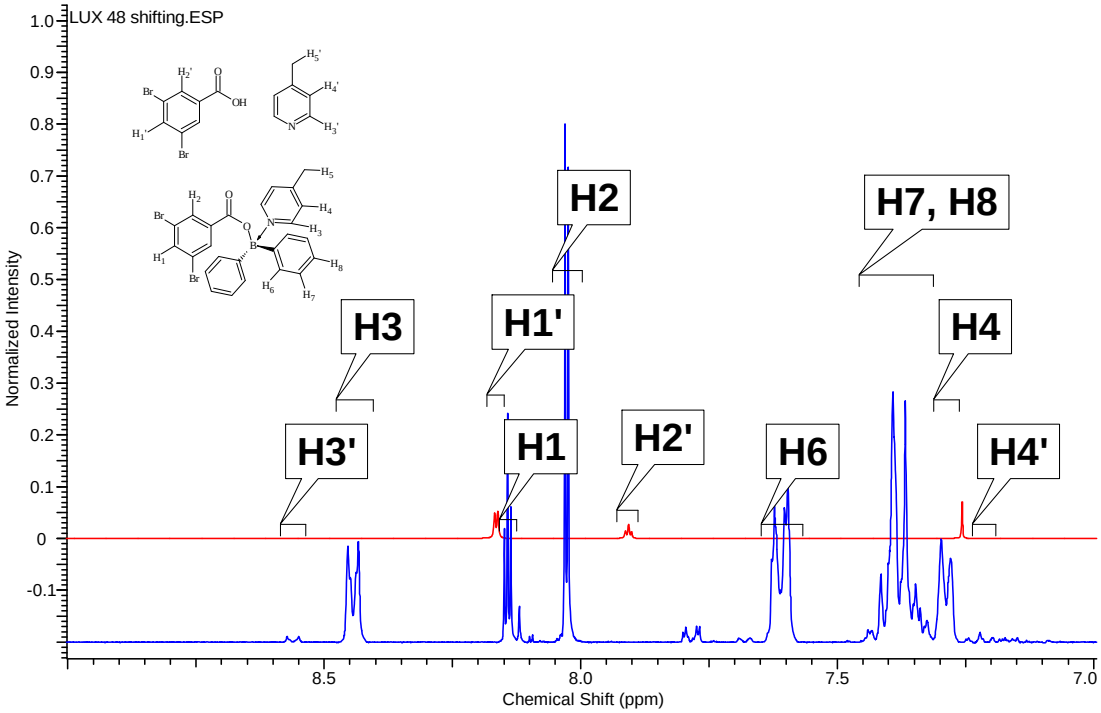

Figure 29. ^{1}H NMR spectra of 3,5-dibromobenzoic acid **35** (red), picoline **5**, and its complex with diphenyl borinic acid **36** (blue)

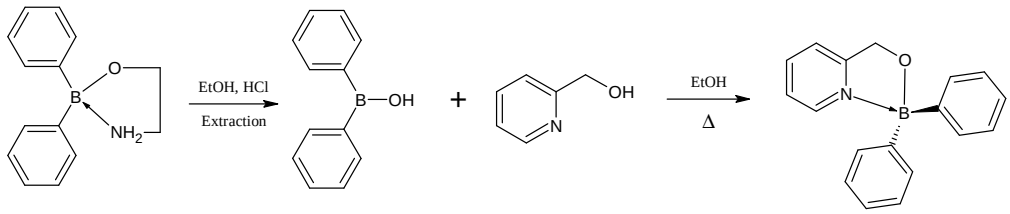

15 **16** **37** **38**

The last reaction with borinic acid **16** to be done was with 2-pyridinemethanol **37** as it is similar to the original borinic acid reaction with picolinic acid **17** that worked so well; the difference being that it contains a methanol functional group in place of the carboxylic acid. This reaction does not need the additional picoline **5** as the previous two did as it already contains a nitrogen atom so the reaction followed the same procedure as the originals.

The starting 2-pyridinemethanol was a brown liquid and the product, before slow evaporation, was a lighter brown liquid. After the solvent had evaporated there were

clear, colorless crystals in the flask surrounded by a brown liquid, this brown liquid was later determined to be starting material **37**. The crystals could not be completely separated from the liquid without destroying them but a sample was able to be isolated enough for a clear ^{1}H NMR. The analysis of this sample showed remaining starting material but also proper integration and shifting of all peaks for the desired product **38** (figure 30). The peak associated with the proton *ortho* to a nitrogen atom, H_1, shifts from 8.47ppm to 8.62ppm, the *meta* H_2 shifts from 7.24ppm to 7.70ppm, the *para* H_3 shifts from 7.78ppm to 8.24ppm, and H_4, *ortho* to the methanol group, shifts from 7.46ppm to 7.85ppm.

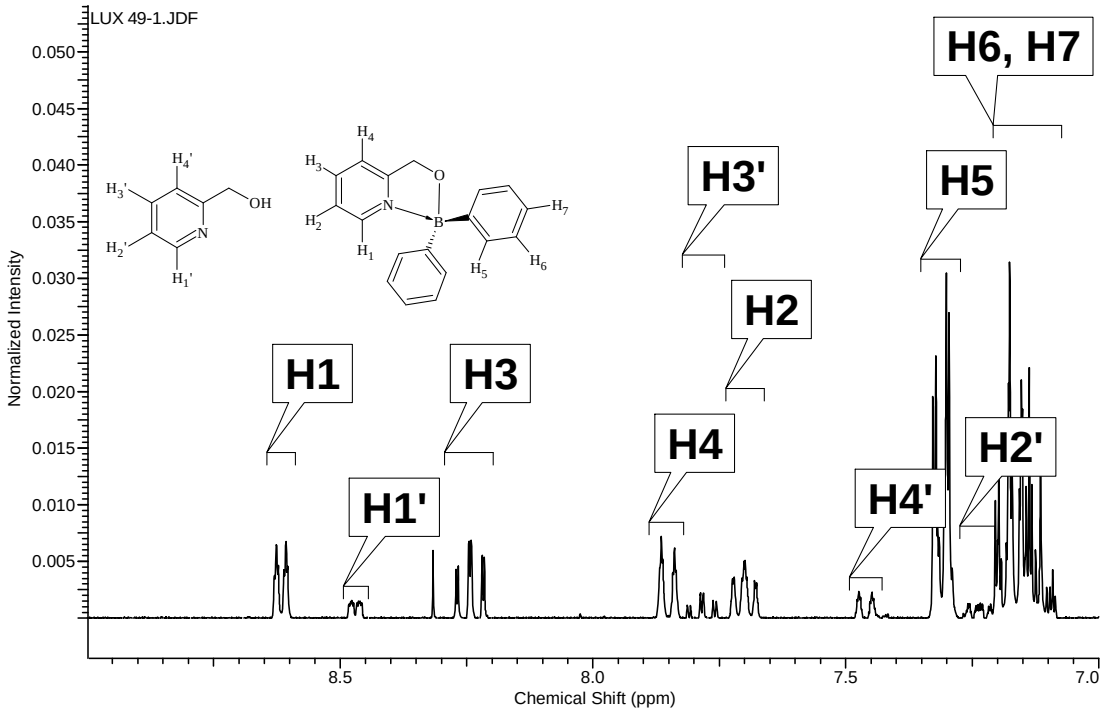

Figure 30. ^{1}H NMR spectrum of 2-pyridinmethanol **37** and its complex with diphenyl borinic acid **38**

2.3 Macrocycles Via Self-Assembly of 9-BBN Derivatives

Due to the difficulties with the diphenyl borinic acids decomposing in the cases of the nicotinic and isonicotinic acids, another boron-based compound was selected in

hopes that it would have the desired results. The compound selected is called 9-borabicyclononane (9-BBN) **39**. 9-BBN has several advantages over borinic acid in that it has no protecting group that needs to be removed, thus removing the time restraint on the reaction once the group is removed. Additionally, the reaction gives off hydrogen gas as a byproduct instead of water giving a clear visual indicator that the reaction is taking place. There are, however, two drawbacks with the 9-BBN. Due to the large aliphatic group, the product is less likely to form crystals for x-ray crystallography and the 9-BBN itself is water sensitive and must be kept in a dry solvent under an inert argon atmosphere.

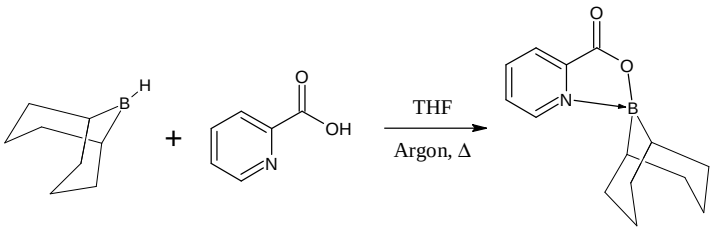

39 **17** **40**

The reaction began by placing the picolinic acid **17** in an RBF with a condenser on top then purging the system with argon gas. Dry tetrahydrofuran (THF) was injected into the system and formed a cloudy white mixture with the carboxylic acid as it did not fully dissolve. To this reaction mixture, 9-BBN (in dry THF) was injected and within a few seconds the solution turned clear. Heat was added to bring the reaction to reflux; before the THF reached boiling, bubbles started to form indicating that hydrogen gas was being given off and the reaction taking place. The reaction solution was refluxed for three hours and turned yellow, but the bubbling of the hydrogen gas stopped before the three hours were complete, indicating that the reactive 9-BBN had been consumed. The solvent of the clear, yellow solution was removed *in vacuo*, yielding a yellow powder with a 99% yield. The change from two white crystalline solid starting materials to a yellow powder was another visual indicator that the reaction worked as hoped.

The product **40** dissolved easily in DMSO-d_6 and the ^{1}H NMR shows a clear shifting of the peaks representing the protons on the picolinic acid (figure 31). The peak associated with the proton *ortho* to a nitrogen atom, H_1, shifts from 8.71ppm to 9.20ppm, the *meta* H_2 and *para* H_3 separate and shift from ~8ppm to 8.35ppm and 8.55ppm respectively, and H_4, *ortho* to the carboxylic acid, shifts from 7.62ppm to 8.09ppm. The separation and shifting of these peaks, as well as the continued presence of the 9-BBN proton peaks, is a clear indicator that the reaction worked as intended.

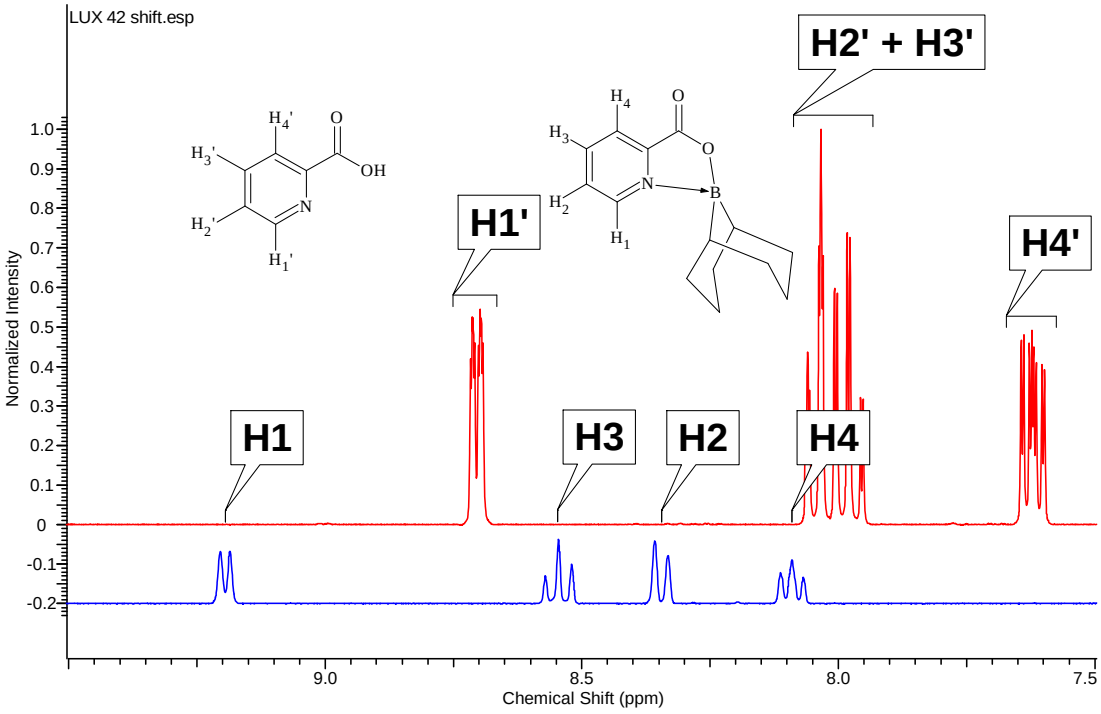

Figure 31. ^{1}H NMR spectra of picolinic acid **17** (red) and its complex with 9-BBN **40** (blue)

Later a sample of the product **40** was dissolved in methanol and injected into a LCMS. The results showed significant presence of both the monomer as [M]+1 at 244.09 $^m/_z$ and [M]+Na at 266.09 $^m/_z$ as well as the dimer, 2[M]+Na, at 509.09 $^m/_z$ with small amounts of picolinic acid+1 at 123.91 $^m/_z$ (figure 32). All of the peaks that represent a compound containing boron also have a peak one $^m/_z$ unit lower at approximately 20% of the relative abundance of its parent peak, indicative of the B^{10} isotope. This is similar to the borinic acid and picolinic acid complex **18**.

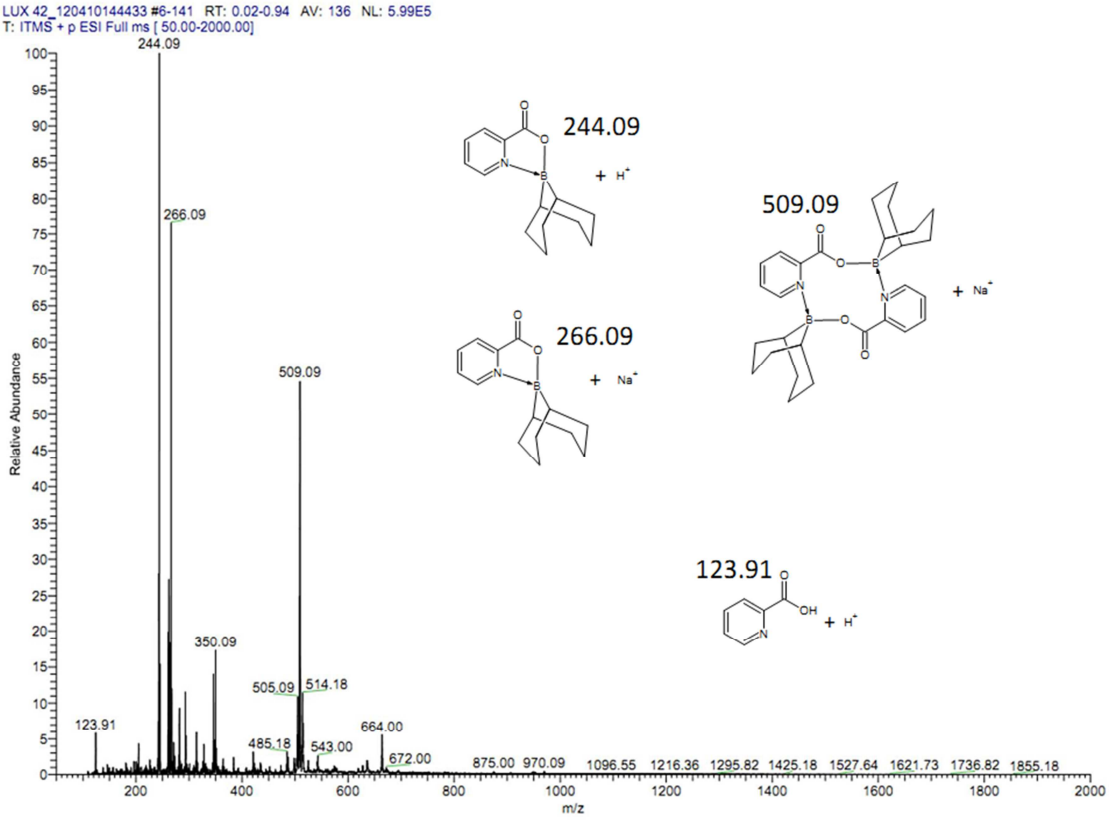

Figure 32. Mass spectrum of the complex formed between picolinic acid and 9-BBN **40** dissolved in methanol

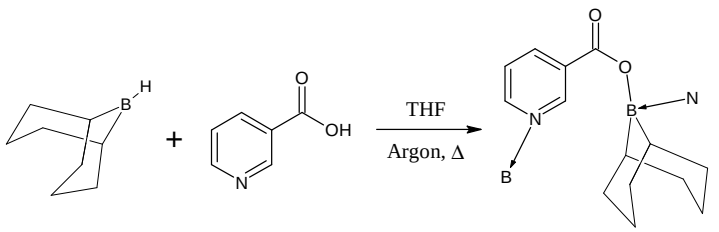

39 **19** **41**

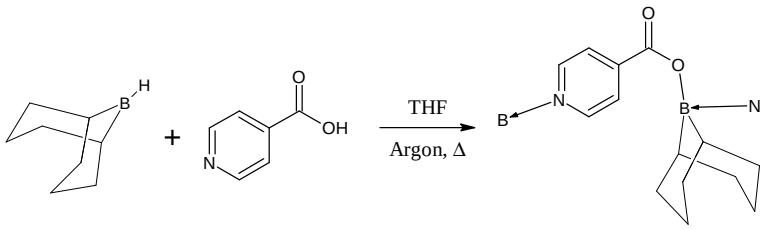

39 **21** **42**

The reaction between 9-BBN **39** and the nicotinic and isonicotinic acids **19** and **21** were a curious case. The initial reactions appeared similar to the previous one with picolinic acid **40**. When the 9-BBN **39** was added to the carboxylic acid and THF

solution it changed from a cloudy solution to clear in a few seconds. During reflux, there was gas being given off; presumably this was the hydrogen gas byproduct, indicating that the reaction was working successfully. However, after the reflux was finished, instead of a clear yellow solution there was a cloudy white solution for the nicotinic acid and cloudy yellow for the isonicotinic acid that precipitated out of solution after allowed to sit for a while. After drying, the product was a waxy yellow solid made from two white crystalline solids, indicating that some reaction had taken place. Both reactions yielded slightly over a 100% yield, indicating that there was solvent remaining in the product.

Trying to characterize these compounds is when the problems began. The nicotinic acid complex **41** would barely dissolve in DMSO-d_6 and the isonicotinic complex **42** seemed not to dissolve at all, even with heat and sonication. Analysis of the NMR spectra confirmed that nothing dissolved in the isonicotinic complex solution and that the only thing dissolved in the DMSO-d_6 for the nicotinic complex was a small amount of starting material, nicotinic acid **19**.

Since hydrogen gas was given off during the reaction yet the majority of the product was insoluble in all of the deuterated solvents available, we suggest that the products were some sort of polymer that was too large to be soluble with both its large aliphatic and polar sections. To confirm this theory, LCMS was attempted. Small amounts of the product were found to be soluble in large quantities of methanol and these solutions were run through the LCMS. There were very small traces of the monomer subunit as [M]-1 at 241.82 $^{m}/_{z}$ present for both but were vastly overwhelmed by the signal for the starting carboxylic acid material+1 at 123.91 $^{m}/_{z}$ (figure 33). Additionally the [M]-1 was not one that could be readily explained, especially since there was no evidence of exact mass or mass plus one, but the [M]-1 peak did have the characteristic -1 peak at ~20% intensity, indicating the presence of boron. Finally, there

was no evidence at all of any larger chains of the polymer even when the voltage was decreased to reduce fracturing.

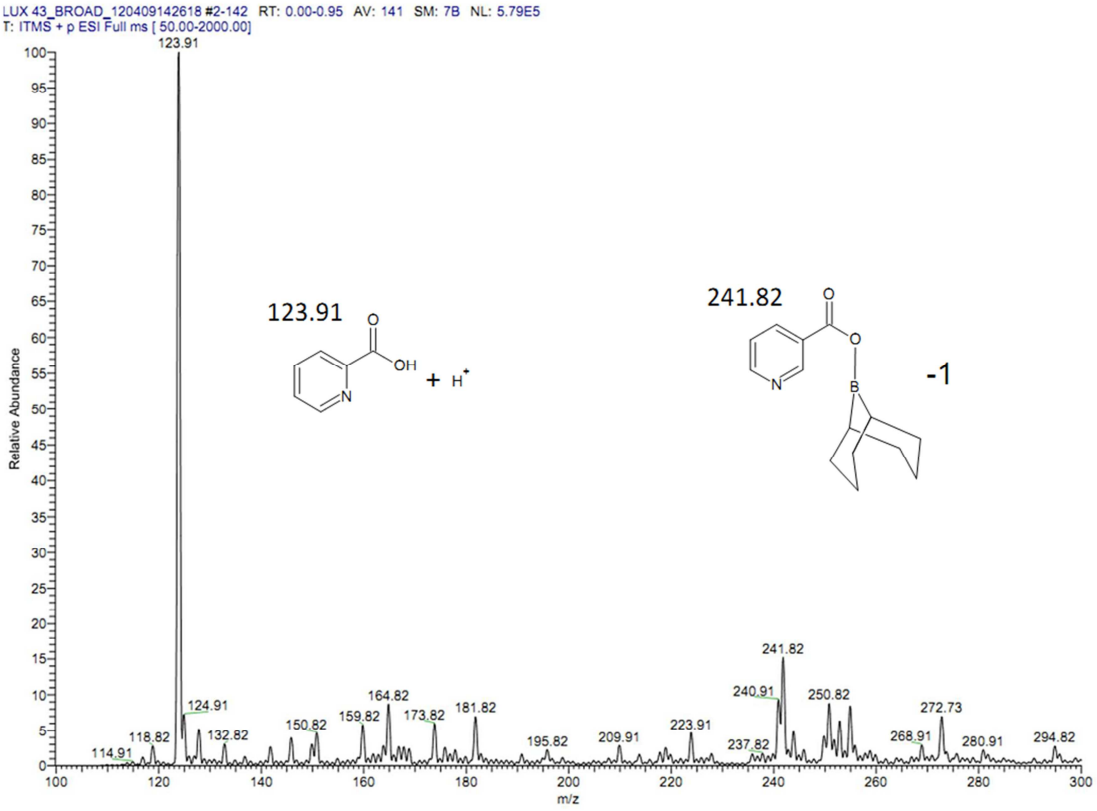

Figure 33. Mass spectrum of the complex formed between nicotinic acid and 9-BBN **41** dissolved in methanol

Based on the visual indicators of color change and gas being given off, it would seem that some sort of reaction took place. Unfortunately, no spectroscopic technique has been able to confirm this and no crystal has been able to be grown. Thus these reactions must be classified as inconclusive.

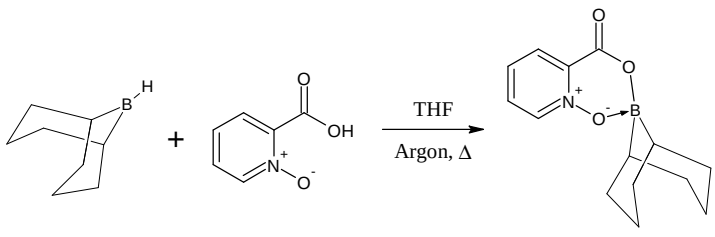

39 **23** **43**

Due to the obvious success of 9-BBN **39** combined with picolinic acid **17**, the uncertain results when combined with nicotinic acid **19** and isonicotinic acid **21**, and the similarities between that and the diphenyl borinic acid **16** series, it was decided that an attempt would be made with 9-BBN and picolinic acid N-Oxide **23**. This reaction was set up the same as the other reactions using 9-BBN **39**. Again the solution of THF and the carboxylic acid turned from cloudy to clear upon addition of the 9-BBN solution. Also the bubbles produced prior to reflux indicated that hydrogen gas was given off. The final solution was yellow-clear and became a yellow waxy substance upon removal of solvents. All of the visual indicators that the reaction had proceeded as predicted.

Additionally, the product **43** readily dissolved in DMSO-d_6 for ^{1}H NMR testing. The results of which showed clear shifting of the peaks associated with the protons on the carboxylic acid (figure 34) and a continued presence of the peaks associated with the aliphatic protons. The peak associated with the proton *ortho* to a nitrogen atom, H_1, shifts from 8.75ppm to 9.14ppm, the *meta* H_2 and *para* H_3 separate and shift from ~7.9ppm to 8.14ppm and 8.35ppm respectively, and H_4, *ortho* to the carboxylic acid, shifts from 8.32ppm to 8.45ppm.

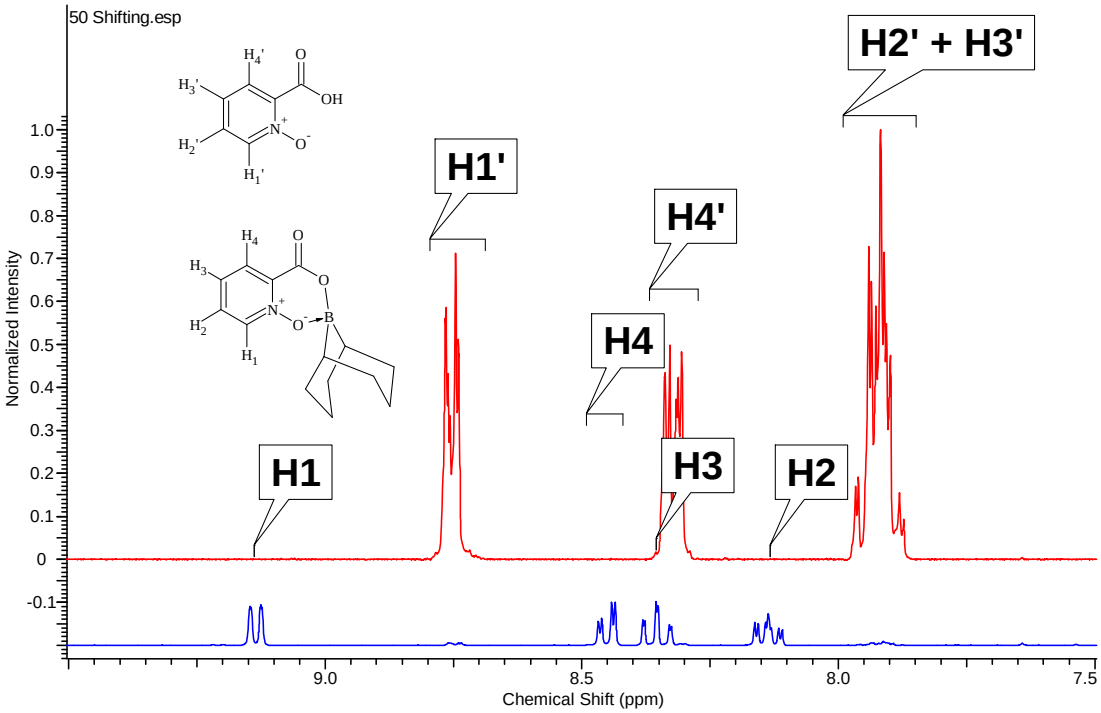

Figure 34. ^{1}H NMR spectra of picolinic acid N-Oxide **23** (red) and its complex with 9-BBN **43** (blue)

CHAPTER THREE: CONCLUSIONS

In our work with ferrocene boroxine systems, we have demonstrated that a variety of Lewis bases, mostly pyridine derivatives, can be successfully complexed with the boroxine ring (table 1). ^{1}H NMR spectroscopy of these complexes showed a high degree of symmetry in the hydrogen signals of the ferrocene ring, indicating a dynamic dative bond. Each reaction was done in a 1:1 ratio, the diamines were also done in 2:1 ratios. Some spectra indicated multiple boroxines for each amine while others suggested the possibility of multiple amines for each boroxine, but these results are not definitive due to contamination of molecular ferrocene. High quality crystals of ferrocene boroxine - 4-aminomethylpyridine complex **4** were prepared and single crystal x-ray diffraction indicated that all three ferrocene groups are below the plane of the boroxine while the amine is above the plane. It is quite possible that a single crystal of a 2:1 ferrocene boroxine : diamine complex could be formed under the right conditions. Judicious choice of diamine structure, as well as careful selection of the solvent system, equivalence, and recrystallization method may have a dramatic impact on the recrystallization results. Though we were unable to create a definitive solid state molecular rotor with ferrocene boroxine, it may still be possible.

The borinic acid system provided an opportunity to use the coordinating ability of the boron atom to form small ring systems. We were able to prepare a total of seven cyclic systems that were verified by ^{1}H NMR (tables 2 and 3). With these ring systems it is evident, through a novel crystal structure and mass spectrum of picolinic diphenylborinate ester **18**, that the same system can exist as an intramolecular monomer ring and a molecule composed of several of these monomer units combined in an intermolecular ring. Additionally, the picolinic 9-BBN ester **40** appears able to exist in both the monomer and dimer configurations according to LCMS. Whether the remaining

systems of picolinic N-Oxide diphenylborinate ester **24**, leucine diphenylborinate ester **30**, phenylalanine diphenylborinate ester **32**, 2-methylpyridine diphenylborinate ester **38**, and picolinic N-Oxide 9-BBN ester **43** were able to exist in both monomer and dimer states is, at this point, unknown. Two additional compounds were synthesized from 9-BBN that could potentially be long chain polymers or macrocycles, but their exact identity could not be ascertained. Their structure could potentially be proven if a proper NMR solvent system could be found that would dissolve them while still allowing them to retain their properties. If these compounds are polymeric and too large to simply dissolve in available solvents, an acidic solvent would dissolve it but would break the dative bond and potentially also the ester linkage; surfactants would also be able to get the compound into solution but lead to difficulty in characterization. Additionally, an IR study could be conducted to characterize key bonds such as the borinic acid-ester linkage and the Lewis base – boron bond. If certain important bonds could be identified by IR, then this method could be quite useful in characterizing many other types of the dative bond complexes as well.

Table 1. Results of ferrocene boroxine rotor series

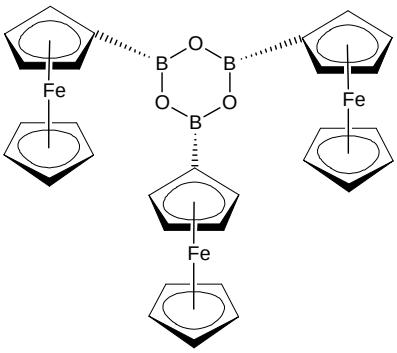	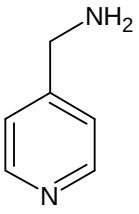	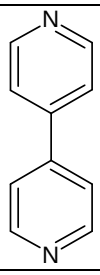	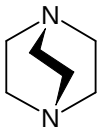
	1:1 ratio formed non-rotor crystal structure	(1-2):1 ratio possible rotor	(>2):1 ratio possible rotor
	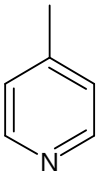	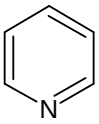	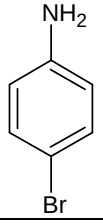
	1:1 ratio non-rotor	1:1 ratio non-rotor	no reaction starting material

Table 2. Results of diphenyl borinic acid macrocycle series

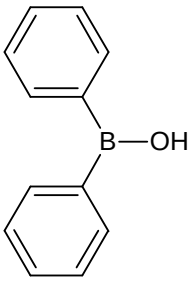		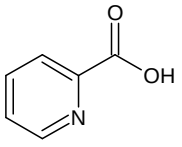	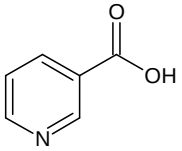	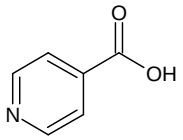
		^{1}H NMR shifting ring formed crystal structure	decomposition	decomposition
		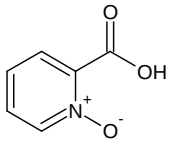	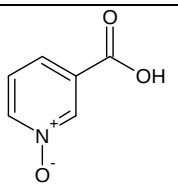	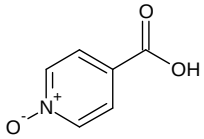
		^{1}H NMR shifting ring formed	decomposition	decomposition
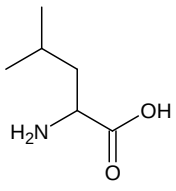	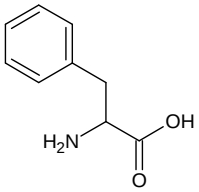	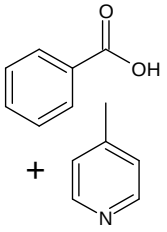	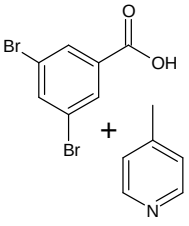	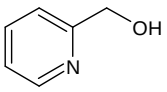
^{1}H NMR peaks present	^{1}H NMR shifting ring formed	^{1}H NMR shifting	^{1}H NMR shifting	^{1}H NMR shifting ring formed

Table 3. Results of 9-BBN macrocycle series

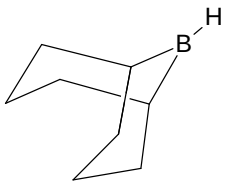	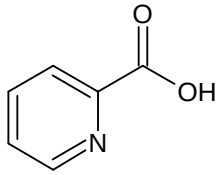	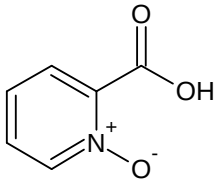
	^{1}H NMR shifting ring formed	^{1}H NMR shifting ring formed
	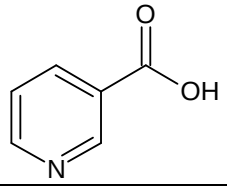	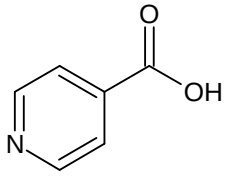
	inconclusive	inconclusive

CHAPTER FOUR: EXPERIMENTAL

4.1 General

All the reagents were purchased from commercial suppliers (Aldrich, Acros or Fisher), unless otherwise stated. ^{1}H, COSY and ^{13}C NMR were recorded on a JEOL Eclipse 300 FT 300 MHz NMR Spectrometer. Mass spectroscopy was done on a Thermo Finnigan LTQ Linear Ion Trap Mass Spectrometer with Electrospray Ionization in positive mode with methanol as the solvent. X-ray crystal structures were determined by Professor Robert Pike from the Department of Chemistry at the College of William & Mary. The rotavap used was BUCHI Rotavapor R- 205. DABCO: 1,4-Diazabicyclo(2.2.2)octane. 9-BBN: 9-borabicyclononane.

4.2 Ferrocene Boroxine Complexes

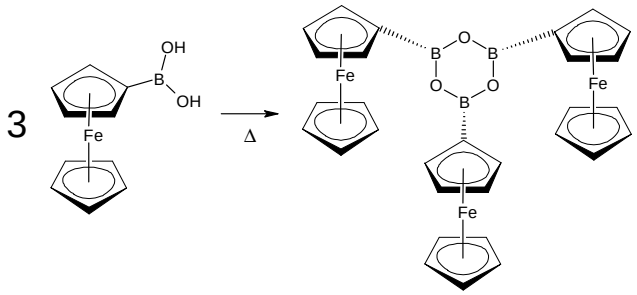

1 **2**

Ferrocene boroxine 2

Ferrocene boronic acid **1** (5g, 21.76mmol) was placed in a beaker and heater for 24 hours in an oven at 80℃ yielding ferrocene boro xine **2** for further experiments. This was analyzed via ^{1}H NMR ($CDCl_3$) 4.68ppm (broad s, 6H), 4.55ppm (broad s, 6H), 4.18ppm (broad s, 15H).

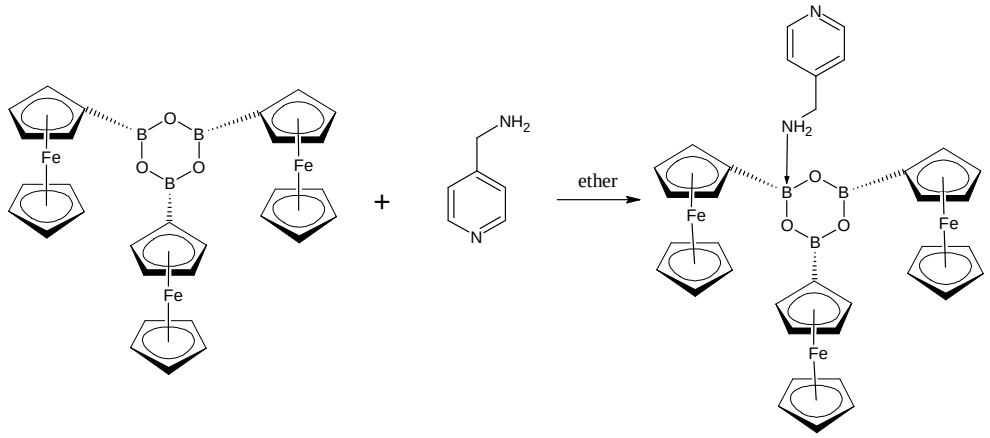

2 **3** **4**

Ferrocene boroxine – 4-Aminomethylpyridine complex 4

Previously synthesized ferrocene boroxines **2** (0.250g, 0.3933mmol) and diethyl ether (50mL) were placed in a 100mL RBF and stirred. 4-aminomethyl pyridine **3** (40µL, 0.394mmol) was added and allowed to stir for 48 hours. The resulting solution was gravity filtered then rotovapped. The final product **4** (0.255g, 87% yield) was analyzed via ^{1}H NMR ($CDCl_3$) 8.67ppm (dd, J1=4.7 J2=1.4 Hz, 2H), 7.36ppm (d, J=6.2 Hz, 2H), 4.61-4.34ppm (m, 10H), 4.16ppm (broad s, 15H), 3.97ppm (s, 2H).

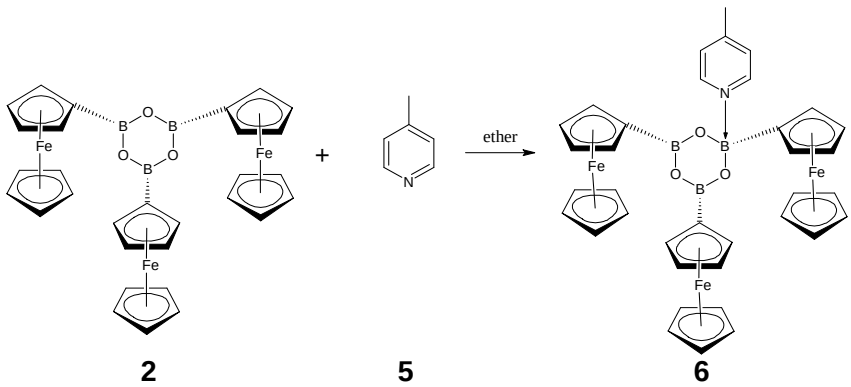

2 **5** **6**

Ferrocene boroxine – Picoline complex 6

Previously synthesized ferrocene boroxines **2** (0.113g, 0.177mmol) and diethyl ether (25mL) were placed in a 50mL RBF and stirred. Picoline **5** (20µL, 0.2055mmol) was added and allowed to stir for 48 hours. The resulting solution was gravity filtered

then rotovapped and placed on a vacuum pump for 6 hours. The final product **6** (0.115g, 90% yield) was analyzed via ^{1}H NMR ($CDCl_3$) 8.54ppm (dd, J1=4.6 J2=1 Hz, 2H), 7.17ppm (d, J=5.2 Hz, 2H), 4.61- 4.35ppm (m 5H), 4.13ppm (m, 12), 2.39ppm (broad s, 3H).

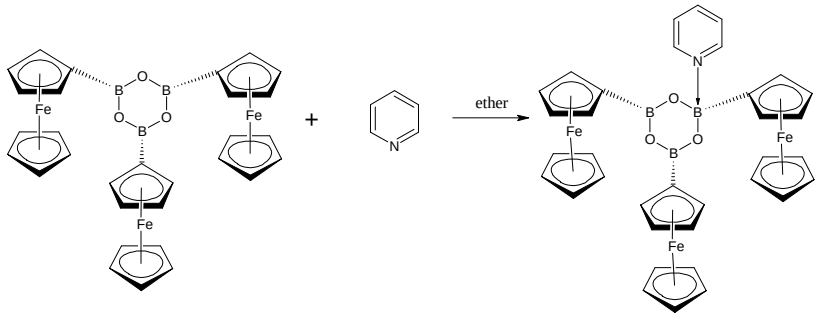

2 **7** **8**

Ferrocene boroxine – Pyridine complex 8

Previously synthesized ferrocene boroxines **2** (0.253g, 0.3962mmol) and diethyl ether (40mL) were placed in a 100mL RBF and stirred. Pyridine **7** (40µL, 0.4965mmol) was added and allowed to stir for 48 hours. The resulting solution was gravity filtered then rotovapped and placed on a vacuum pump for 6 hours. The final product **8** (0.233g, 83% yield) was analyzed via ^{1}H NMR ($CDCl_3$) 8.8ppm (d, J=4.3 Hz, 2H), 7.82ppm (tt, J1=7.6 J2=1.6 Hz, 1H), 7.43ppm (dd, J1=7.5 J2=6 Hz, 2H), 4.64-4.3ppm (m, 10H), 4.15ppm (broad s, 15H).

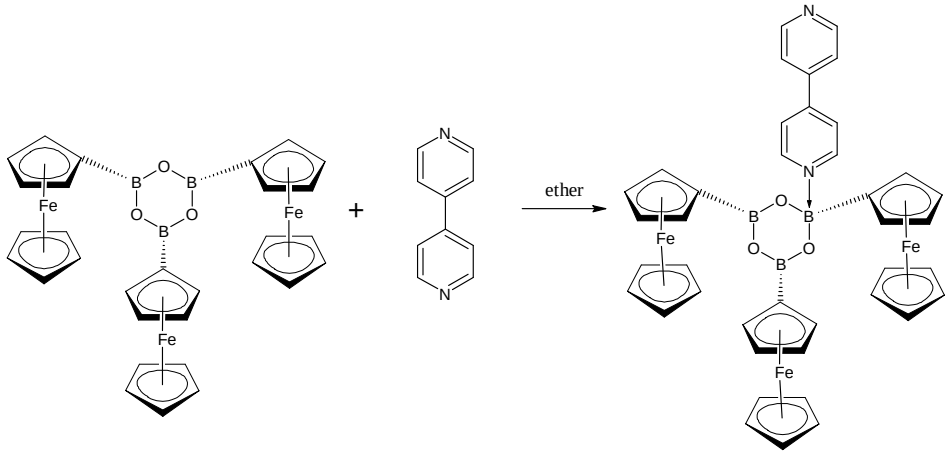

2 **11** **12**

Ferrocene boroxine – 4,4'-Bipyridine complex 12

Previously synthesized ferrocene boroxines **2** (0.1096g, 0.1716mmol) and diethyl ether (50mL) were placed in a 100mL RBF and stirred. 4,4'-bipyridine **11** (0.0155g, 0.0992mmol) was added and allowed to stir for 48 hours. The resulting solution was gravity filtered then rotovapped and placed on a vacuum pump for 6 hours. The final product **12** (0.106g, 84.7% mass balance) was analyzed via ^{1}H NMR ($CDCl_3$) 8.89ppm (s, 4H), 7.65ppm (s, 4H), 3.9-4.9ppm (m, 38H).

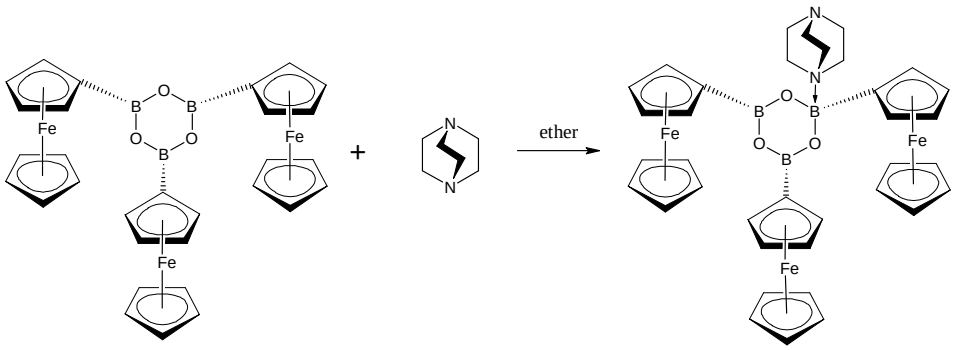

2 **13** **14**

Ferrocene boroxine – DABCO complex 14

Previously synthesized ferrocene boroxines **2** (0.1079g, 0.1690mmol) and diethyl ether (50mL) were placed in a 100mL RBF and stirred. DABCO **13** (0.0100g, 0.0892mmol) was added and allowed to stir for 48 hours. The resulting solution was

gravity filtered then rotovapped and placed on a vacuum pump for 6 hours. The final product **14** (0.103g, 87.4% mass balance) was analyzed via ^{1}H NMR ($CDCl_3$) 3.9-4.9ppm (m, 72H), 3.03ppm (broad s, 12H).

4.3 Borinic Acid Derivatives

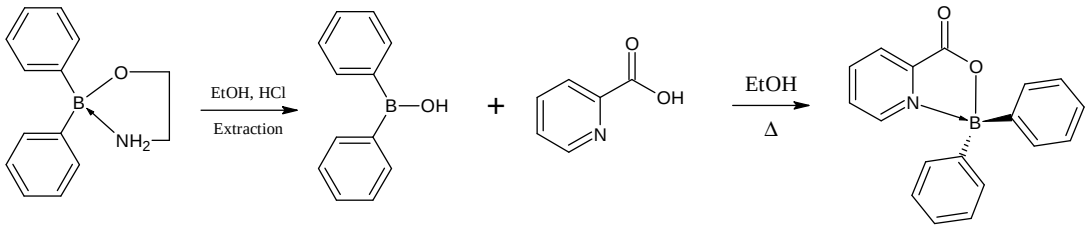

15 **16** **17** **18**

Picolinic diphenylborinate ester 18

2-aminoethyl diphenylborinate **15** (0.5032g, 2.235mmol) and ethanol (20mL) were placed in a 100mL RBF and stirred. HCl (20mL of 1M) was slowly added to the RBF and allowed to stir for 22 minutes. The solution was extracted four times with diethyl ether. The ether layers were combined and extracted with a brine solution then dried with magnesium sulfate. The ether solution, in a 250mL RBF, was rotovapped and placed on a vacuum pump for 30 minutes. Ethanol (100mL) was added to the RBF and stirred. Picolinic acid **17** (0.2480g, 2.014mmol) was added to the RBF and refluxed for 15 minutes. The resulting solution was distilled through short path distillation until approximately 25% of the volume remained. This was allowed to recrystallize over 48 hours followed by being placed on a vacuum pump for 2 hours. The final product **18** (0.3962g, 69% yield) was analyzed via ^{1}H NMR (DMSO-d_6) 9.19ppm (dt, J1=5.6 J2=1 Hz, 1H), 8.64ppm (td, J1=7.7 J2=1.2 Hz, 1H), 8.47 (dt, J1=7.8 J2=1 Hz, 1H), 8.19ppm (ddd, J1=7.7 J2=5.6 J3=1.3 Hz, 1H), 1.18-7.35ppm (m, 10H) and LCMS 288.09 $^{m}/_{z}$ ([M]+1), 310.09 $^{m}/_{z}$ ([M]+Na), 597.00 $^{m}/_{z}$ (2[M]+Na).

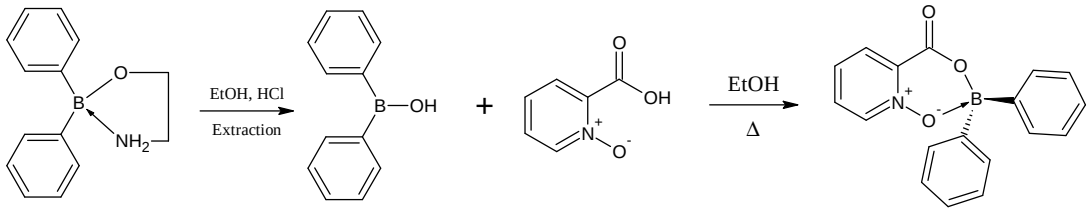

15 **16** **23** **24**

Picolinic N-Oxide diphenylborinate ester 24

2-aminoethyl diphenylborinate **15** (0.2488g, 1.1053mmol) and ethanol (20mL) were placed in a 100mL RBF and stirred. Concentrated HCl (0.5mL) was slowly added to the RBF followed by deionized water (12 mL) and allowed to stir for 20 minutes. The solution was extracted four times with diethyl ether. The ether layers were combined and extracted with a brine solution then dried with magnesium sulfate. The ether solution, in a 250mL RBF, was rotovapped and placed on a vacuum pump for 30 minutes. Ethanol (100mL) was added to the RBF and stirred. Picolinic acid N-Oxide **23** (0.1395g, 0.9948mmol) was added to the RBF and refluxed for 15 minutes. The resulting solution was distilled through short path distillation until approximately 30% of the volume remained. This was allowed to recrystallize over 48 hours followed by being vacuum filtered. The final product **24** (0.2356g, 78% yield) was analyzed via ^{1}H NMR ($CDCl_3$) 8.52ppm (dq, J1=6.4 J2=0.5 Hz, 1H), 8.44ppm (dd, J1=7.9 J2=2 Hz, 1H), 7.99ppm (td, J1=7.8 J2=1.3 Hz, 1H), 7.75ppm (ddd, J1=7.9 J2=6.2 J3=2 Hz, 1H), 7.53ppm (m, 4H), 7.13-7.25ppm (m, 6H).

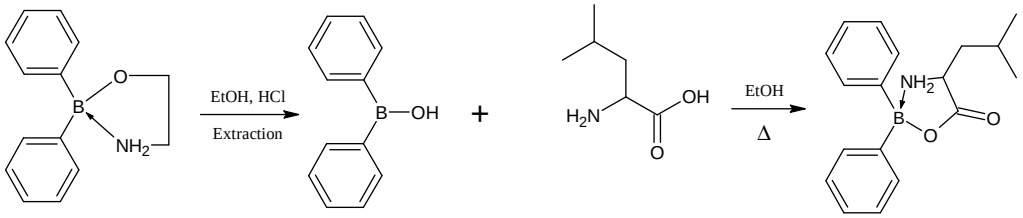

15 **16** **29** **30**

Leucine diphenylborinate ester 30

2-aminoethyl diphenylborinate **15** (0.2560g, 1.137mmol) and ethanol (25mL) were placed in a 100mL RBF and stirred. Concentrated HCl (12 drops) was slowly added to the RBF followed by deionized water (16mL) and allowed to stir for 40 minutes. The solution was extracted four times with diethyl ether. The ether layers were combined and extracted with a brine solution then dried with magnesium sulfate. The ether solution, in a 250mL RBF, was rotovapped. Ethanol (100mL) was added to the RBF and stirred. Leucine **29** (0.1541g, 1.174mmol) was added to the RBF and refluxed for 30 minutes. The resulting solution was distilled through short path distillation until approximately 15% of the volume remained. This was allowed to recrystallize over 48 hours followed by being placed on a vacuum pump for 2 hours. The final product **30** (0.3339g, 99% yield) was analyzed via ^{1}H NMR (DMSO-d_6) 7.4ppm (m, 4H), 7.18-7.26ppm (m, 4H), 7.09-7.17ppm (m, 2H), 1.74-1.9ppm (m, 1H), 1.44-1.64ppm (m, 2H), 0.76-0.9ppm (dd, J1=7.7 J2=6.7 Hz, 6H).

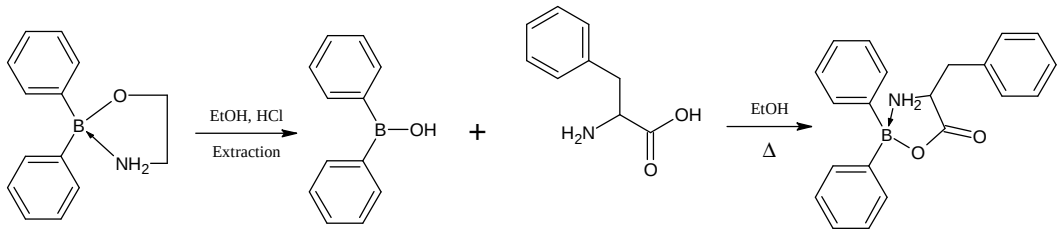

15 **16** **31** **32**

Phenylalanine diphenylborinate ester 32

2-aminoethyl diphenylborinate **15** (0.2684g, 1.192mmol) and ethanol (22mL) were placed in a 100mL RBF and stirred. Concentrated HCl (12 drops) was slowly added to the RBF followed by deionized water (12mL) and allowed to stir for 30 minutes. The solution was extracted four times with diethyl ether. The ether layers were combined and extracted with a brine solution then dried with magnesium sulfate. The ether solution, in a 250mL RBF, was rotovapped. Ethanol (100mL) was added to the RBF and stirred. Phenylalanine **31** (0.2090g, 1.265mmol) was added to the RBF and refluxed for 15 minutes. The resulting solution was distilled through short path distillation until approximately 15% of the volume remained. This was allowed to recrystallize over 48 hours followed by being placed on a vacuum pump for 2 hours. The final product **32** (0.3640g, 92% yield) was analyzed via ^{1}H NMR (DMSO-d_6) 7.05-7.45ppm (m, 15H), 3.7ppm (m, 1H), 2.78-3.23ppm (m, 2H).

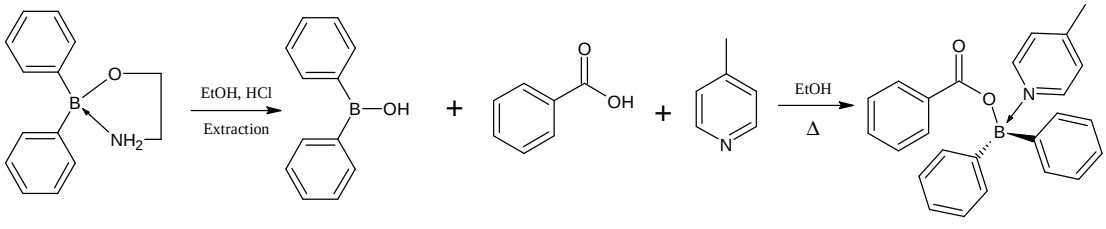

15 **16** **33** **5** **34**

Benzoic diphenylborinate ester – Picoline complex 34

2-aminoethyl diphenylborinate **15** (0.2476g, 1.099mmol) and ethanol (23mL) were placed in a 100mL RBF and stirred. Concentrated HCl (13 drops) was slowly added to

the RBF followed by deionized water (18mL) and allowed to stir for 20 minutes. The solution was extracted four times with diethyl ether. The ether layers were combined and extracted with a brine solution then dried with magnesium sulfate. The ether solution, in a 250mL RBF, was rotovapped and placed on a vacuum pump for 30 minutes. Ethanol (100mL) was added to the RBF and stirred. Benzoic acid **33** (0.1384g, 1.093mmol) and pyridine **5** (0.110mL, 1.130mmol) were added to the RBF and refluxed for 20 minutes. The resulting solution was distilled through short path distillation until approximately 15% of the volume remained. This was allowed to recrystallize over 48 hours followed by being placed on a vacuum pump for 2 hours. The final product **34** (0.3552g, 85% yield) was analyzed via ^{1}H NMR ($CdCl_3$) 8.65ppm (d, J=6.6 Hz, 2H), 8.23ppm (d, J=7.1 Hz, 2H), 7.16-7.65ppm (m, 29H), 2.45ppm (s, 3H).

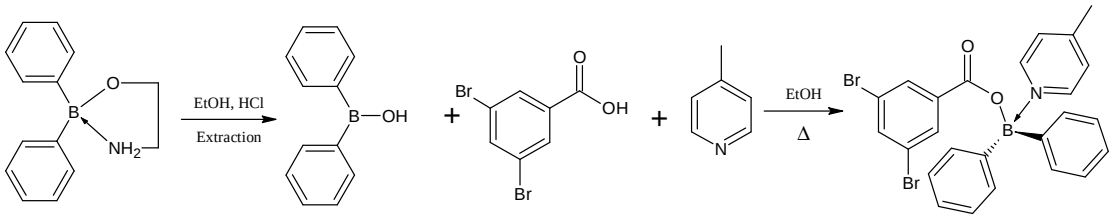

15 **16** **35** **5** **36**

3,5-dibromobenzoic diphenylborinate ester – Picoline complex 36

2-aminoethyl diphenylborinate **15** (0.2599g, 1.155mmol) and ethanol (21mL) were placed in a 100mL RBF and stirred. Concentrated HCl (12 drops) was slowly added to the RBF followed by deionized water (17mL) and allowed to stir for 20 minutes. The solution was extracted four times with diethyl ether. The ether layers were combined and extracted with a brine solution then dried with magnesium sulfate. The ether solution, in a 250mL RBF, was rotovapped. Ethanol (100mL) was added to the RBF and stirred. 3,5-dibromobenzoic acid **35** (0.3234g, 1.155mmol) and pyridine **5** (0.115mL, 1.181mmol) were added to the RBF and refluxed for 30 minutes. The resulting solution was distilled through short path distillation until approximately 15% of the volume

remained. This was allowed to recrystallize over 48 hours followed by being placed on a vacuum pump for 2 hours. The final product **36** (0.5265g, 85% yield) was analyzed via ^{1}H NMR (DMSO-d_6) 8.45ppm (dd, J1=2.7 J2=2.7 Hz, 2H), 8.15ppm (t, J=1.8 Hz, 1H), 8.03ppm (d, J=1.8 Hz, 2H), 7.32-7.64ppm (m, 10H), 7.29ppm (d, J=5.5 Hz, 2H), 2.35ppm (s, 3H).

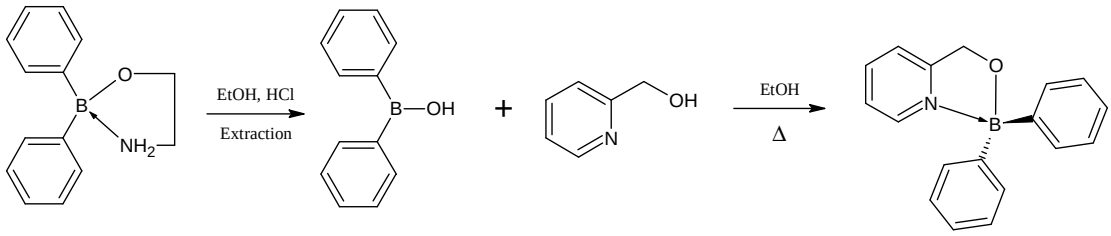

15 **16** **37** **38**

2-Methylpyridine diphenylborinate ester 38

2-aminoethyl diphenylborinate **15** (0.2407g, 1.069mmol) and ethanol (25mL) were placed in a 100mL RBF and stirred. Concentrated HCl (10 drops) was slowly added to the RBF followed by deionized water (17mL) and allowed to stir for 40 minutes. The solution was extracted four times with diethyl ether. The ether layers were combined and extracted with a brine solution then dried with magnesium sulfate. The ether solution, in a 250mL RBF, was rotovapped. Ethanol (100mL) was added to the RBF and stirred. 2-pyridinmethanol **37** (0.105mL, 1.087mmol) was added to the RBF and refluxed for 20 minutes. The resulting solution was distilled through short path distillation until approximately 15% of the volume remained. This was allowed to recrystallize over 48 hours followed by being placed on a vacuum pump for 2 hours. The final product **38** was analyzed via ^{1}H NMR (DMSO-d_6) 8.62ppm (dt, J1=5.7 J2=1.1 Hz, 1H), 8.24ppm (td, J1=7.7 J2=1.4 Hz, 1H), 7.86ppm (dt, J1=7.9 J2=0.9 Hz, 1H), 7.70ppm (ddd, J1=7.5 J2=5.7 J3=1.1 Hz, 1H), 7.32ppm (m, 4H), 7.08-7.21ppm (m, 6H), 5.16ppm (s, 2H).

4.4 9-BBN Derivatives

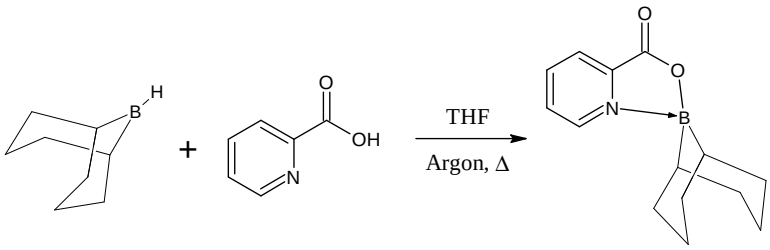

39 **17** **40**

Picolinic 9-BBN ester 40

Picolinic acid **17** (0.1558g, 1.266mmol) was placed in a 100mL RBF with a water cooled condensing tube on top. The system was sealed and purged with argon gas. Anhydrous THF (50mL) was added to the RBF and stirred followed by 9-borabicyclononane **39** in anhydrous THF (2.7mL, 1.350mmol). This was refluxed for three hours then rotovapped and placed on a vacuum pump for two hours. The final product **40** (0.3052g 99% yield) was analyzed via ^{1}H NMR (300MHz, DMSO-d_6) 9.2ppm (d, J=5.7 Hz , 1H), 8.55ppm (t, J=7.7 Hz, 1H), 8.34 (d, J=7.8 Hz , 1H), 8.09ppm (t, J=6.7 Hz, 1H), 1.15-2.18ppm (m, 15H) and LCMS 244.09 $^{m}/_{z}$ ([M]+1), 266.09 $^{m}/_{z}$ ([m]+Na), 509.09 $^{m}/_{z}$ (2[M]+Na).

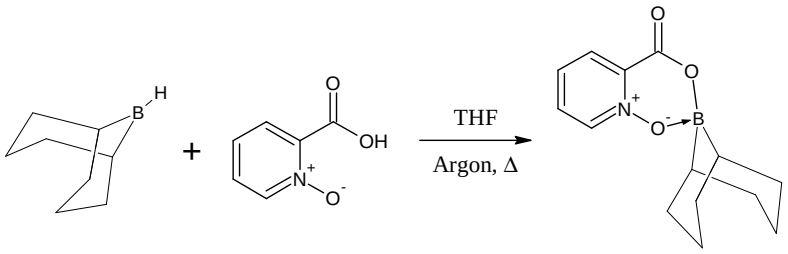

39 **23** **43**

Picolinic N-Oxide 9-BBN ester 43

Picolinic acid N-Oxide **23** (0.1582g, 1.137mmol) was placed in a 100mL RBF with a water cooled condensing tube on top. The system was sealed and purged with argon gas. Anhydrous THF (50mL) was added to the RBF and stirred followed by 9-borabicyclononane **39** in anhydrous THF (2.5mL, 1.250mmol). This was refluxed for

three hours and allowed to stand for 18 hours. It was then rotovapped and placed on a vacuum pump for two hours. The final product **43** (0.3192g 108% yield) was analyzed via ^{1}H NMR (300MHz, DMSO-d_6) 9.14ppm (dd, J1=6.3 J2=0.7 Hz, 1H), 8.45ppm (m, 1H), 8.35ppm (td, J1=7.8 J2=1.1 Hz, 1H), 8.15ppm (ddd, J1=7.9 J2=6.2 J3=2 Hz, 1H), 1.3-1.85ppm (m, 14H).

REFERENCES

[1] Beckett, A. Michael; Strickland, C. Gary; Varma, K. Sukumar; Hibbs, E. David; Hursthouse, B. Michael; Malik, K.M. Abdul. Amine adducts of triarylboroxines: synthesis and characterization of adducts of tri(2-tolyl) boroxine and crystal structures of $(4\text{-}MeC_6H_4)_3B_3O_3$ and $(4\text{-}MeC_6H_4)_3B_3O_3 \cdot 4$-picoline. *Journal of Organometallic Chemistry*. 535 (**1997**) 33-41.

[2] Rodriguez-Molina, Braulio; Ochoa, Ma. Eugenia; Farfán, Norberto; Santillan, Rosa; Garcia-Garibay, A. Miguel. Synthesis, characterization, and rotational dynamics of crystalline molecular compasses with N-heterocyclic rotators. *Journal of Organic Chemistry*. **2009**, 74, 8554-8565.

[3] Stang, P.J. *The Journal of Organic Chemistry* **2009**, *74*, 2-20.

[4] Christinat, Nicolas; Scopelliti, Rosario; Severin, Kay. A new method for the synthesis of boronate macrocyles. *Chem. Commun.* **2004**, 1158-1159.

[5] Baker, J. Stephen; Akama, Tsutomu; Zhang, Yong-Kang; Sauro, Vittorio; Pandit, Chetan; Singh, Rajeshwar; Kully, Maureen; Khan, Jehangir; Plattner, J. Jacob; Benkovic, J. Stephen; Lee, Ving; and Maples, R. Kirk. Identification of a novel boron-containing antibacterial agent (AN0128) with anti-inflammatory activity, for the potential treatment of cutaneous diseases. *Bioinorganic & Medical Chemistry Letters*. 16 (**2006**) 5963-5967.

APPENDIX A: ^{1}H NMR SPECTRA OF PRODUCTS

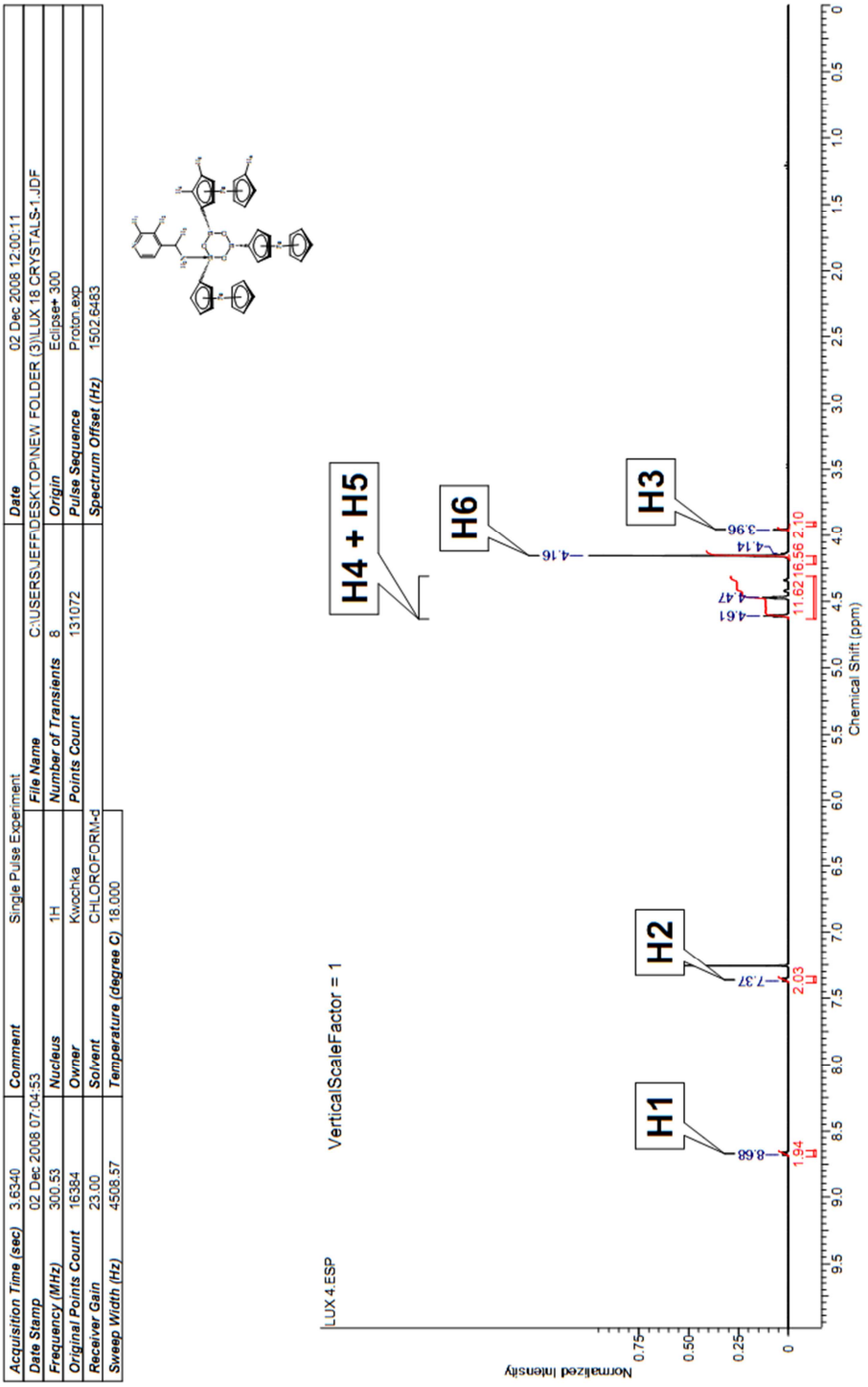

Figure 35. ^{1}H NMR spectrum of product **4** of ferrocene boroxine **2** and 4-aminomethyl pyridine **3**.

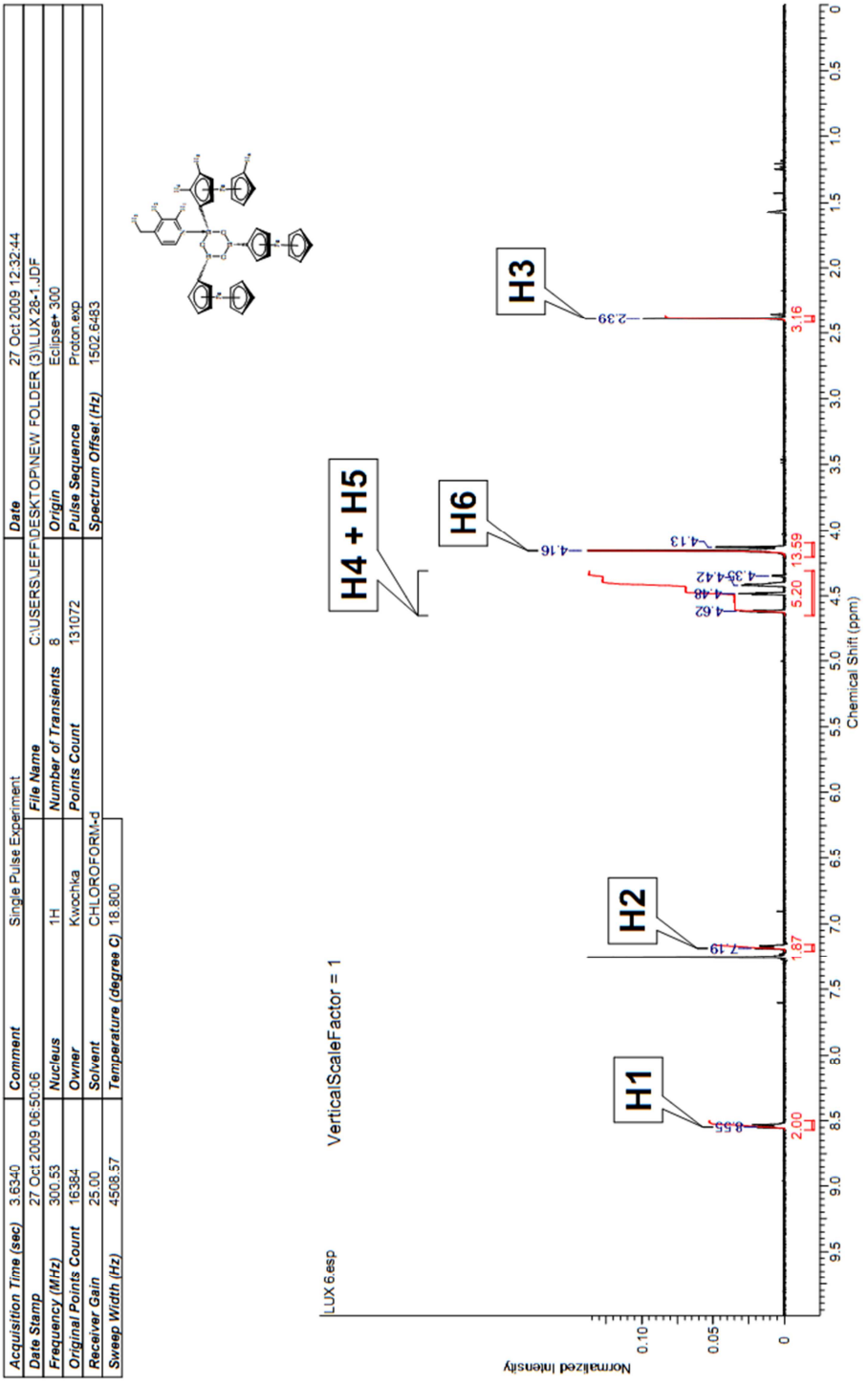

Figure 36. ^{1}H NMR spectrum of product **6** of ferrocene boroxine **2** and picoline **5**.

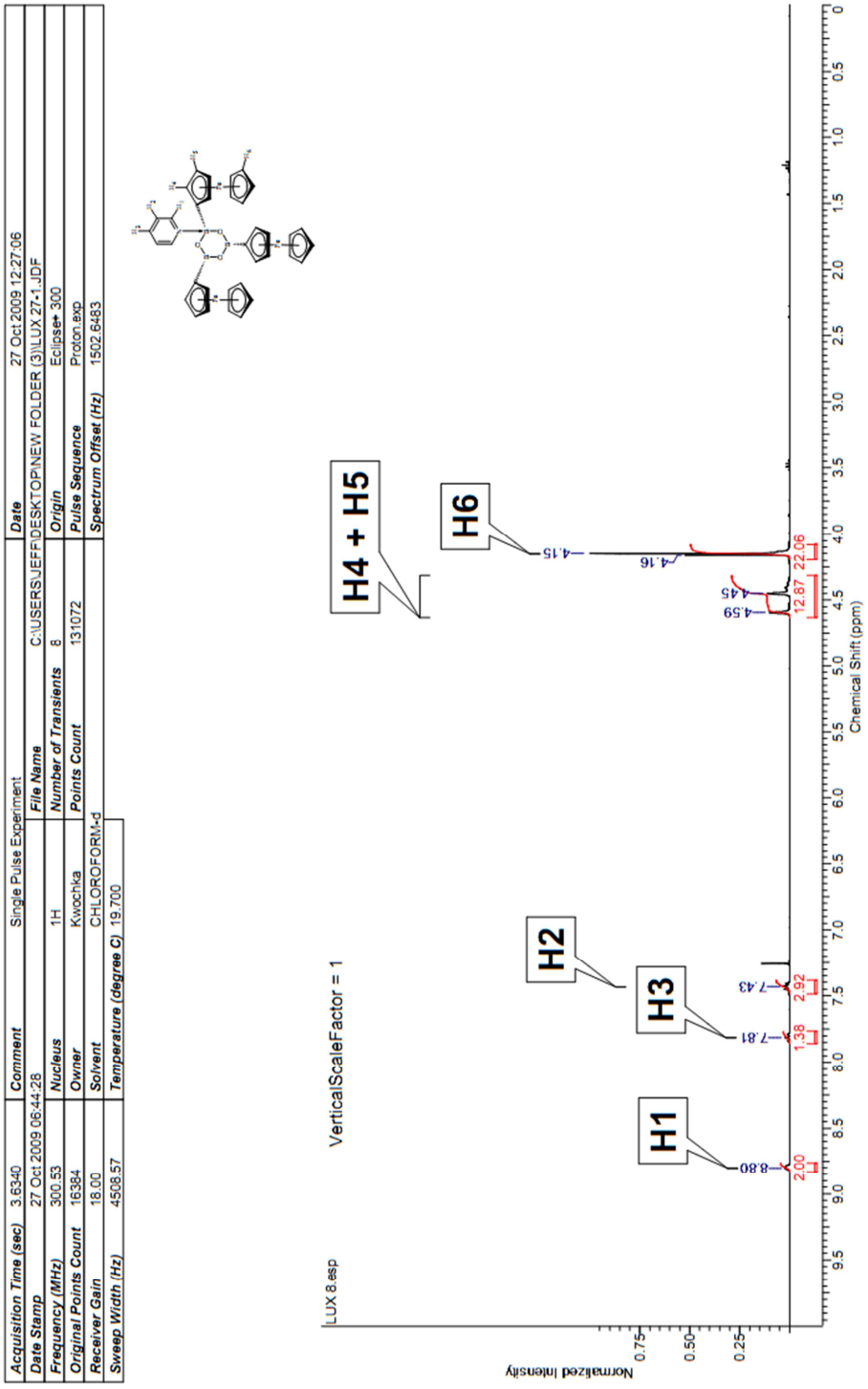

Figure 37. ^{1}H NMR spectrum of product **8** of ferrocene boroxine **2** and pyridine **7**.

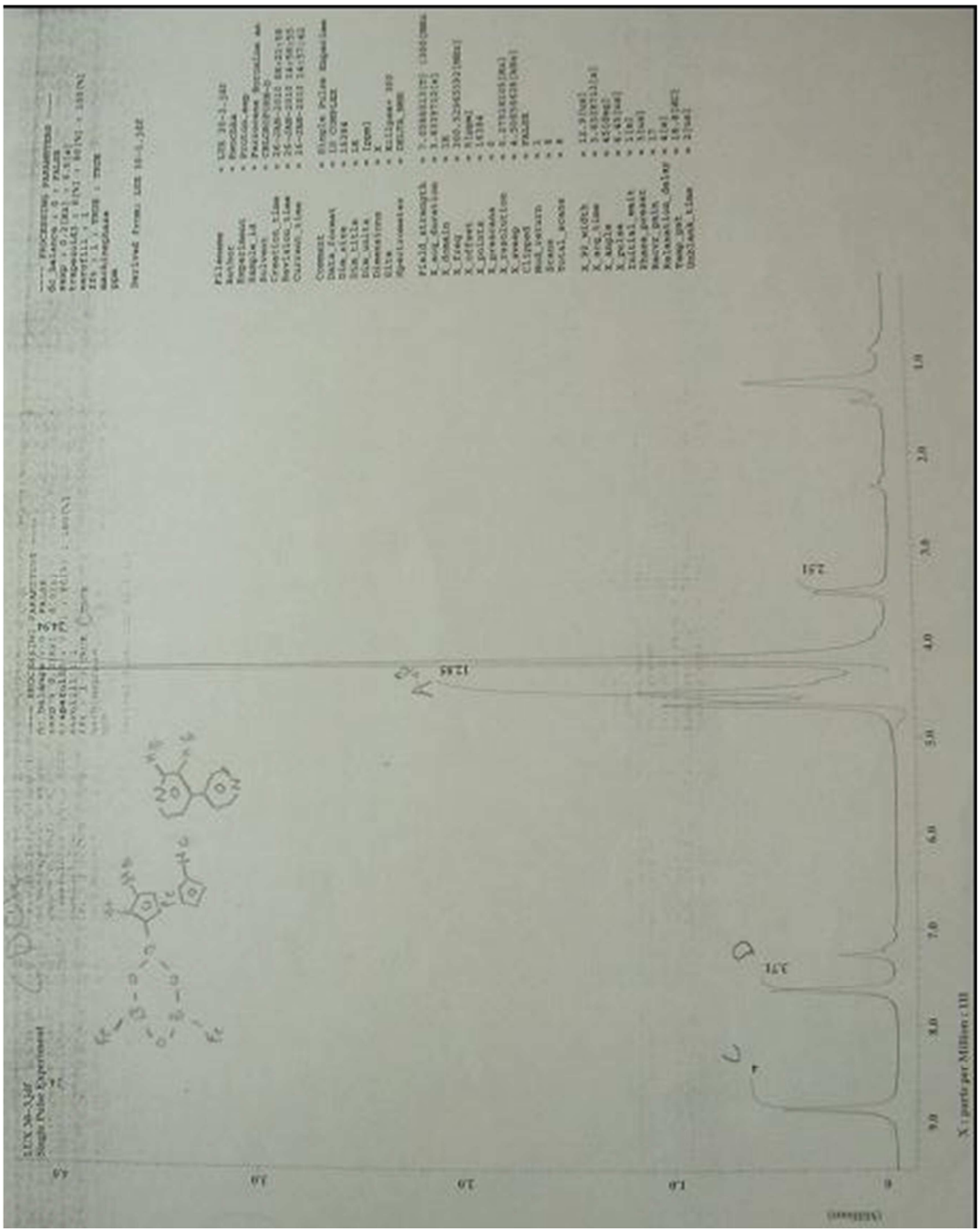

Figure 38. ^{1}H NMR spectrum of product **12** of ferrocene boroxine **2** and 4,4'-bipyridine **11**.

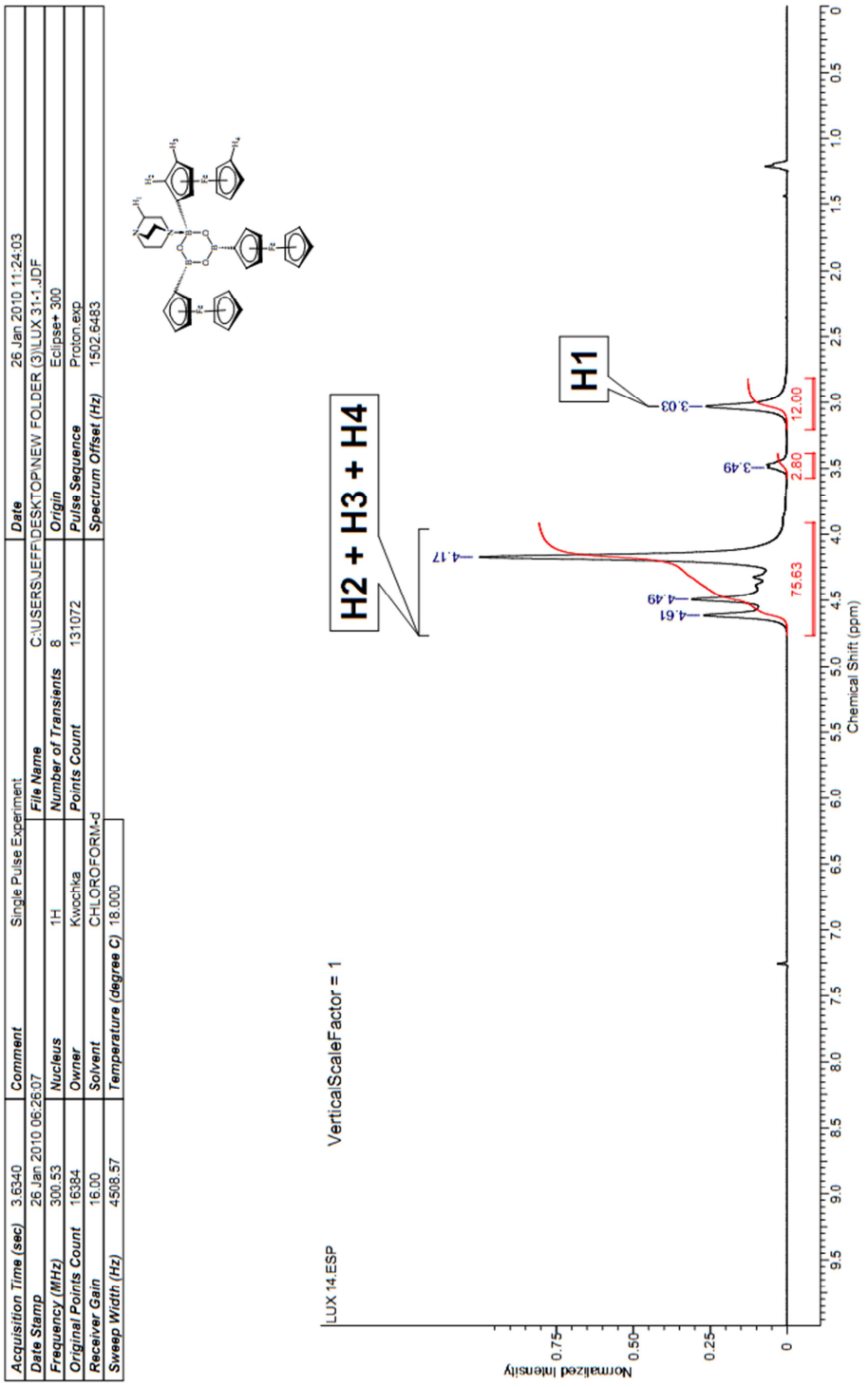

Figure 39. ^{1}H NMR spectrum of product **14** of ferrocene boroxine **2** and DABCO **13**.

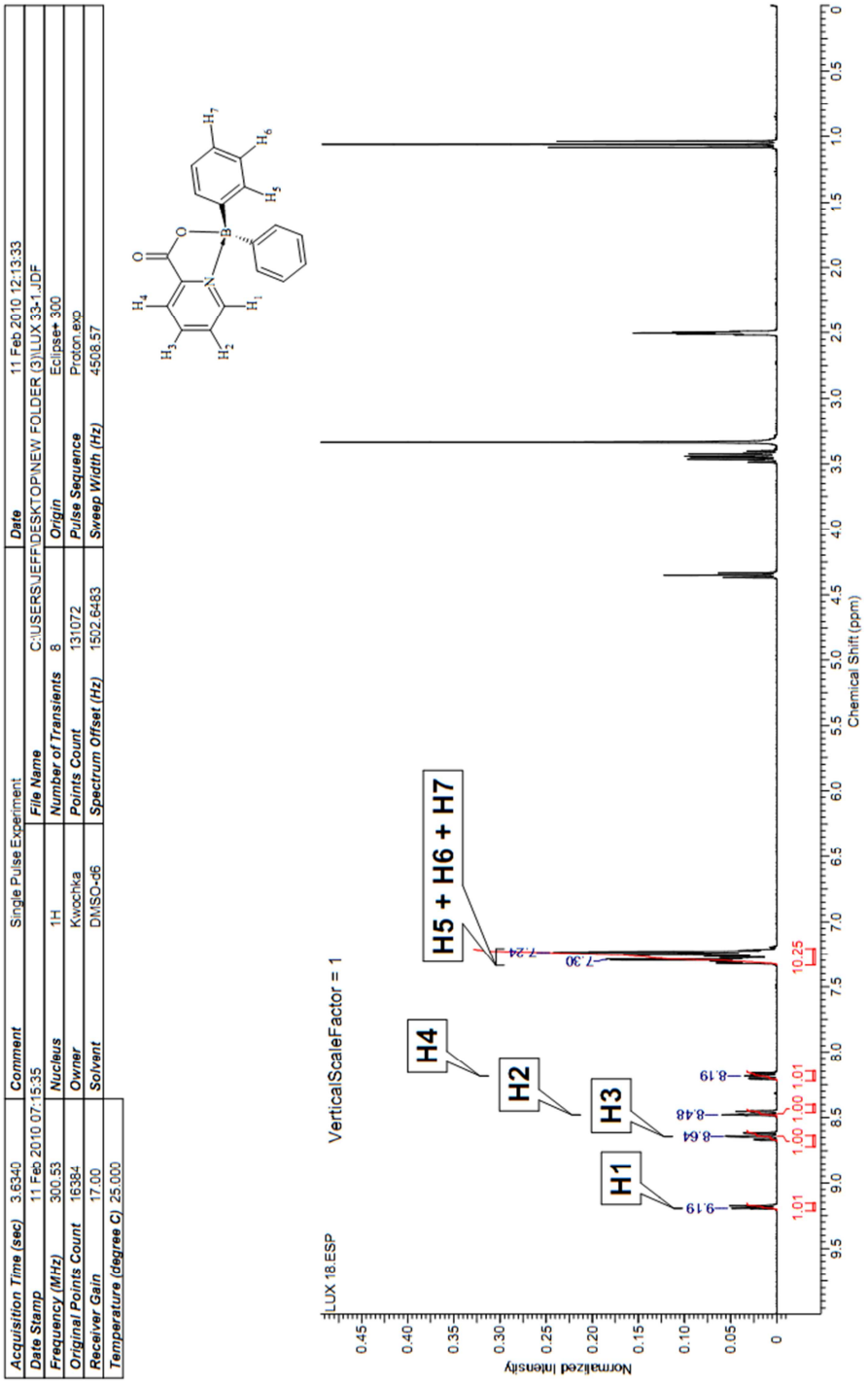

Figure 40. ^{1}H NMR spectrum of product **18** of diphenyl borinic acid **16** and picolinic acid **17**.

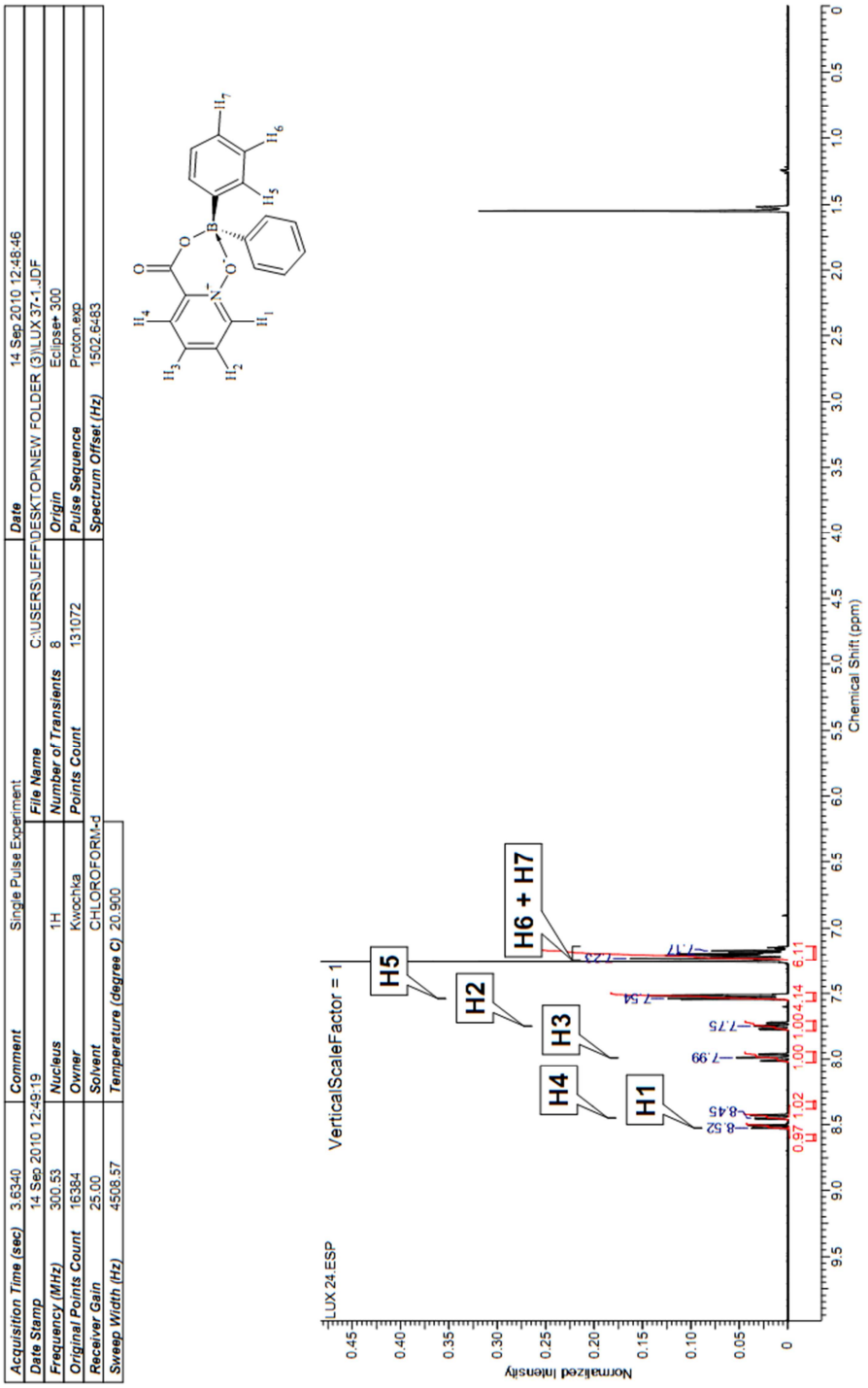

Figure 41. ^{1}H NMR spectrum of product **24** of diphenyl borinic acid **16** and picolinic acid N-Oxide **23**.

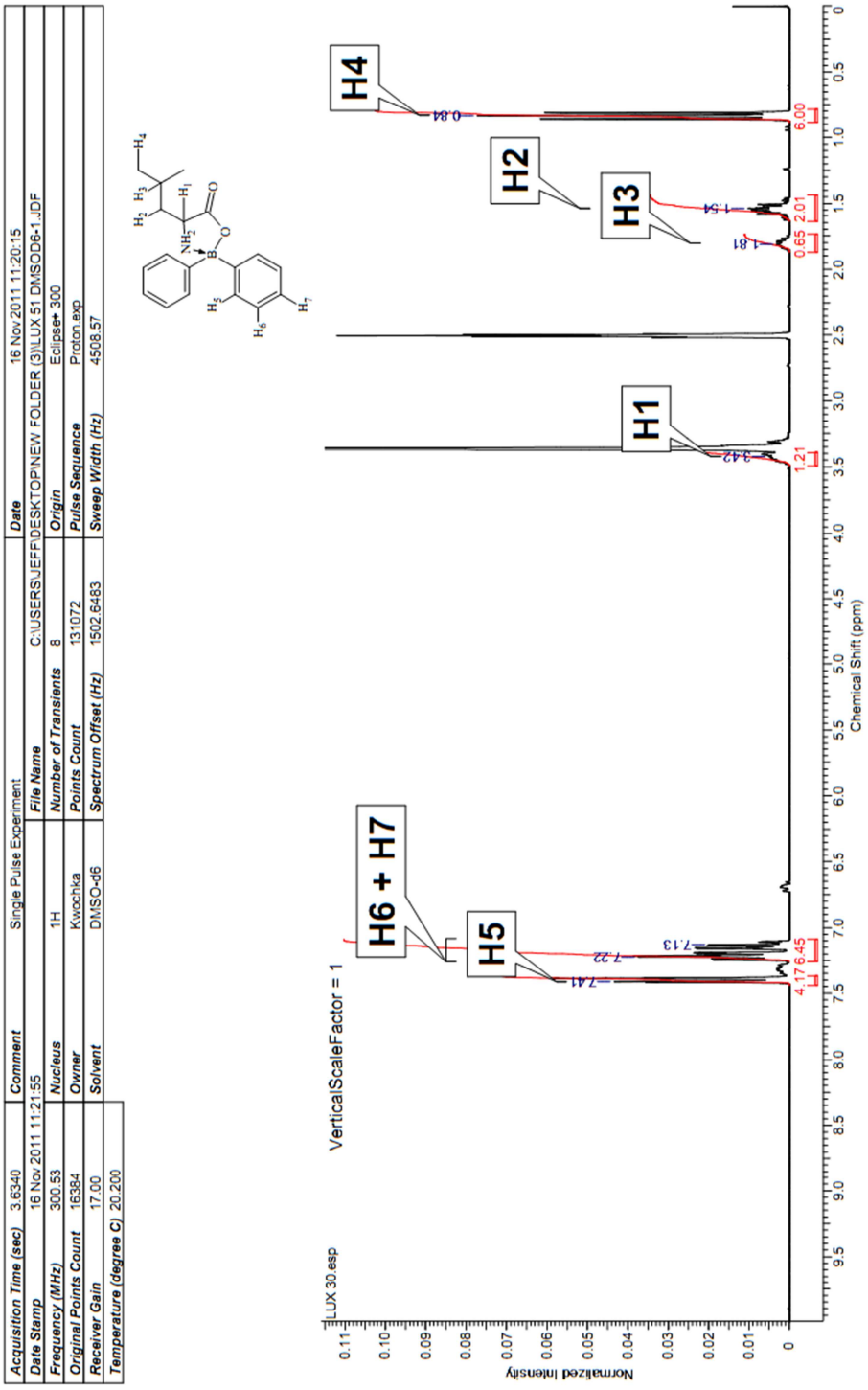

Figure 42. ^{1}H NMR spectrum of product **30** of diphenyl borinic acid **16** and leucine **29**.

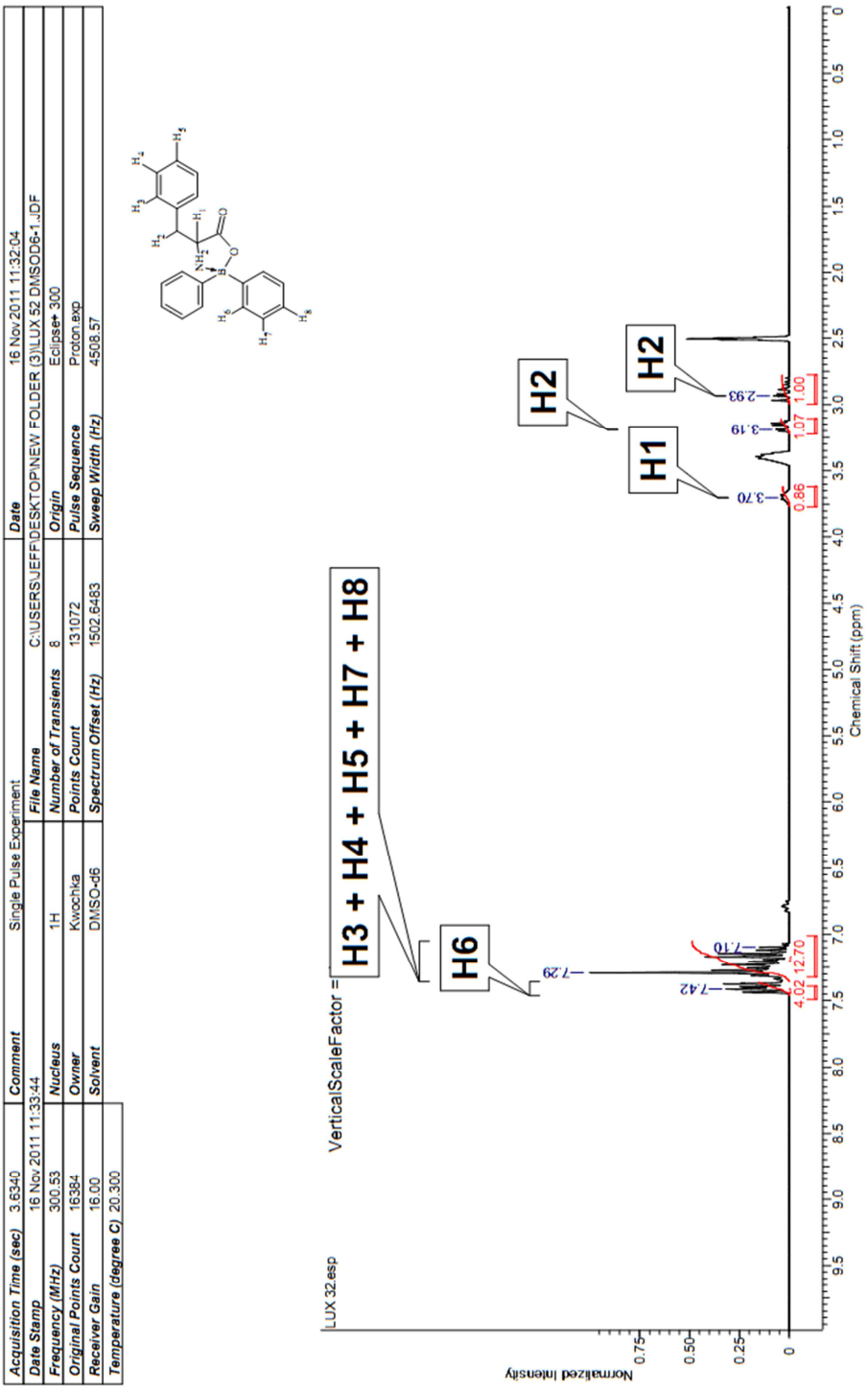

Figure 43. ^{1}H NMR spectrum of product **32** of diphenyl borinic acid **16** and phenylalanine **31**.

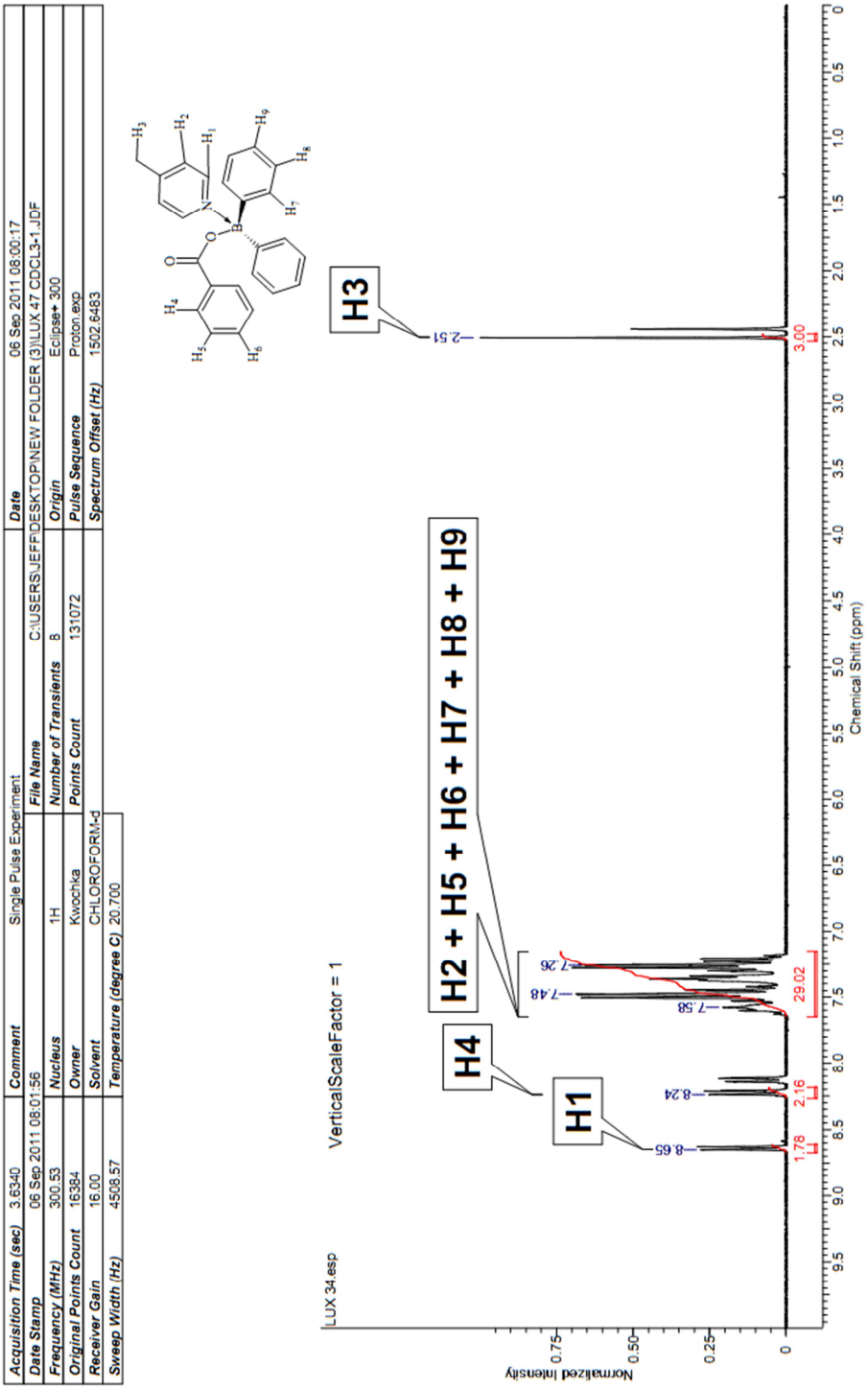

Figure 44. [1]H NMR spectrum of product **34** of diphenyl borinic acid **16**, benzoic acid **33**, and picoline **5**.

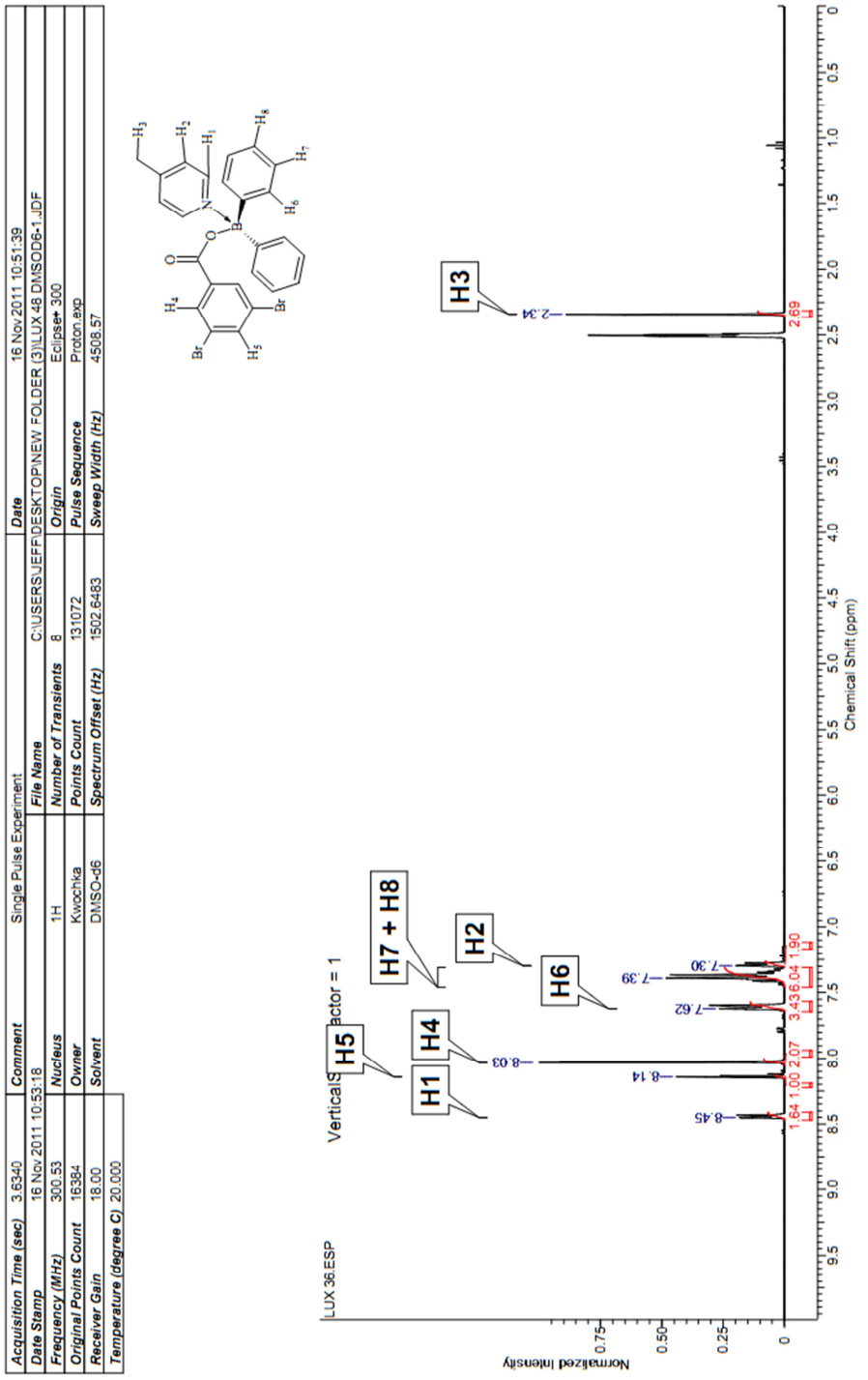

Figure 45. ^{1}H NMR spectrum of product **36** of diphenyl borinic acid **16**, 3,5-dibromobenzoic acid **35** and picoline **5**.

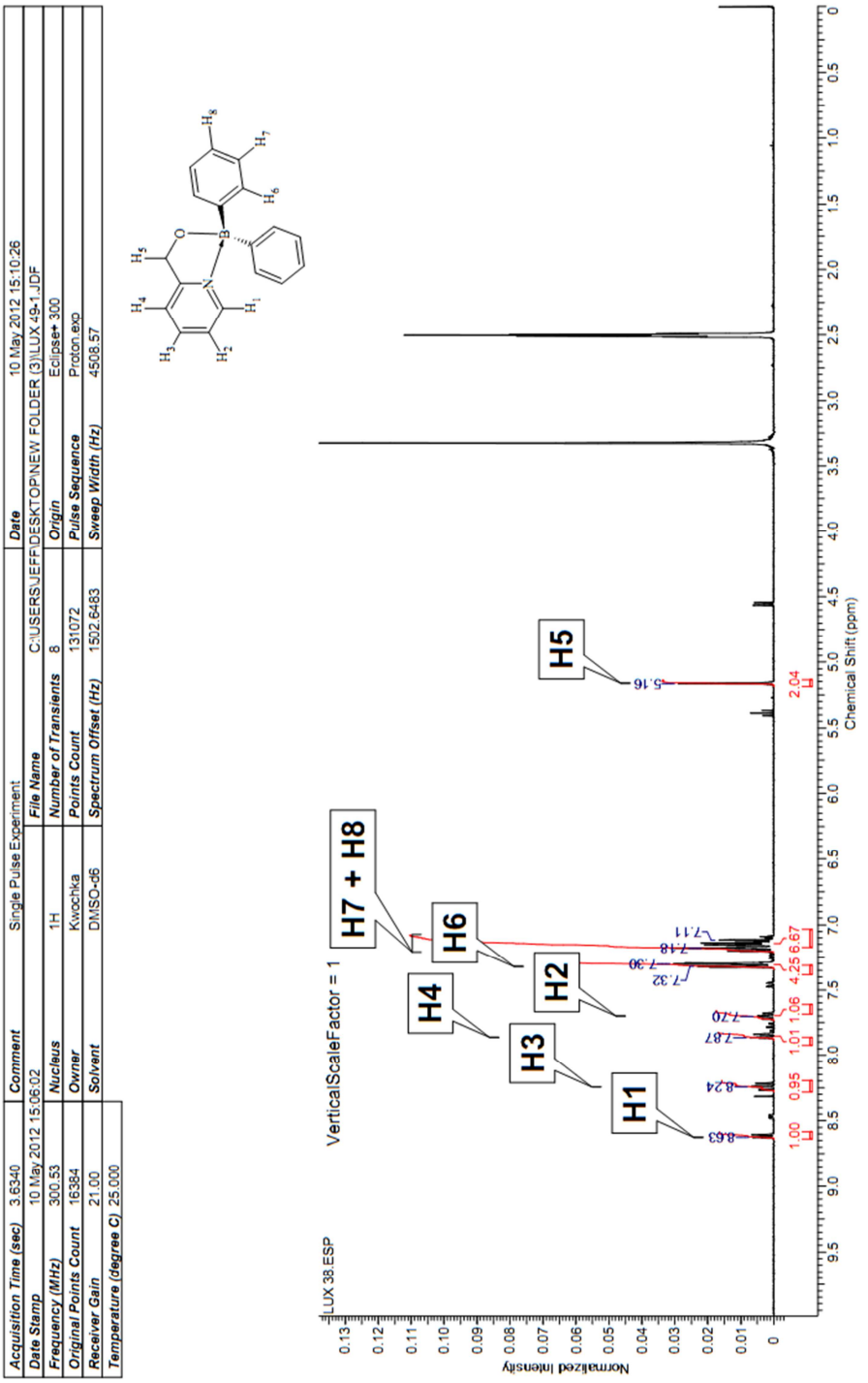

Figure 46. ^{1}H NMR spectrum of product **38** of diphenyl borinic acid **16** and 2-methylpyridine **37**.

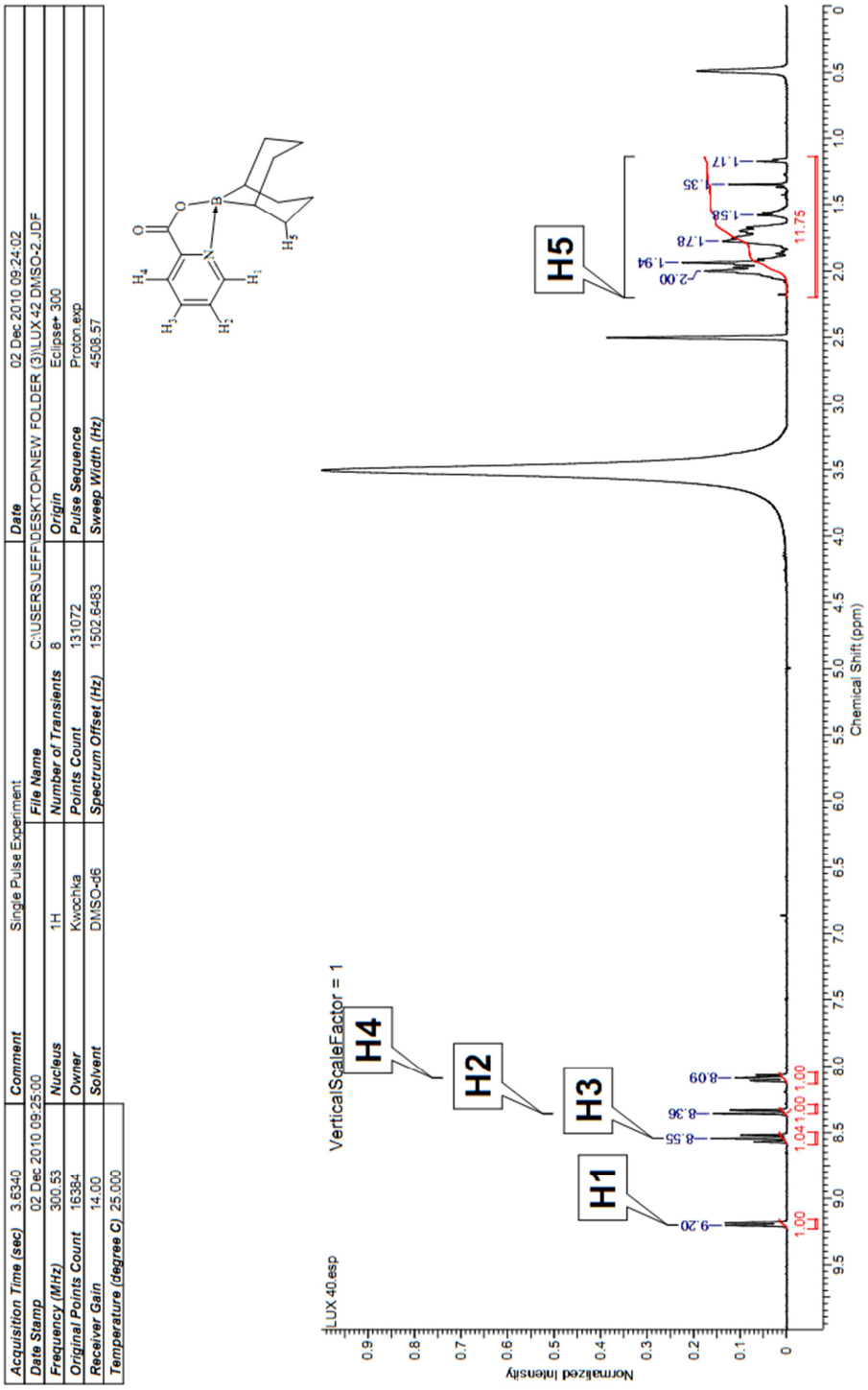

Figure 47. ^{1}H NMR spectrum of product **40** of 9-BBN **39** and picolinic acid **17**.

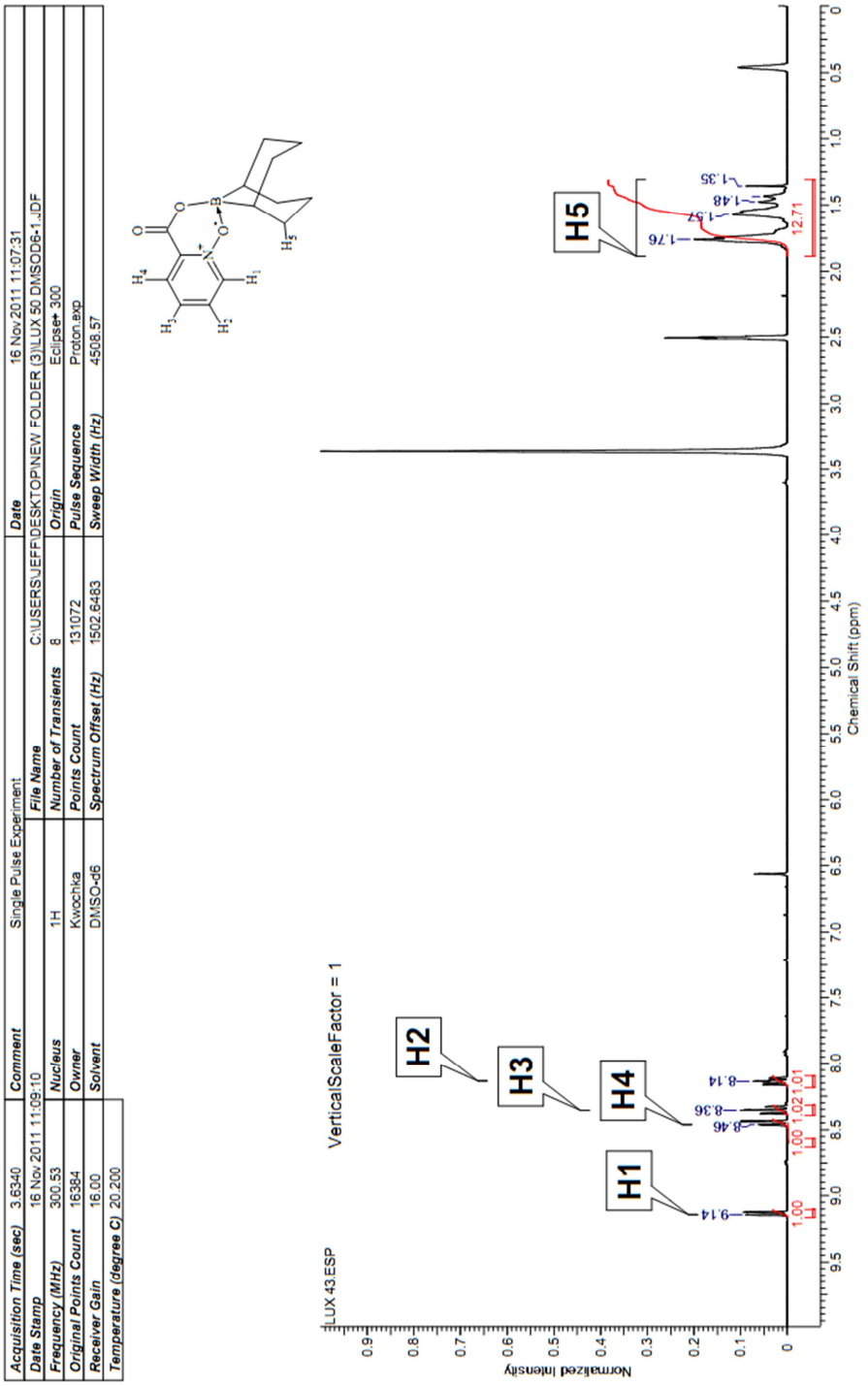

Figure 48. ^{1}H NMR spectrum of product **43** of 9-BBN **39** and picolinic acid N-Oxide **23**.

APPENDIX B: MASS SPECTRA OF PRODUCTS

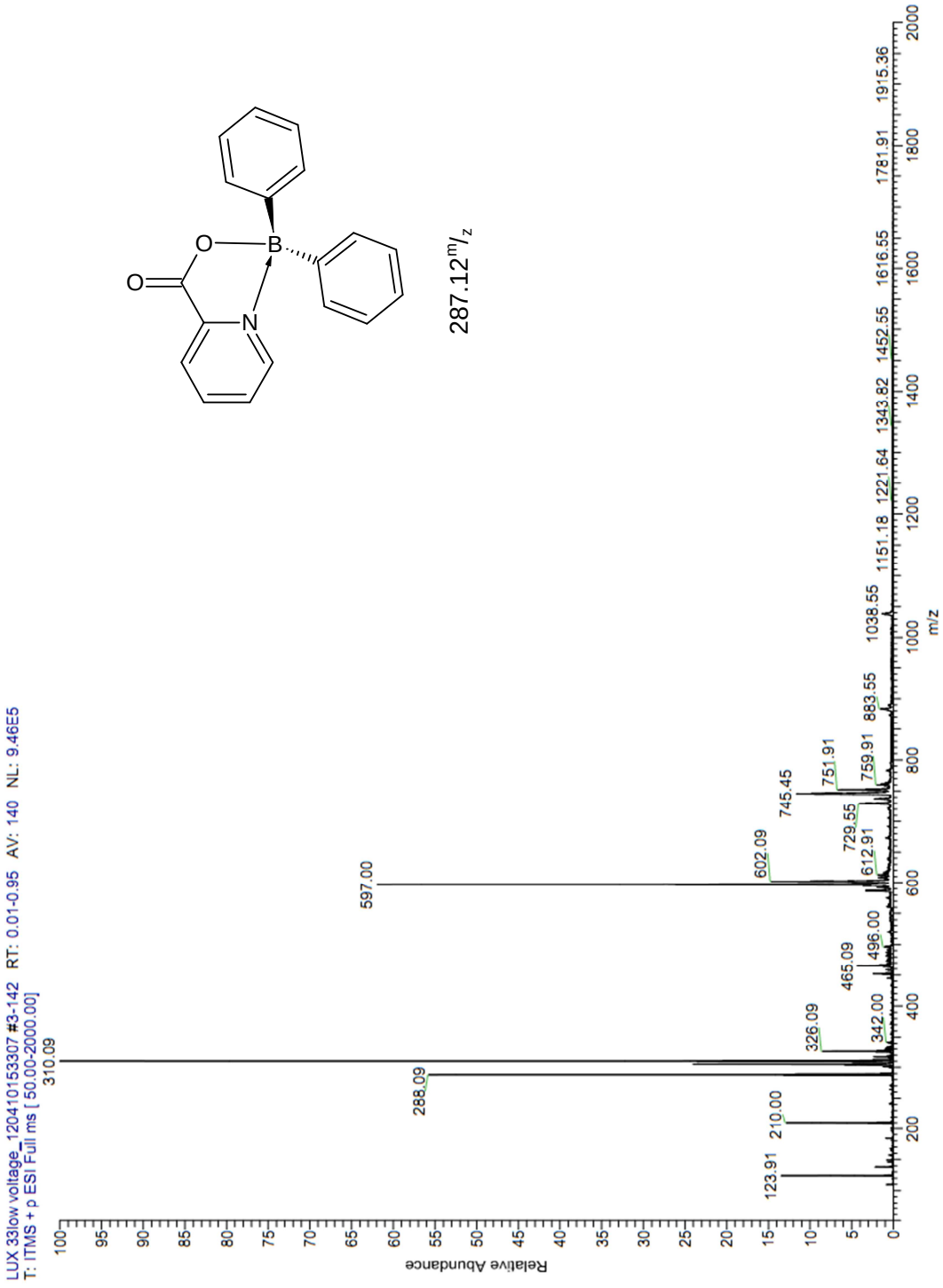

Figure 49. Mass spectrum of product **18** of diphenyl borinic acid **16** and picolinic acid **17**.

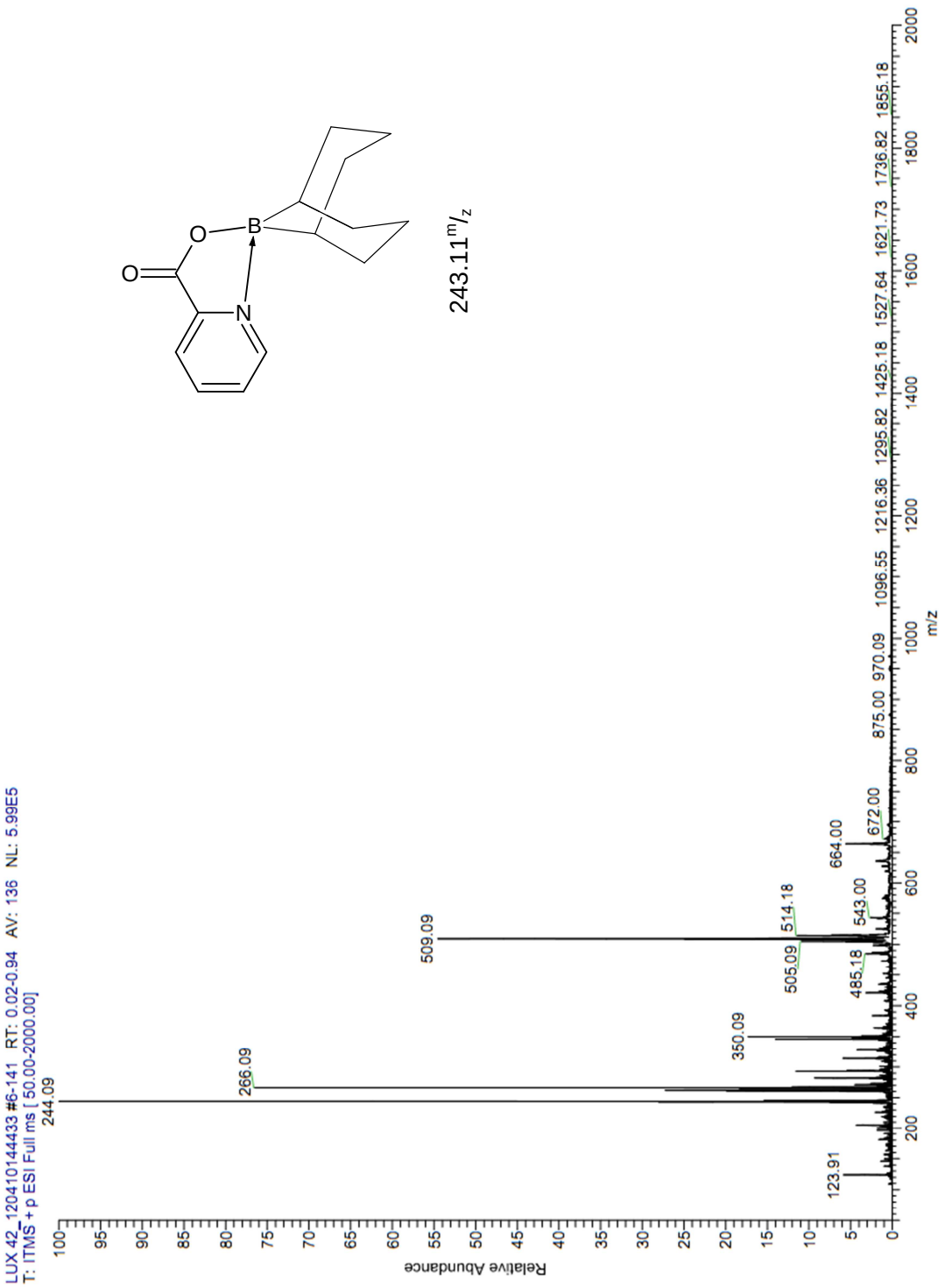

Figure 50. Mass spectrum of product **40** of 9-BBN **39** and picolinic acid **17**.

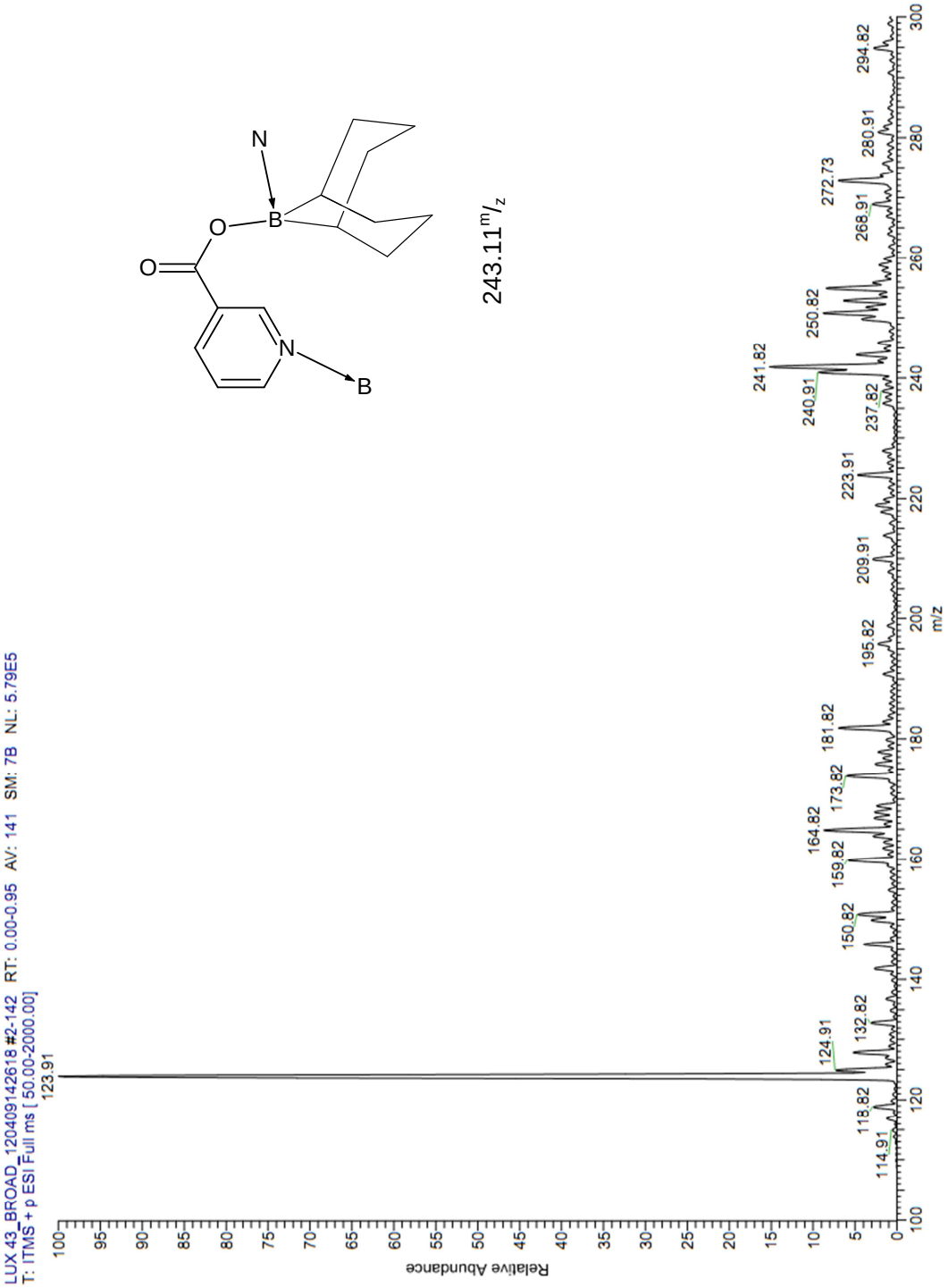

Figure 51. Mass spectrum of product of 9-BBN **39** and nicotinic acid **18**.

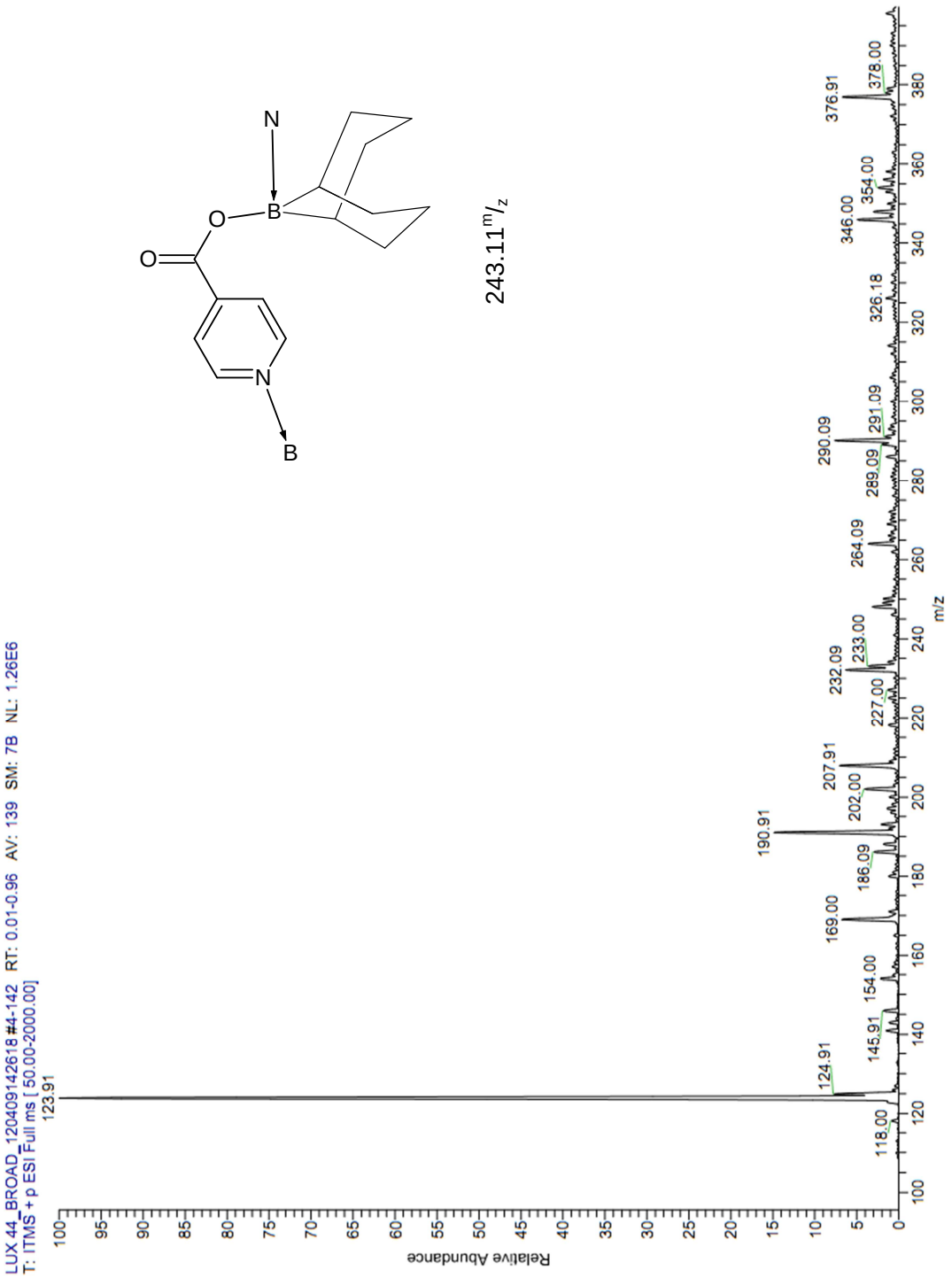

Figure 52. Mass spectrum of product of 9-BBN **39** and isonicotinic acid **19**.

APPENDIX C: SINGLE CRYSTAL X-RAY DIFFRACTION

Ferrocene Boroxine – 4-Aminomethyl Pyridine Complex 4

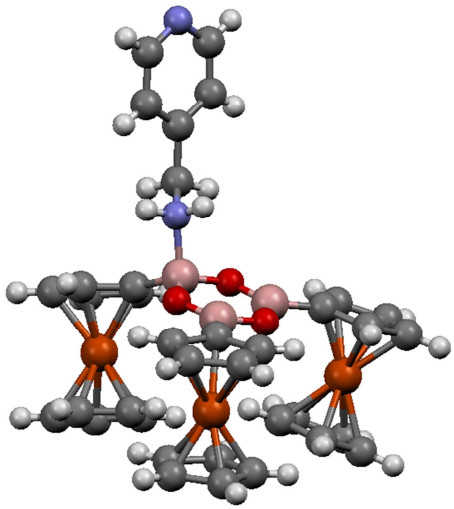

Table 4. Crystal data and structure refinement for p212121.

Identification code	p212121	
Empirical formula	C36 H35 B3 Fe3 N2 O3	
Formula weight	743.64	
Temperature	100(2) K	
Wavelength	1.54178 Å	
Crystal system, space group	Orthorhombic, P2(1)2(1)2(1)	
Unit cell dimensions	a = 10.6202(5) Å	α = 90 deg.
	b = 16.1745(7) Å	β = 90 deg.
	c = 18.7829(8) Å	γ = 90 deg.
Volume	3226.5(2) $Å^3$	
Z, Calculated density	4, 1.531 Mg/m^3	
Absorption coefficient	10.989 mm^{-1}	
F(000)	1528	
Crystal size	0.27 x 0.22 x 0.11 mm	
Theta range for data collection	3.61 to 67.00°	
Limiting indices	-12<=h<=11, -18<=k<=19, -22<=l<=22	
Reflections collected / unique	31963 / 5467 [R(int) = 0.0497]	
Completeness to theta = 67.00	99.2 %	
Absorption correction	Numerical	
Max. and min. transmission	0.3778 and 0.1553	
Refinement method	Full-matrix least-squares on F^2	
Data / restraints / parameters	5467 / 0 / 424	
Goodness-of-fit on F^2	0.939	
Final R indices [I>2sigma(I)]	R1 = 0.0247, wR2 = 0.0480	
R indices (all data)	R1 = 0.0309, wR2 = 0.0491	
Absolute structure parameter	0.010(3)	
Largest diff. peak and hole	0.226 and -0.226 e. $Å^{-3}$	

Table 5. Atomic coordinates (x 10^4) and equivalent isotropic displacement parameters (Å ^{2} x 10^3) for p212121. U(eq) is defined as one third of the trace of the orthogonalized U^{ij} tensor.

	x	y	z	U(eq)
Fe(1)	330(1)	3456(1)	6974(1)	11(1)
Fe(2)	4722(1)	6115(1)	7931(1)	13(1)
Fe(3)	4863(1)	4319(1)	4808(1)	11(1)
O(1)	1541(1)	5680(1)	6752(1)	12(1)
O(2)	3368(2)	5830(1)	6023(1)	14(1)
O(3)	1595(2)	5120(1)	5540(1)	12(1)
N(1)	-162(2)	6017(1)	5929(1)	11(1)
N(2)	-3511(2)	7677(1)	4564(1)	22(1)
C(1)	-1034(2)	5775(2)	5357(1)	19(1)
C(2)	-1867(2)	6466(2)	5095(1)	16(1)
C(3)	-2503(3)	6996(2)	5546(2)	23(1)
C(4)	-3303(3)	7588(2)	5260(2)	26(1)
C(5)	-2878(3)	7161(2)	4134(2)	22(1)
C(6)	-2053(2)	6565(2)	4368(1)	18(1)
C(7)	-22(2)	4522(1)	6402(1)	10(1)
C(8)	-835(2)	4459(2)	7010(1)	14(1)
C(9)	-1551(2)	3718(2)	6960(1)	17(1)
C(10)	-1194(2)	3312(2)	6325(1)	16(1)
C(11)	-263(2)	3802(1)	5985(1)	14(1)
C(12)	2126(2)	3535(2)	7346(1)	22(1)
C(13)	1287(3)	3398(2)	7916(2)	35(1)
C(14)	658(3)	2646(2)	7783(2)	38(1)
C(15)	1105(2)	2316(2)	7132(2)	24(1)
C(16)	2014(2)	2869(2)	6865(1)	19(1)
C(17)	3390(2)	6521(2)	7216(1)	12(1)
C(18)	2993(2)	6684(1)	7928(1)	14(1)
C(19)	3898(2)	7199(2)	8263(1)	18(1)
C(20)	4856(3)	7369(1)	7761(1)	20(1)
C(21)	4552(2)	6948(2)	7120(1)	18(1)
C(22)	4567(3)	4950(2)	8353(1)	21(1)
C(23)	5231(3)	5487(2)	8823(1)	26(1)
C(24)	6314(3)	5773(2)	8459(2)	31(1)
C(25)	6309(3)	5425(2)	7771(2)	32(1)
C(26)	5240(3)	4917(2)	7704(1)	24(1)
C(27)	3591(2)	5263(1)	4791(1)	12(1)
C(28)	4848(2)	5565(1)	4678(1)	14(1)
C(29)	5358(2)	5185(1)	4061(1)	16(1)
C(30)	4423(2)	4646(2)	3782(1)	15(1)
C(31)	3351(2)	4694(2)	4226(1)	15(1)
C(32)	4623(3)	3781(2)	5776(1)	19(1)
C(33)	5859(3)	4104(2)	5722(1)	21(1)
C(34)	6452(3)	3709(2)	5133(2)	24(1)
C(35)	5590(2)	3149(2)	4830(2)	22(1)
C(36)	4448(3)	3189(2)	5226(1)	24(1)
B(1)	851(3)	5278(2)	6178(2)	12(1)
B(2)	2718(3)	5974(2)	6650(2)	13(1)
B(3)	2793(3)	5404(2)	5476(2)	12(1)

Table 6. Bond lengths [Å] and angles [°] for p212121.

Fe(1)-C(14)	2.035(3)
Fe(1)-C(12)	2.035(3)
Fe(1)-C(16)	2.036(2)
Fe(1)-C(10)	2.040(2)
Fe(1)-C(11)	2.040(2)
Fe(1)-C(15)	2.040(3)
Fe(1)-C(8)	2.041(2)
Fe(1)-C(13)	2.042(3)
Fe(1)-C(9)	2.042(2)
Fe(1)-C(7)	2.066(2)
Fe(2)-C(23)	2.034(2)
Fe(2)-C(24)	2.038(3)
Fe(2)-C(21)	2.041(2)
Fe(2)-C(25)	2.043(3)
Fe(2)-C(22)	2.051(3)
Fe(2)-C(18)	2.055(2)
Fe(2)-C(19)	2.057(3)
Fe(2)-C(26)	2.058(2)
Fe(2)-C(17)	2.058(2)
Fe(2)-C(20)	2.058(2)
Fe(3)-C(28)	2.031(2)
Fe(3)-C(32)	2.032(2)
Fe(3)-C(31)	2.036(2)
Fe(3)-C(36)	2.038(3)
Fe(3)-C(27)	2.040(2)
Fe(3)-C(35)	2.045(2)
Fe(3)-C(33)	2.045(3)
Fe(3)-C(34)	2.048(3)
Fe(3)-C(29)	2.052(2)
Fe(3)-C(30)	2.053(2)
O(1)-B(2)	1.351(3)
O(1)-B(1)	1.458(3)
O(2)-B(3)	1.380(3)
O(2)-B(2)	1.387(3)
O(3)-B(3)	1.358(3)
O(3)-B(1)	1.458(3)
N(1)-C(1)	1.471(3)
N(1)-B(1)	1.675(3)
N(1)-H(1A)	0.9200
N(1)-H(1B)	0.9200
N(2)-C(4)	1.335(3)
N(2)-C(5)	1.340(3)
C(1)-C(2)	1.507(3)
C(1)-H(1C)	0.9900
C(1)-H(1D)	0.9900
C(2)-C(3)	1.382(4)
C(2)-C(6)	1.388(3)
C(3)-C(4)	1.389(4)
C(3)-H(3)	0.9500
C(4)-H(4)	0.9500

C(5)-C(6)	1.376(3)
C(5)-H(5)	0.9500
C(6)-H(6)	0.9500
C(7)-C(11)	1.426(3)
C(7)-C(8)	1.436(3)
C(7)-B(1)	1.591(3)
C(8)-C(9)	1.422(3)
C(8)-H(8)	0.9500
C(9)-C(10)	1.413(4)
C(9)-H(9)	0.9500
C(10)-C(11)	1.420(3)
C(10)-H(10)	0.9500
C(11)-H(11)	0.9500
C(12)-C(13)	1.410(4)
C(12)-C(16)	1.412(4)
C(12)-H(12)	0.9500
C(13)-C(14)	1.410(5)
C(13)-H(13)	0.9500
C(14)-C(15)	1.415(4)
C(14)-H(14)	0.9500
C(15)-C(16)	1.409(4)
C(15)-H(15)	0.9500
C(16)-H(16)	0.9500
C(17)-C(21)	1.426(3)
C(17)-C(18)	1.428(3)
C(17)-B(2)	1.555(4)
C(18)-C(19)	1.418(3)
C(18)-H(18)	0.9500
C(19)-C(20)	1.414(4)
C(19)-H(19)	0.9500
C(20)-C(21)	1.421(3)
C(20)-H(20)	0.9500
C(21)-H(21)	0.9500
C(22)-C(26)	1.414(3)
C(22)-C(23)	1.424(4)
C(22)-H(22)	0.9500
C(23)-C(24)	1.417(4)
C(23)-H(23)	0.9500
C(24)-C(25)	1.411(4)
C(24)-H(24)	0.9500
C(25)-C(26)	1.408(4)
C(25)-H(25)	0.9500
C(26)-H(26)	0.9500
C(27)-C(31)	1.428(3)
C(27)-C(28)	1.437(3)
C(27)-B(3)	1.558(4)
C(28)-C(29)	1.420(3)
C(28)-H(28)	0.9500
C(29)-C(30)	1.422(3)
C(29)-H(29)	0.9500
C(30)-C(31)	1.413(3)

C(30)-H(30)	0.9500
C(31)-H(31)	0.9500
C(32)-C(33)	1.416(4)
C(32)-C(36)	1.422(4)
C(32)-H(32)	0.9500
C(33)-C(34)	1.423(4)
C(33)-H(33)	0.9500
C(34)-C(35)	1.408(4)
C(34)-H(34)	0.9500
C(35)-C(36)	1.425(4)
C(35)-H(35)	0.9500
C(36)-H(36)	0.9500
C(14)-Fe(1)-C(12)	67.92(12)
C(14)-Fe(1)-C(16)	67.96(11)
C(12)-Fe(1)-C(16)	40.59(10)
C(14)-Fe(1)-C(10)	120.52(12)
C(12)-Fe(1)-C(10)	162.97(11)
C(16)-Fe(1)-C(10)	125.72(10)
C(14)-Fe(1)-C(11)	155.34(12)
C(12)-Fe(1)-C(11)	125.79(11)
C(16)-Fe(1)-C(11)	107.90(10)
C(10)-Fe(1)-C(11)	40.73(9)
C(14)-Fe(1)-C(15)	40.62(12)
C(12)-Fe(1)-C(15)	68.22(11)
C(16)-Fe(1)-C(15)	40.43(10)
C(10)-Fe(1)-C(15)	107.69(11)
C(11)-Fe(1)-C(15)	120.33(11)
C(14)-Fe(1)-C(8)	126.18(11)
C(12)-Fe(1)-C(8)	120.43(10)
C(16)-Fe(1)-C(8)	155.05(10)
C(10)-Fe(1)-C(8)	68.26(10)
C(11)-Fe(1)-C(8)	67.98(10)
C(15)-Fe(1)-C(8)	163.25(11)
C(14)-Fe(1)-C(13)	40.46(13)
C(12)-Fe(1)-C(13)	40.45(12)
C(16)-Fe(1)-C(13)	68.20(11)
C(10)-Fe(1)-C(13)	155.13(12)
C(11)-Fe(1)-C(13)	162.76(12)
C(15)-Fe(1)-C(13)	68.39(12)
C(8)-Fe(1)-C(13)	108.02(11)
C(14)-Fe(1)-C(9)	108.09(11)
C(12)-Fe(1)-C(9)	155.23(11)
C(16)-Fe(1)-C(9)	162.75(11)
C(10)-Fe(1)-C(9)	40.50(10)
C(11)-Fe(1)-C(9)	68.23(10)
C(15)-Fe(1)-C(9)	125.72(11)
C(8)-Fe(1)-C(9)	40.77(9)
C(13)-Fe(1)-C(9)	120.51(12)
C(14)-Fe(1)-C(7)	163.00(12)
C(12)-Fe(1)-C(7)	107.19(10)
C(16)-Fe(1)-C(7)	119.71(10)

C(10)-Fe(1)-C(7)	68.96(10)
C(11)-Fe(1)-C(7)	40.64(9)
C(15)-Fe(1)-C(7)	154.50(11)
C(8)-Fe(1)-C(7)	40.94(9)
C(13)-Fe(1)-C(7)	125.39(12)
C(9)-Fe(1)-C(7)	69.10(9)
C(23)-Fe(2)-C(24)	40.73(11)
C(23)-Fe(2)-C(21)	165.53(11)
C(24)-Fe(2)-C(21)	128.01(11)
C(23)-Fe(2)-C(25)	68.24(12)
C(24)-Fe(2)-C(25)	40.45(12)
C(21)-Fe(2)-C(25)	108.88(11)
C(23)-Fe(2)-C(22)	40.81(10)
C(24)-Fe(2)-C(22)	68.21(11)
C(21)-Fe(2)-C(22)	152.64(10)
C(25)-Fe(2)-C(22)	67.77(11)
C(23)-Fe(2)-C(18)	117.59(11)
C(24)-Fe(2)-C(18)	149.80(11)
C(21)-Fe(2)-C(18)	67.88(10)
C(25)-Fe(2)-C(18)	169.07(12)
C(22)-Fe(2)-C(18)	109.96(10)
C(23)-Fe(2)-C(19)	106.75(10)
C(24)-Fe(2)-C(19)	115.84(11)
C(21)-Fe(2)-C(19)	68.06(10)
C(25)-Fe(2)-C(19)	149.40(11)
C(22)-Fe(2)-C(19)	129.14(11)
C(18)-Fe(2)-C(19)	40.36(9)
C(23)-Fe(2)-C(26)	68.23(10)
C(24)-Fe(2)-C(26)	67.91(11)
C(21)-Fe(2)-C(26)	119.41(10)
C(25)-Fe(2)-C(26)	40.15(11)
C(22)-Fe(2)-C(26)	40.25(10)
C(18)-Fe(2)-C(26)	131.35(11)
C(19)-Fe(2)-C(26)	168.18(11)
C(23)-Fe(2)-C(17)	151.65(11)
C(24)-Fe(2)-C(17)	167.18(11)
C(21)-Fe(2)-C(17)	40.70(9)
C(25)-Fe(2)-C(17)	130.20(11)
C(22)-Fe(2)-C(17)	119.40(10)
C(18)-Fe(2)-C(17)	40.64(9)
C(19)-Fe(2)-C(17)	68.51(10)
C(26)-Fe(2)-C(17)	110.46(10)
C(23)-Fe(2)-C(20)	126.94(10)
C(24)-Fe(2)-C(20)	106.53(12)
C(21)-Fe(2)-C(20)	40.58(9)
C(25)-Fe(2)-C(20)	117.26(12)
C(22)-Fe(2)-C(20)	166.05(10)
C(18)-Fe(2)-C(20)	67.63(10)
C(19)-Fe(2)-C(20)	40.19(10)
C(26)-Fe(2)-C(20)	151.33(11)
C(17)-Fe(2)-C(20)	68.43(10)

C(28)-Fe(3)-C(32)	122.13(9)
C(28)-Fe(3)-C(31)	68.49(10)
C(32)-Fe(3)-C(31)	120.64(11)
C(28)-Fe(3)-C(36)	159.25(10)
C(32)-Fe(3)-C(36)	40.89(10)
C(31)-Fe(3)-C(36)	107.65(11)
C(28)-Fe(3)-C(27)	41.34(9)
C(32)-Fe(3)-C(27)	104.61(10)
C(31)-Fe(3)-C(27)	41.03(10)
C(36)-Fe(3)-C(27)	122.32(10)
C(28)-Fe(3)-C(35)	157.59(10)
C(32)-Fe(3)-C(35)	68.44(10)
C(31)-Fe(3)-C(35)	125.77(11)
C(36)-Fe(3)-C(35)	40.84(10)
C(27)-Fe(3)-C(35)	160.70(10)
C(28)-Fe(3)-C(33)	105.93(10)
C(32)-Fe(3)-C(33)	40.64(10)
C(31)-Fe(3)-C(33)	155.44(10)
C(36)-Fe(3)-C(33)	68.66(11)
C(27)-Fe(3)-C(33)	118.93(10)
C(35)-Fe(3)-C(33)	68.27(11)
C(28)-Fe(3)-C(34)	121.41(11)
C(32)-Fe(3)-C(34)	68.28(11)
C(31)-Fe(3)-C(34)	162.51(11)
C(36)-Fe(3)-C(34)	68.35(11)
C(27)-Fe(3)-C(34)	155.73(10)
C(35)-Fe(3)-C(34)	40.23(10)
C(33)-Fe(3)-C(34)	40.69(10)
C(28)-Fe(3)-C(29)	40.70(9)
C(32)-Fe(3)-C(29)	159.54(10)
C(31)-Fe(3)-C(29)	68.34(10)
C(36)-Fe(3)-C(29)	158.67(10)
C(27)-Fe(3)-C(29)	69.34(10)
C(35)-Fe(3)-C(29)	123.33(10)
C(33)-Fe(3)-C(29)	123.92(11)
C(34)-Fe(3)-C(29)	108.81(11)
C(28)-Fe(3)-C(30)	68.23(9)
C(32)-Fe(3)-C(30)	157.23(11)
C(31)-Fe(3)-C(30)	40.42(9)
C(36)-Fe(3)-C(30)	122.92(10)
C(27)-Fe(3)-C(30)	68.94(10)
C(35)-Fe(3)-C(30)	110.12(10)
C(33)-Fe(3)-C(30)	161.70(10)
C(34)-Fe(3)-C(30)	126.31(11)
C(29)-Fe(3)-C(30)	40.52(9)
B(2)-O(1)-B(1)	121.2(2)
B(3)-O(2)-B(2)	119.7(2)
B(3)-O(3)-B(1)	121.4(2)
C(1)-N(1)-B(1)	114.76(18)
C(1)-N(1)-H(1A)	108.6
B(1)-N(1)-H(1A)	108.6

C(1)-N(1)-H(1B)	108.6
B(1)-N(1)-H(1B)	108.6
H(1A)-N(1)-H(1B)	107.6
C(4)-N(2)-C(5)	116.1(2)
N(1)-C(1)-C(2)	114.3(2)
N(1)-C(1)-H(1C)	108.7
C(2)-C(1)-H(1C)	108.7
N(1)-C(1)-H(1D)	108.7
C(2)-C(1)-H(1D)	108.7
H(1C)-C(1)-H(1D)	107.6
C(3)-C(2)-C(6)	117.5(2)
C(3)-C(2)-C(1)	123.1(2)
C(6)-C(2)-C(1)	119.3(2)
C(2)-C(3)-C(4)	119.3(3)
C(2)-C(3)-H(3)	120.4
C(4)-C(3)-H(3)	120.4
N(2)-C(4)-C(3)	123.7(3)
N(2)-C(4)-H(4)	118.1
C(3)-C(4)-H(4)	118.1
N(2)-C(5)-C(6)	124.3(3)
N(2)-C(5)-H(5)	117.8
C(6)-C(5)-H(5)	117.8
C(5)-C(6)-C(2)	119.0(3)
C(5)-C(6)-H(6)	120.5
C(2)-C(6)-H(6)	120.5
C(11)-C(7)-C(8)	105.7(2)
C(11)-C(7)-B(1)	126.0(2)
C(8)-C(7)-B(1)	127.9(2)
C(11)-C(7)-Fe(1)	68.72(12)
C(8)-C(7)-Fe(1)	68.62(12)
B(1)-C(7)-Fe(1)	132.36(16)
C(9)-C(8)-C(7)	109.2(2)
C(9)-C(8)-Fe(1)	69.65(13)
C(7)-C(8)-Fe(1)	70.45(12)
C(9)-C(8)-H(8)	125.4
C(7)-C(8)-H(8)	125.4
Fe(1)-C(8)-H(8)	126.1
C(10)-C(9)-C(8)	107.7(2)
C(10)-C(9)-Fe(1)	69.67(14)
C(8)-C(9)-Fe(1)	69.58(13)
C(10)-C(9)-H(9)	126.1
C(8)-C(9)-H(9)	126.1
Fe(1)-C(9)-H(9)	126.2
C(9)-C(10)-C(11)	107.9(2)
C(9)-C(10)-Fe(1)	69.84(14)
C(11)-C(10)-Fe(1)	69.65(14)
C(9)-C(10)-H(10)	126.1
C(11)-C(10)-H(10)	126.1
Fe(1)-C(10)-H(10)	126.0
C(10)-C(11)-C(7)	109.5(2)
C(10)-C(11)-Fe(1)	69.63(13)

C(7)-C(11)-Fe(1)	70.64(13)
C(10)-C(11)-H(11)	125.2
C(7)-C(11)-H(11)	125.2
Fe(1)-C(11)-H(11)	126.1
C(13)-C(12)-C(16)	108.2(3)
C(13)-C(12)-Fe(1)	70.02(16)
C(16)-C(12)-Fe(1)	69.72(14)
C(13)-C(12)-H(12)	125.9
C(16)-C(12)-H(12)	125.9
Fe(1)-C(12)-H(12)	126.0
C(12)-C(13)-C(14)	107.5(3)
C(12)-C(13)-Fe(1)	69.53(15)
C(14)-C(13)-Fe(1)	69.52(17)
C(12)-C(13)-H(13)	126.2
C(14)-C(13)-H(13)	126.2
Fe(1)-C(13)-H(13)	126.3
C(13)-C(14)-C(15)	108.6(3)
C(13)-C(14)-Fe(1)	70.02(16)
C(15)-C(14)-Fe(1)	69.89(15)
C(13)-C(14)-H(14)	125.7
C(15)-C(14)-H(14)	125.7
Fe(1)-C(14)-H(14)	126.0
C(16)-C(15)-C(14)	107.4(3)
C(16)-C(15)-Fe(1)	69.60(14)
C(14)-C(15)-Fe(1)	69.49(15)
C(16)-C(15)-H(15)	126.3
C(14)-C(15)-H(15)	126.3
Fe(1)-C(15)-H(15)	126.2
C(15)-C(16)-C(12)	108.3(2)
C(15)-C(16)-Fe(1)	69.96(14)
C(12)-C(16)-Fe(1)	69.69(14)
C(15)-C(16)-H(16)	125.9
C(12)-C(16)-H(16)	125.9
Fe(1)-C(16)-H(16)	126.1
C(21)-C(17)-C(18)	106.5(2)
C(21)-C(17)-B(2)	125.9(2)
C(18)-C(17)-B(2)	127.6(2)
C(21)-C(17)-Fe(2)	69.02(13)
C(18)-C(17)-Fe(2)	69.56(13)
B(2)-C(17)-Fe(2)	125.41(17)
C(19)-C(18)-C(17)	108.9(2)
C(19)-C(18)-Fe(2)	69.91(14)
C(17)-C(18)-Fe(2)	69.80(13)
C(19)-C(18)-H(18)	125.5
C(17)-C(18)-H(18)	125.5
Fe(2)-C(18)-H(18)	126.3
C(20)-C(19)-C(18)	107.8(2)
C(20)-C(19)-Fe(2)	69.94(14)
C(18)-C(19)-Fe(2)	69.73(14)
C(20)-C(19)-H(19)	126.1
C(18)-C(19)-H(19)	126.1

Fe(2)-C(19)-H(19)	125.8
C(19)-C(20)-C(21)	108.0(2)
C(19)-C(20)-Fe(2)	69.87(14)
C(21)-C(20)-Fe(2)	69.08(13)
C(19)-C(20)-H(20)	126.0
C(21)-C(20)-H(20)	126.0
Fe(2)-C(20)-H(20)	126.6
C(20)-C(21)-C(17)	108.8(2)
C(20)-C(21)-Fe(2)	70.34(14)
C(17)-C(21)-Fe(2)	70.28(14)
C(20)-C(21)-H(21)	125.6
C(17)-C(21)-H(21)	125.6
Fe(2)-C(21)-H(21)	125.3
C(26)-C(22)-C(23)	107.9(2)
C(26)-C(22)-Fe(2)	70.14(14)
C(23)-C(22)-Fe(2)	68.96(14)
C(26)-C(22)-H(22)	126.0
C(23)-C(22)-H(22)	126.0
Fe(2)-C(22)-H(22)	126.4
C(24)-C(23)-C(22)	107.6(2)
C(24)-C(23)-Fe(2)	69.78(15)
C(22)-C(23)-Fe(2)	70.23(14)
C(24)-C(23)-H(23)	126.2
C(22)-C(23)-H(23)	126.2
Fe(2)-C(23)-H(23)	125.4
C(25)-C(24)-C(23)	108.0(3)
C(25)-C(24)-Fe(2)	70.00(16)
C(23)-C(24)-Fe(2)	69.49(15)
C(25)-C(24)-H(24)	126.0
C(23)-C(24)-H(24)	126.0
Fe(2)-C(24)-H(24)	126.1
C(26)-C(25)-C(24)	108.5(3)
C(26)-C(25)-Fe(2)	70.47(15)
C(24)-C(25)-Fe(2)	69.56(16)
C(26)-C(25)-H(25)	125.8
C(24)-C(25)-H(25)	125.8
Fe(2)-C(25)-H(25)	125.8
C(25)-C(26)-C(22)	108.0(2)
C(25)-C(26)-Fe(2)	69.38(16)
C(22)-C(26)-Fe(2)	69.61(14)
C(25)-C(26)-H(26)	126.0
C(22)-C(26)-H(26)	126.0
Fe(2)-C(26)-H(26)	126.6
C(31)-C(27)-C(28)	106.0(2)
C(31)-C(27)-B(3)	127.6(2)
C(28)-C(27)-B(3)	125.3(2)
C(31)-C(27)-Fe(3)	69.34(14)
C(28)-C(27)-Fe(3)	69.00(13)
B(3)-C(27)-Fe(3)	117.12(16)
C(29)-C(28)-C(27)	109.1(2)
C(29)-C(28)-Fe(3)	70.45(13)

C(27)-C(28)-Fe(3)	69.66(13)
C(29)-C(28)-H(28)	125.4
C(27)-C(28)-H(28)	125.4
Fe(3)-C(28)-H(28)	126.0
C(28)-C(29)-C(30)	107.4(2)
C(28)-C(29)-Fe(3)	68.85(13)
C(30)-C(29)-Fe(3)	69.78(14)
C(28)-C(29)-H(29)	126.3
C(30)-C(29)-H(29)	126.3
Fe(3)-C(29)-H(29)	126.6
C(31)-C(30)-C(29)	108.2(2)
C(31)-C(30)-Fe(3)	69.13(14)
C(29)-C(30)-Fe(3)	69.69(13)
C(31)-C(30)-H(30)	125.9
C(29)-C(30)-H(30)	125.9
Fe(3)-C(30)-H(30)	126.9
C(30)-C(31)-C(27)	109.2(2)
C(30)-C(31)-Fe(3)	70.46(14)
C(27)-C(31)-Fe(3)	69.63(13)
C(30)-C(31)-H(31)	125.4
C(27)-C(31)-H(31)	125.4
Fe(3)-C(31)-H(31)	126.1
C(33)-C(32)-C(36)	108.5(2)
C(33)-C(32)-Fe(3)	70.18(15)
C(36)-C(32)-Fe(3)	69.78(14)
C(33)-C(32)-H(32)	125.8
C(36)-C(32)-H(32)	125.8
Fe(3)-C(32)-H(32)	125.9
C(32)-C(33)-C(34)	107.5(2)
C(32)-C(33)-Fe(3)	69.19(14)
C(34)-C(33)-Fe(3)	69.75(15)
C(32)-C(33)-H(33)	126.2
C(34)-C(33)-H(33)	126.2
Fe(3)-C(33)-H(33)	126.4
C(35)-C(34)-C(33)	108.4(2)
C(35)-C(34)-Fe(3)	69.78(15)
C(33)-C(34)-Fe(3)	69.56(14)
C(35)-C(34)-H(34)	125.8
C(33)-C(34)-H(34)	125.8
Fe(3)-C(34)-H(34)	126.4
C(34)-C(35)-C(36)	108.3(2)
C(34)-C(35)-Fe(3)	69.99(15)
C(36)-C(35)-Fe(3)	69.33(15)
C(34)-C(35)-H(35)	125.9
C(36)-C(35)-H(35)	125.9
Fe(3)-C(35)-H(35)	126.4
C(32)-C(36)-C(35)	107.3(2)
C(32)-C(36)-Fe(3)	69.33(14)
C(35)-C(36)-Fe(3)	69.83(15)
C(32)-C(36)-H(36)	126.3
C(35)-C(36)-H(36)	126.3

Fe(3)-C(36)-H(36)	126.1
O(1)-B(1)-O(3)	114.5(2)
O(1)-B(1)-C(7)	116.1(2)
O(3)-B(1)-C(7)	113.5(2)
O(1)-B(1)-N(1)	102.17(18)
O(3)-B(1)-N(1)	104.14(18)
C(7)-B(1)-N(1)	104.39(18)
O(1)-B(2)-O(2)	121.5(2)
O(1)-B(2)-C(17)	121.9(2)
O(2)-B(2)-C(17)	116.6(2)
O(3)-B(3)-O(2)	121.2(2)
O(3)-B(3)-C(27)	122.2(2)
O(2)-B(3)-C(27)	116.5(2)

Table 7. Anisotropic displacement parameters ($Å^2 \times 10^3$) for p212121. The anisotropic displacement factor exponent takes the form: $-2\pi^2 [h^2 a^{*2} U^{11} + ... + 2 h k a^* b^* U^{12}]$

	U^{11}	U^{22}	U^{33}	U^{23}	U^{13}	U^{12}
Fe(1)	13(1)	9(1)	12(1)	3(1)	-1(1)	3(1)
Fe(2)	11(1)	14(1)	13(1)	-2(1)	-3(1)	1(1)
Fe(3)	14(1)	9(1)	9(1)	1(1)	1(1)	0(1)
O(1)	13(1)	12(1)	11(1)	-1(1)	-1(1)	-1(1)
O(2)	12(1)	18(1)	12(1)	-3(1)	1(1)	-2(1)
O(3)	12(1)	13(1)	12(1)	-2(1)	-1(1)	0(1)
N(1)	12(1)	8(1)	13(1)	2(1)	0(1)	-2(1)
N(2)	19(1)	13(1)	33(1)	9(1)	-3(1)	1(1)
C(1)	23(1)	11(1)	24(2)	-5(1)	-11(1)	3(1)
C(2)	11(1)	10(1)	28(2)	-1(1)	-6(1)	-2(1)
C(3)	28(2)	20(2)	22(2)	1(1)	-10(1)	2(1)
C(4)	23(2)	18(2)	36(2)	-5(2)	-4(1)	7(1)
C(5)	21(2)	20(2)	26(2)	12(1)	-2(1)	0(1)
C(6)	15(1)	15(1)	23(2)	1(1)	0(1)	0(1)
C(7)	9(1)	8(1)	12(1)	3(1)	-6(1)	5(1)
C(8)	13(1)	13(1)	18(1)	3(1)	-2(1)	7(1)
C(9)	8(1)	20(2)	24(1)	9(1)	2(1)	1(1)
C(10)	17(1)	11(1)	19(1)	3(1)	-7(1)	-4(1)
C(11)	15(1)	13(1)	13(1)	3(1)	-4(1)	1(1)
C(12)	18(2)	17(2)	31(2)	-5(1)	-15(1)	4(1)
C(13)	49(2)	44(2)	13(2)	-7(2)	-11(1)	34(2)
C(14)	28(2)	53(2)	32(2)	34(2)	10(1)	21(2)
C(15)	22(2)	12(1)	39(2)	5(1)	-6(1)	5(1)
C(16)	18(2)	19(2)	19(2)	-4(1)	-2(1)	8(1)
C(17)	9(1)	11(1)	16(1)	4(1)	-3(1)	1(1)
C(18)	12(1)	9(1)	19(1)	-1(1)	1(1)	3(1)
C(19)	20(2)	15(1)	18(1)	-6(1)	-6(1)	3(1)
C(20)	18(1)	13(1)	28(2)	0(1)	-9(1)	-4(1)
C(21)	18(1)	20(1)	17(1)	5(1)	-2(1)	-2(1)
C(22)	23(2)	15(1)	25(2)	5(1)	0(1)	5(1)
C(23)	46(2)	18(2)	14(1)	1(1)	-8(1)	8(1)
C(24)	26(2)	25(2)	42(2)	7(2)	-24(1)	2(1)
C(25)	17(2)	37(2)	43(2)	9(2)	9(1)	13(1)
C(26)	25(2)	24(2)	24(1)	-8(1)	-1(1)	13(1)
C(27)	13(1)	10(1)	13(1)	4(1)	-2(1)	4(1)
C(28)	19(1)	10(1)	12(1)	3(1)	1(1)	0(1)
C(29)	17(1)	15(1)	15(1)	6(1)	3(1)	1(1)
C(30)	19(1)	15(1)	10(1)	2(1)	-1(1)	0(1)
C(31)	17(1)	19(1)	10(1)	3(1)	-1(1)	2(1)
C(32)	35(2)	14(1)	9(1)	5(1)	2(1)	6(1)
C(33)	27(2)	20(2)	15(2)	6(1)	-7(1)	4(1)
C(34)	20(2)	25(2)	26(2)	8(1)	1(1)	11(1)
C(35)	36(2)	10(1)	21(2)	4(1)	4(1)	8(1)
C(36)	35(2)	15(2)	24(2)	7(1)	2(1)	-3(1)
B(1)	13(2)	10(2)	12(2)	2(1)	-3(1)	1(1)
B(2)	13(2)	10(2)	16(2)	3(1)	-4(1)	5(1)
B(3)	16(2)	7(2)	14(2)	3(1)	-3(1)	2(1)

Table 8. Hydrogen coordinates (x 10^4) and isotropic displacement parameters (Å ^{2} x 10^3) for p212121.

	x	y	z	U(eq)
H(1A)	-626	6174	6320	13
H(1B)	290	6470	5780	13
H(1C)	-1574	5319	5531	23
H(1D)	-538	5561	4951	23
H(3)	-2393	6956	6047	28
H(4)	-3727	7950	5578	31
H(5)	-3009	7211	3636	27
H(6)	-1616	6226	4037	21
H(8)	-886	4850	7386	17
H(9)	-2159	3530	7293	21
H(10)	-1520	2801	6156	19
H(11)	137	3671	5547	16
H(12)	2672	3997	7295	26
H(13)	1167	3748	8316	42
H(14)	37	2402	8080	46
H(15)	840	1815	6916	29
H(16)	2474	2804	6434	22
H(18)	2244	6482	8143	16
H(19)	3866	7394	8740	21
H(20)	5576	7705	7840	24
H(21)	5042	6950	6697	22
H(22)	3807	4665	8458	25
H(23)	4990	5627	9295	31
H(24)	6935	6136	8646	37
H(25)	6924	5518	7412	39
H(26)	5010	4607	7295	29
H(28)	5270	5957	4970	16
H(29)	6175	5275	3869	19
H(30)	4504	4312	3369	18
H(31)	2591	4394	4159	18
H(32)	4014	3935	6123	23
H(33)	6226	4509	6023	25
H(34)	7287	3806	4973	28
H(35)	5745	2803	4431	27
H(36)	3705	2877	5138	29

Table 9. Hydrogen bonds for p212121 [A and deg.].

D-H...A	d(D-H)	d(H...A)	d(D...A)	<(DHA)
N(1)-H(1B)...N(2)#1	0.92	1.99	2.898(3)	170.9

Symmetry transformations used to generate equivalent atoms:
#1 x+1/2,-y+3/2,-z+1

Picolinic Diphenylborinate Ester 18

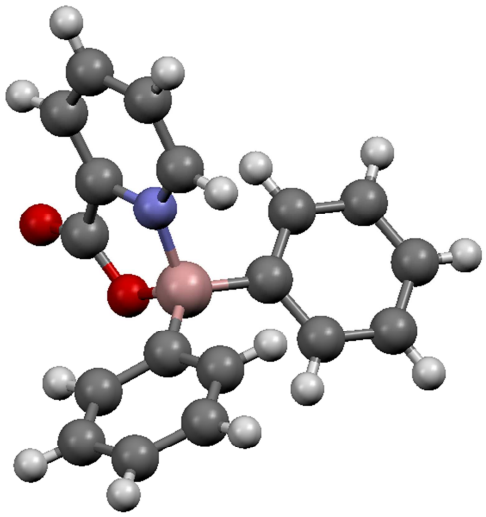

Table 10. Crystal data and structure refinement for p212121.

Identification code	p212121	
Empirical formula	C18 H14 B N O2	
Formula weight	287.11	
Temperature	100(2) K	
Wavelength	1.54178 Å	
Crystal system	Orthorhombic	
Space group	P2(1)2(1)2(1)	
Unit cell dimensions	a = 9.71220(10) Å	α= 90°.
	b = 11.28620(10) Å	β= 90°.
	c = 13.2458(2) Å	γ = 90°.
Volume	1451.92(3) $Å^3$	
Z	4	
Density (calculated)	1.313 Mg/m^3	
Absorption coefficient	0.675 mm^{-1}	
F(000)	600	
Crystal size	0.45 x 0.26 x 0.22 mm^3	
Theta range for data collection	5.15 to 66.97°.	
Index ranges	-10<=h<=11, -11<=k<=13, -15<=l<=15	
Reflections collected	15926	
Independent reflections	2549 [R(int) = 0.0273]	
Completeness to theta = 66.97°	99.7 %	
Absorption correction	Numerical	
Max. and min. transmission	0.8668 and 0.7501	
Refinement method	Full-matrix least-squares on F^2	
Data / restraints / parameters	2549 / 0 / 255	
Goodness-of-fit on F^2	1.064	
Final R indices [I>2sigma(I)]	R1 = 0.0250, wR2 = 0.0643	
R indices (all data)	R1 = 0.0253, wR2 = 0.0645	
Absolute structure parameter	0.05(15)	
Largest diff. peak and hole	0.125 and -0.194 $e.Å^{-3}$	

Table 11. Atomic coordinates (x 10^4) and equivalent isotropic displacement parameters (Å^{2}x 10^3) for p212121. U(eq) is defined as one third of the trace of the orthogonalized U^{ij} tensor.

	x	y	z	U(eq)
O(1)	1532(1)	7623(1)	1596(1)	20(1)
O(2)	311(1)	8355(1)	296(1)	27(1)
N(1)	-158(1)	6291(1)	2200(1)	17(1)
C(1)	-937(1)	5492(1)	2679(1)	19(1)
C(2)	-2223(1)	5206(1)	2304(1)	21(1)
C(3)	-2697(1)	5740(1)	1428(1)	22(1)
C(4)	-1869(1)	6560(1)	933(1)	21(1)
C(5)	-610(1)	6819(1)	1352(1)	18(1)
C(6)	447(1)	7683(1)	1004(1)	19(1)
C(7)	2430(1)	5703(1)	2444(1)	19(1)
C(8)	2666(1)	4967(1)	3280(1)	23(1)
C(9)	3545(1)	3995(1)	3227(1)	28(1)
C(10)	4181(1)	3707(1)	2321(1)	31(1)
C(11)	3951(1)	4410(1)	1477(1)	30(1)
C(12)	3107(1)	5402(1)	1546(1)	24(1)
C(13)	1234(1)	7543(1)	3518(1)	18(1)
C(14)	2325(1)	7633(1)	4202(1)	21(1)
C(15)	2230(1)	8329(1)	5065(1)	25(1)
C(16)	1040(1)	8962(1)	5266(1)	24(1)
C(17)	-48(1)	8913(1)	4588(1)	22(1)
C(18)	51(1)	8208(1)	3731(1)	20(1)
B(1)	1355(1)	6782(1)	2493(1)	19(1)

Table 12. Bond lengths [Å] and angles [°] for p212121.

O(1)-C(6)	1.3159(13)
O(1)-B(1)	1.5309(13)
O(2)-C(6)	1.2132(14)
N(1)-C(1)	1.3380(15)
N(1)-C(5)	1.3448(14)
N(1)-B(1)	1.6169(15)
C(1)-C(2)	1.3827(16)
C(1)-H(1)	0.995(15)
C(2)-C(3)	1.3871(17)
C(2)-H(2)	0.995(15)
C(3)-C(4)	1.3895(17)
C(3)-H(3)	0.975(15)
C(4)-C(5)	1.3740(16)
C(4)-H(4)	0.969(14)
C(5)-C(6)	1.4897(16)
C(7)-C(12)	1.4012(16)
C(7)-C(8)	1.4032(17)
C(7)-B(1)	1.6049(16)
C(8)-C(9)	1.3920(18)
C(8)-H(8)	0.984(15)
C(9)-C(10)	1.389(2)
C(9)-H(9)	0.984(15)
C(10)-C(11)	1.389(2)
C(10)-H(10)	0.996(18)
C(11)-C(12)	1.3913(18)
C(11)-H(11)	0.989(17)
C(12)-H(12)	1.004(15)
C(13)-C(14)	1.3973(15)
C(13)-C(18)	1.4016(16)
C(13)-B(1)	1.6104(16)
C(14)-C(15)	1.3905(16)
C(14)-H(14)	1.002(16)
C(15)-C(16)	1.3847(18)
C(15)-H(15)	0.981(15)
C(16)-C(17)	1.3877(17)
C(16)-H(16)	0.960(15)
C(17)-C(18)	1.3890(16)
C(17)-H(17)	0.995(15)
C(18)-H(18)	0.998(14)
C(6)-O(1)-B(1)	113.88(8)
C(1)-N(1)-C(5)	120.64(10)
C(1)-N(1)-B(1)	129.11(9)
C(5)-N(1)-B(1)	110.25(9)
N(1)-C(1)-C(2)	119.88(10)
N(1)-C(1)-H(1)	116.9(8)
C(2)-C(1)-H(1)	123.3(8)
C(1)-C(2)-C(3)	119.92(11)
C(1)-C(2)-H(2)	117.5(8)
C(3)-C(2)-H(2)	122.6(8)
C(2)-C(3)-C(4)	119.48(11)

C(2)-C(3)-H(3)	121.8(8)
C(4)-C(3)-H(3)	118.7(8)
C(5)-C(4)-C(3)	117.78(11)
C(5)-C(4)-H(4)	120.5(9)
C(3)-C(4)-H(4)	121.7(8)
N(1)-C(5)-C(4)	122.28(11)
N(1)-C(5)-C(6)	108.87(9)
C(4)-C(5)-C(6)	128.84(10)
O(2)-C(6)-O(1)	125.47(10)
O(2)-C(6)-C(5)	125.04(10)
O(1)-C(6)-C(5)	109.47(9)
C(12)-C(7)-C(8)	116.71(10)
C(12)-C(7)-B(1)	121.59(10)
C(8)-C(7)-B(1)	121.56(10)
C(9)-C(8)-C(7)	121.80(11)
C(9)-C(8)-H(8)	117.0(8)
C(7)-C(8)-H(8)	121.2(8)
C(10)-C(9)-C(8)	120.11(12)
C(10)-C(9)-H(9)	121.7(9)
C(8)-C(9)-H(9)	118.2(9)
C(9)-C(10)-C(11)	119.34(11)
C(9)-C(10)-H(10)	120.4(9)
C(11)-C(10)-H(10)	120.3(9)
C(12)-C(11)-C(10)	120.11(12)
C(12)-C(11)-H(11)	117.8(10)
C(10)-C(11)-H(11)	122.1(10)
C(11)-C(12)-C(7)	121.87(12)
C(11)-C(12)-H(12)	118.3(8)
C(7)-C(12)-H(12)	119.8(8)
C(14)-C(13)-C(18)	116.90(10)
C(14)-C(13)-B(1)	121.98(10)
C(18)-C(13)-B(1)	121.00(10)
C(15)-C(14)-C(13)	121.57(11)
C(15)-C(14)-H(14)	118.2(8)
C(13)-C(14)-H(14)	120.2(8)
C(16)-C(15)-C(14)	120.33(11)
C(16)-C(15)-H(15)	120.3(8)
C(14)-C(15)-H(15)	119.4(8)
C(15)-C(16)-C(17)	119.38(10)
C(15)-C(16)-H(16)	121.1(9)
C(17)-C(16)-H(16)	119.6(9)
C(16)-C(17)-C(18)	119.93(11)
C(16)-C(17)-H(17)	121.3(8)
C(18)-C(17)-H(17)	118.7(8)
C(17)-C(18)-C(13)	121.86(10)
C(17)-C(18)-H(18)	118.4(8)
C(13)-C(18)-H(18)	119.8(8)
O(1)-B(1)-C(7)	111.47(9)
O(1)-B(1)-C(13)	109.36(9)
C(7)-B(1)-C(13)	119.08(9)
O(1)-B(1)-N(1)	97.36(8)

C(7)-B(1)-N(1)	108.75(9)
C(13)-B(1)-N(1)	108.59(9)

Table 13. Anisotropic displacement parameters ($Å^2 x\ 10^3$)for p212121. The anisotropic displacement factor exponent takes the form: $-2\pi^2[\ h^2 a^{*2} U^{11} + ... + 2\ h\ k\ a^*\ b^*\ U^{12}\ ]$

	U^{11}	U^{22}	U^{33}	U^{23}	U^{13}	U^{12}
O(1)	20(1)	23(1)	18(1)	2(1)	0(1)	-3(1)
O(2)	28(1)	31(1)	22(1)	8(1)	0(1)	-1(1)
N(1)	18(1)	16(1)	16(1)	-3(1)	1(1)	0(1)
C(1)	22(1)	16(1)	18(1)	-2(1)	3(1)	1(1)
C(2)	20(1)	17(1)	26(1)	-4(1)	5(1)	0(1)
C(3)	17(1)	22(1)	27(1)	-5(1)	-1(1)	1(1)
C(4)	21(1)	22(1)	21(1)	-2(1)	-2(1)	3(1)
C(5)	20(1)	18(1)	16(1)	-2(1)	1(1)	4(1)
C(6)	20(1)	20(1)	17(1)	-1(1)	1(1)	2(1)
C(7)	17(1)	19(1)	22(1)	-2(1)	-2(1)	-5(1)
C(8)	24(1)	20(1)	25(1)	-1(1)	-2(1)	-3(1)
C(9)	27(1)	21(1)	37(1)	2(1)	-5(1)	-2(1)
C(10)	21(1)	22(1)	50(1)	-7(1)	-1(1)	0(1)
C(11)	21(1)	31(1)	37(1)	-9(1)	6(1)	-3(1)
C(12)	19(1)	26(1)	26(1)	-3(1)	1(1)	-4(1)
C(13)	20(1)	16(1)	19(1)	3(1)	0(1)	-4(1)
C(14)	24(1)	18(1)	23(1)	2(1)	-3(1)	0(1)
C(15)	31(1)	23(1)	22(1)	0(1)	-9(1)	1(1)
C(16)	35(1)	21(1)	17(1)	-1(1)	-1(1)	-2(1)
C(17)	23(1)	20(1)	22(1)	2(1)	4(1)	-1(1)
C(18)	19(1)	22(1)	18(1)	3(1)	-1(1)	-3(1)
B(1)	18(1)	20(1)	17(1)	2(1)	-1(1)	-3(1)

Table 14. Hydrogen coordinates (x 10^4) and isotropic displacement parameters (Å^{2}x 10^3) for p212121.

	x	y	z	U(eq)
H(1)	-536(15)	5120(12)	3294(11)	23(3)
H(2)	-2769(16)	4603(12)	2680(11)	28(4)
H(3)	-3604(16)	5564(13)	1150(10)	25(3)
H(4)	-2156(15)	6933(12)	308(10)	25(3)
H(8)	2229(15)	5127(13)	3937(11)	27(4)
H(9)	3691(15)	3524(14)	3843(12)	32(4)
H(10)	4796(18)	3002(15)	2276(12)	43(4)
H(11)	4362(17)	4225(15)	812(12)	39(4)
H(12)	2991(16)	5912(13)	930(11)	30(4)
H(14)	3198(16)	7181(13)	4082(10)	27(3)
H(15)	3012(16)	8362(12)	5534(10)	25(3)
H(16)	952(15)	9425(13)	5869(11)	31(4)
H(17)	-911(15)	9367(13)	4705(10)	21(3)
H(18)	-739(14)	8200(12)	3249(10)	22(3)